CHARACTERIZATION OF CHARGE INJECTION PROCESSES OF THIN FILMS ON INDIUM TIN OXIDE ELECTRODES USING A NOVEL SPECTROELECTROCHEMICAL TECHNIQUE: POTENTIAL-MODULATED ATTENUATED TOTAL REFLECTANCE SPECTROSCOPY

by

Zeynep Ozkan Araci

_____

A Dissertation Submitted to the Faculty of the

DEPARTMENT OF CHEMISTRY AND BIOCHEMISTRY

In the partial Fullfilment of the Requirements
For the Degree of

DOCTOR OF PHILOSOPHY
WITH A MAJOR IN CHEMISTRY

In the Graduate College

THE UNIVERSITY OF ARIZONA

2 0 10

THE UNIVERSITY OF ARIZONA
GRADUATE COLLEGE

As members of the Dissertation Committee, we certify that we have read the dissertation

prepared by Zeynep Araci

entitled Characterization of Charge Injection Processes of Thin Films on Indium Tin Oxide Electrodes Using a Novel Spectroelectrochemical Technique: Potential Modulated Attenuated Total Reflectance Spectroscopy

and recommend that it be accepted as fulfilling the dissertation requirement for the

Degree of Doctor of Philosophy

S. Scott Saavedra Date: 7/20/10

Neal Armstrong Date: 7/20/10

Jeanne Pemberton Date: 7/20/10

John Enemark Date: 7/20/10

Final approval and acceptance of this dissertation is contingent upon the candidate's submission of the final copies of the dissertation to the Graduate College.

I hereby certify that I have read this dissertation prepared under my direction and recommend that it be accepted as fulfilling the dissertation requirement.

S. Scott Saavedra Date: 7/20/10

Dissertation Director

STATEMENT BY AUTHOR

This dissertation has been submitted in partial fulfillment of requirements for an advanced degree at The University of Arizona and is deposited in the University Library to be made available to borrowers under rules of the Library.

Brief quotations from this thesis are allowable without special permission, provided that accurate acknowledgment of source is made. Requests for permission for extended quotation from or reproduction of this manuscript in whole or in part may be granted by the head of the major department or the Dean of the Graduate College when in his or her judgment the proposed use of the material is in the interests of scholarship. In all other instances, however, permission must be obtained from the author.

SIGNED: Zeynep Araci

ACKNOWLEDGMENTS

I would like to thank my research advisor, Dr. Scott Saavedra, for his scientific advice and encouragement throughout this project. I have been very fortunate to have an advisor who I have taken as a good example of a great scientist. His dedication to science and his erudition always inspire and enlighten me. Special thanks to the members of my dissertation committee, Dr. Neal Armstrong, Dr. Jeanne Pemberton and Dr. John Enemark for their scientific expertise and encouragement.

I would like to thank Dr. Anne F. Runge, who has been a wonderful teacher and a great friend who worked on some parts of this project with me. I would also like to acknowledge all the other people who helped me on this project: Walter Doherty, James Joubert, Chenhao Ge, Dr. Zhijie Sui, Michael Brumbach, Clayton Shallcross, Dr. Andrea Munro, Dr. Erin Ratcliff, Sergio Paniagua, and Saneeha Marikkar.

I would like to express gratitude to all the members of the Saavedra research group (past, present and adopted) for their support and friendship over the years. The life at the graduate school and the research becomes easier, fun and more valuable with their friendship.

I would like to thank some of the stuff members and facility scientists at the Department of Chemistry and Biochemistry who were willing to help all the time, excellent in advising and making our lifes easier at the Department: Lori Boyd, Selin Demir, Stacey Tutas, Lee Macomber, Ken Nebesny, Paul Lee, Dr. Brooke Beam, Brittany Douglas, and Daniel Moseke.

I would like to express my appreciation to all my dear and close friends. Without them, it is hard to imagine living through the stressing days in pursuing my degree. Particularly, I would like to mention that this research would not have been completed without the support and encouragements of the following people: Han Zhang, Kristina Orosz, Anne Simon, James Joubert, Mariola Macech, Nurcin Celik, Esra Buyuktahtakin, Ozlem Kepenekci, Mine Yildiz, Pinar Erduran, Asli Karatas, Halise Celik, Fran Braverman, Karen Phelps, Alejandra Lopez, Ayse Tay, Perihan Sarikaya, Cihan Kurter and Lauran Caris.

I would like to thank to my parents, my sisters, and my parent in-laws for their love and encouragements over the phone lines and through the internet: Huriye and Mehmet Ozkan, Sibel Ozkan, Dilsat Ozkan Ariksoysal, Filiz and Aziz Araci. Their support and prayers sustain and inspire me throughout all these years.

This dissertation is dedicated to my husband I. Emre Araci. Without his unconditional love, patience and support, I couldn’t have survived from this challenging process. His encouragements, concern, and strength has been the major driving forces for all the successes throughout my graduate career.

TABLE OF CONTENTS

TABLE OF CONTENTS - *Continued*

TABLE OF CONTENTS - *Continued*

TABLE OF CONTENTS - *Continued*

LIST OF FIGURES

LIST OF FIGURES – *Continued*

LIST OF FIGURES – *Continued*

LIST OF FIGURES – *Continued*

LIST OF FIGURES – *Continued*

LIST OF FIGURES – *Continued*

LIST OF TABLES

ABSTRACT

Understanding interfacial charge injection processes is one of the key factors needed for development of efficient organic electronic devices, such as biosensors and energy conversion systems, since these processes control the electrical characteristics of these devices. Spectroelectrochemical characterization of electron transfer processes occurring at the electrode – electroactive thin film interface has been evaluated to improve our understanding of charge transfer kinetics using a novel form of electroreflectance spectroscopy, potential-modulated attenuated total reflectance (PM-ATR), which makes it possible to sensitively monitor spectroscopic changes in thin films as a function of applied potential.

PM-ATR was used to evaluate three different redox-active films deposited on indium tin oxide (ITO) electrodes to investigate: i) the orientation dependence of charge transfer rates of thin films of biomolecules, ii) surface treatment and modification effects on charge transfer kinetics of conducting polymers and, iii) estimation of rates of electron injection and conduction band edge of semiconductor nanocrystalline materials.

First, Prussian blue film as a model system was used successfully to examine the PM-ATR technique for determination of the charge transfer rate constant between ITO and a molecular film.

Second, an anisotropic and redox active protein film, cytochrome *c*, was used to probe charge transfer rates with respect to molecular orientation. The electron transfer rate measured using TM polarized light was four-fold greater than that measured using

TE polarized light. These data are the first to correlate a distribution of molecular orientations with a distribution of electron transfer rates in a redox-active molecular film.

Third, the effects of ITO surface treatment and modification on charge transfer kinetics on a conducting polymer, poly(3,4-ethylenedioxythiophene/)/poly(styrenesulfonate) (PEDOT/PSS), were studied. The apparent interfacial charge transfer rate constant for PEDOT/PSS on ITO has been reported for the first time which cannot be measured otherwise with conventional electrochemistry due to high non-Faradaic background of PEDOT/PSS films.

Fourth, PM-ATR enabled characterization of reversible redox processes between submonolayer coverages of surface-tethered, CdSe nanocrystals and ITO for the first time. Optically determined onset potentials for electron injection were used for estimation for the conduction band and valance band energies (E_{CB} and E_{VB}, respectively).

1. INTRODUCTION TO POTENTIAL MODULATED ATTENUATED TOTAL REFLECTANCE SPECTOSCOPY

1.1 Spectroelectrochemistry of Adsorbed Thin Films

It has been long recognized by electrochemists that measurements of electrochemical currents, voltages, charges or capacitances do not provide unequivocal identification of electroactive molecules. Although a diffusion current might be correlated to a particular species, with its peak or half-wave potentials for reduction or oxidation and a diffusion coefficient appropriate to the medium, the molecular and structural identity of that species can not be fully understood from these properties, especially for complex and biochemical redox systems.[1] The ability to utilize additional specific and physical characteristics of molecules to monitor electrode processes would be useful.

The information content of electrochemical techniques can be substantially increased by combining them with spectroscopic techniques as a second dimension of analysis. The coupling of optical and electrochemical methods – *spectroelectrochemistry* – has been employed for over five decades to investigate a wide variety of inorganic, organic and biological redox systems.[2, 3]

The advantages of spectroelectrochemistry are well established. Specifically, the current flow of a Faradaic electrochemical event may be monitored through spectroscopic changes, therefore eliminating interferences from non-Faradaic current.[4] Spectral information can provide structural and/or orientational information as a function of redox

state, and can also increase sensitivity for detection of reactant, intermediate or product species.[1]

To improve our understanding of electron transfer reaction pathways and molecular structure at interfaces, a variety of optical methods have been coupled to electrochemical techniques. Spectroscopic methods that have been adapted to spectroelectrochemistry include X-ray absorption[5], ellipsometry[6], IR[7, 8] and Raman[9] spectroscopy. This introduction will focus on UV-VIS absorption spectroscopic techniques applicable to thin films which have been frequently employed due to their simplicity.

Monitoring absorbance in an electrochemical experiment introduces wavelength selectivity to allow the separation of poorly resolved or unresolved electrochemical signals. Also, absorbance spectroelectrochemistry can be utilized to acquire kinetic data for irreversible electrode reactions that can not be obtained through electrochemical methods.[10]

There are different absorbance geometries which can be used to perform spectroelectrochemical measurements on thin films. Two of the possible geometries and their corresponding relative sensitivities are shown in Figure 1.1.

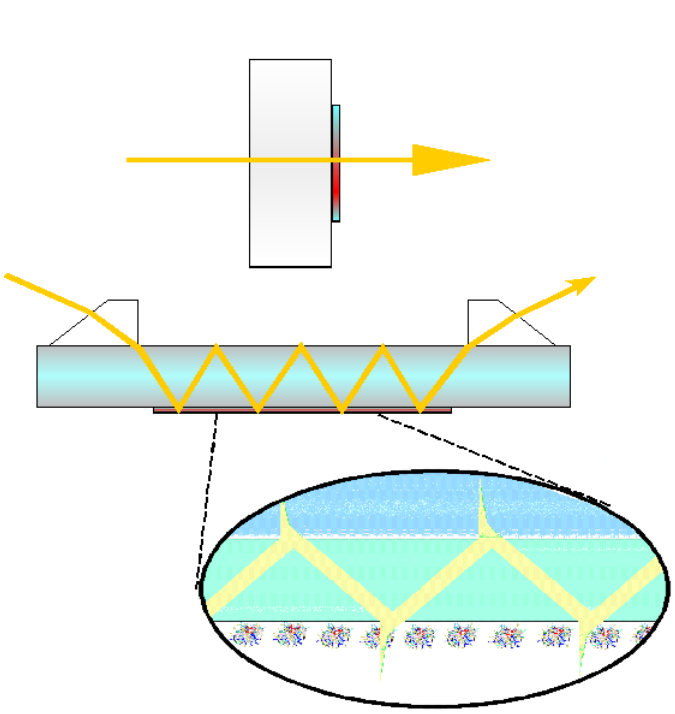

Figure 1.1 Possible absorbance geometries that can be applied for spectroelectrochemical detection of thin films and their relative sensitivities.

A major disadvantage of a transmission absorbance geometry is its low sensitivity since the pathlength is short for a thin film sample. In addition, the absorbance spectra of thin films acquired in transmission geometries are often complicated with the presence of interference fringes.[11] For experiments where the surface coverage and molar absorptivity of a thin film is high enough to measure an adequate absorbance, the low sensitivity of transmission geometry may not be a problem. But in the fields where higher sensitivity is required such as protein electrochemistry, a transmission geometry may not be adequate. In this case, using a multiple pass geometry such as in attenuated total reflectance (ATR) spectroscopy can be a better option since the pathlength of light will be larger and therefore sensitivity will be relatively higher. Multiple internal reflection spectroscopy in a planar waveguide is used to increase absorbance sensitivity for molecules at or near transparent electrode surfaces and this technique is emphasized in this project.

The first spectroscopic planar waveguide experiments, performed in the late 1950's,[12] were based on attenuating an internally reflected beam of light at the surface of a prism; later experiments were performed using a planar crystal. Harrick used this approach to spectroscopically measure chemical species in very close proximity (i.e. a few hundred nanometers) of the surface of the waveguiding structure and several researchers followed in the field of planar waveguide spectroscopy afterwards.[13, 14]

The first combination of electroactive coatings with ATR spectroscopy was done using a glass internal reflection element (IRE) coated with a thin, conductive, transparent electrode (tin-oxide) to study the electron transfer kinetics of *o*-tolidine.[15, 16] In those

studies, changes in the surface coverage of oxidized product as a function of time by application of an anodic potential step were monitored spectroscopically.

The first application of optical waveguides to electrochemistry was reported by Itoh and Fujishima[17] in 1988. They used a potassium ion-exchange (PIE) waveguide coated with a thin layer of conductive tin-oxide (SnO_2) to study the electrochemical reduction of methylene blue (MB). Using attenuation of the guided light due to adsorbed MB, 8 μm thick, gradient-index and four-mode waveguide, they achieved an increased sensitivity relative to a transmission experiment taken with a spectrophotometer by a factor of ~20 - 40.[17] Dunphy and coworkers[18] employed an alternate strategy in which a thin, low-refractive index buffer layer (SiO_2) was placed between the waveguiding layer and the indium tin oxide (ITO) film to create a multilayer stacked structure. They used a step-index guide which was inherently more sensitive than gradient-index design.[18] They also claimed that the ITO, because of its high refractive index, shifts the mode distribution toward the superstrate, increasing the field strength at the ITO/superstrate interface and therefore increasing the sensitivity.[18]

A spectroelectrochemical waveguide sensor for chlorine was developed by Piraud and coworkers.[19] The absorbance of a lutetium biphthalocyanine ($Lu(PC)_2$) film, deposited over an ITO layer, coated onto a PIE waveguide, responded to chlorine which oxidized the film. The sensor could be regenerated by applying a suitable cathodic potential to the ITO layer.

A series of publications, by Heineman and coworkers, outline the design, characterization, and applicability of an ATR spectroelectrochemical sensor format. The

technique employs chemically selective ion-exchange films, such as polyelectrolyte-SiO_2 sol-gel composites[20-25] and polymer blends,[26-28] deposited on glass slide IREs coated with ITO (thickness ~1 mm).[2, 20-23, 26-29] These extensive studies clearly illustrate the advantages of spectroelectrochemical ATR techniques.

1.2 Electron Transfer Theories

Electron transfer (ET) reactions have a central position in chemistry and biochemistry. The key steps in photosynthesis and metabolism, as well as many simple chemical reactions, involve ET reactions.[30-33]

Since the early work of Marcus[34-39], the theory of electrochemical electron transfer has been greatly expanded to outer- and inner-sphere electron transfers,[40, 41]the application of quantum theory, consideration of the role of electrode material and double layer effects (for heterogeneous transfers),[42, 43] the nature of the donor and acceptor species (for homogeneous transfers), and the role of the solvent dynamics.[44-48]

Strategies for studying ET reactions can be divided into two types: homogeneous ET, where the ET occurs between two species in solution, or heterogeneous ET, where a single redox species undergoes ET at an electrode.[49]

It is also useful to distinguish between inner sphere and outer-sphere electron transfer reactions at electrodes. The term “outer-sphere” denotes a reaction between two species in which electron transfer occurs from one primary bond system to another.[50, 51] In an outer-sphere electrode reaction, the reactant and product do not interact with the electrode surface, and they are generally at a distance of at least a solvent layer from the

electrode.[50, 51] Heterogeneous reduction of $Ru(NH_3)_6^{3+}$ at the Au electrode is an example since the reactant at the electrode surface is essentially the same as in the bulk.[51]

In contrast, "inner-sphere" reactions occur in an activated complex (and ions that share a ligand) where electron transfer takes place within a primary bond system.[50, 51] In an inner-sphere electrode reaction, strong interactions of reactant or product with the electrode such as specific adsorption of species involved in the reaction to the electrode surface are observed.[51]

Due to practical convenience, a great deal of experimental work has been devoted to studying homogeneous electron transfer.[52] The field of heterogeneous electron transfer has been relatively neglected as a result. There have been more efforts focused on heterogeneous electron transfer in recent years.[52-55] Knowledge of electron transfer between adsorbed molecules and a metal electrode was greatly advanced by introducing redox molecules into self-assembled monolayers (SAMs).[56]

In this research, our focus is on electroactive monolayers and thicker films on conductive substrates which are frequently called chemically modified electrodes. A number of reviews discussing the preparation, characterization and electrochemical behavior of modified electrodes are available in the literature.[51, 57-60] Organic films on solid substrates have been the focus of considerable research effort since rationally designed interfacial structures could potentially play important roles in wetting, adhesion, biocompatibility, nonlinear optics, catalysis, and numerous other applications such as fuel cells, batteries, electronic-organic devices and display technologies.[51, 61]

Many theories of kinetics have been constructed to illuminate the factors controlling reaction rates and to describe how molecular structure and environment affect the electron-transfer process from major contributions by Marcus. In here, Marcus electron transfer theory and others that are relevant for this research will be presented briefly.

1.2.1 Marcus Theory of Electron Transfer

Marcus theory explains the rates of electron transfer reactions – the rate at which an electron can be transfered from a donor to an acceptor by introducing reorganization energy and reaction coordinate diagram where the Gibbs' Free Energy and thermodynamic transition state are typically portrayed.[34] It was originally formulated to address outer sphere electron transfer reactions, in which the two chemical species aren't directly bonded to each other, but it was also extended to inner sphere electron transfer reactions, in which the two chemical species are attached by a chemical bridge, by Noel S. Hush (known as Marcus-Hush theory). Besides the inner and outer-sphere applications, this theory has also been extended to address heterogeneous electron transfer.[52] Marcus received the Nobel Prize in Chemistry in 1992 for his theory. A brief summary of this theory will be given here but comprehensive reviews are available in the literature.[34, 62-64]

In Marcus theory, the rate constant k for intramolecular electron transfer is given by;[51]

$$k_s = K_{P,O}\nu_n\kappa_{el}\exp(-\Delta G_f^{\ddagger}/RT) \qquad (1.1)$$

where $\Delta G_f^{\ddagger}$ is the activation energy for reduction of O; $K_{P,O}$ is a precursor equilibrium constant which is related to ratio of reactant concentration at the electrode (precursor state) to bulk concentration; ν_n is the nuclear frequency factor which is associated with bond vibrations and solvent motion; and κ_{el} is the electronic transmission coefficient which is related to the probability of the electron tunneling.[51] Equation 1.1 can be used both for a heterogeneous reduction at an electrode or a homogeneous ET.

A description of electron transfer may be presented by using a reaction coordinate based on the potential energy surfaces of the reactant and product. Figure 1.2 illustrates the free energy change during a reaction. This description is derived from the semi-classical treatment of electron transfer by Marcus and later elaborated by Hush and Sutin.[37, 63, 65-67] Electron transfer (Figure 1.2) may be defined as the crossing from the well of the reactant potential energy surface to the well of the product potential energy surface (O is the oxidant and R is the reductant). Changes in nuclear coordinates are due to vibrational and rotational motion in O and R, and fluctuations in the position and orientation of the solvent molecules.[51] To plot this, two general assumptions are made: i) reactant, O, is centered at some fixed position with respect to the electrode (or for a homogeneous reaction, O and R are at a fixed distance from each other) and ii) the standard free energies of O and R (G_O^0 and G_R^0) depend on the reaction coordinate, q.[51] This diagram applies either to a heterogeneous reaction in which O and R react at an electrode or a homogeneous reaction in which O and R react with each other such as O + R' → R + O'. [51] $\Delta G_f^{\ddagger}$ is the activation energy for reduction of O, ΔG^0 is either the standard free energy of the reaction for homogeneous ET or $F(E-E^0)$ for heterogeneous

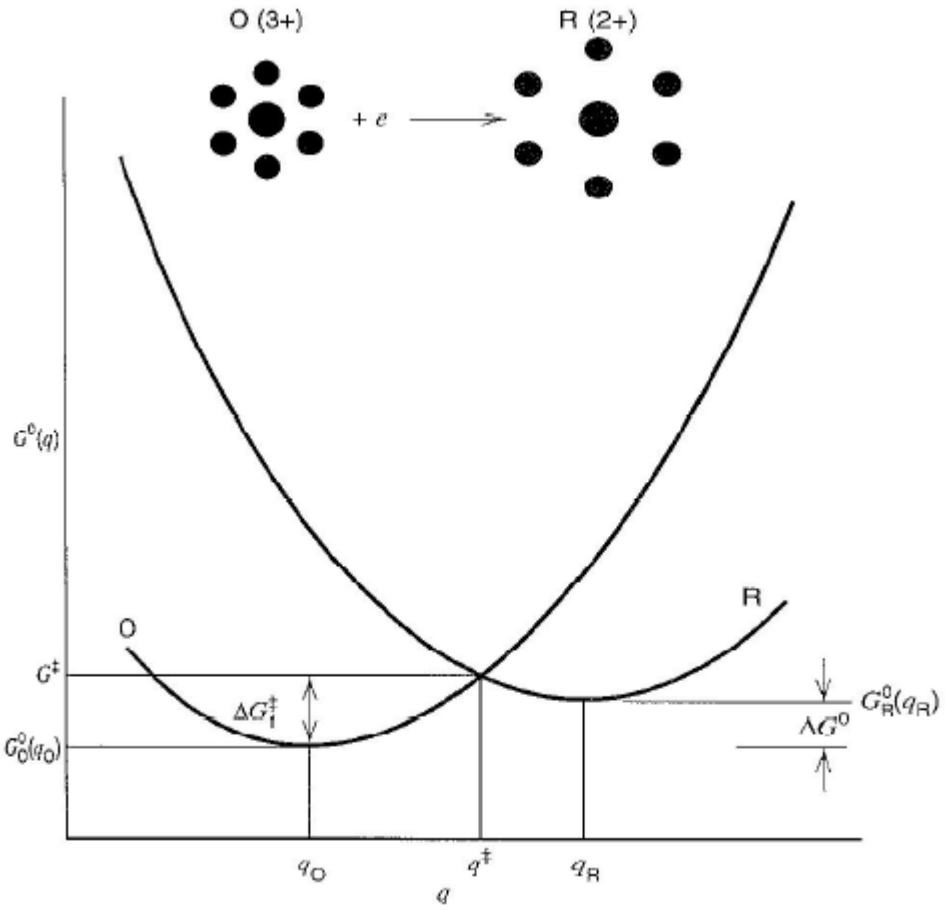

Figure 1.2 Standard free energy, G^0, as a function of reaction coordinate, q, for an ET reaction, such as $O^{3+} + e^- \rightarrow R^{2+}$. The picture at the top is a general representation of structural changes that might accompany electron transfer.[51]

ET where F is the Faraday constant, and E and E^0 are potential and standard potential of the reaction, respectively. q_O and q_R are the values of the coordinate for the equilibrium atomic configurations in O and R. Molecules shown at the top of the diagram represent stable configurations of the reactant and product and provide a view of the change in nuclear configuration upon reduction.[51] In the figure, the changes in spacing of the six surrounding dots could represent change in bond lengths within the species and/or the restructuring of the surrounding solvent.[51]

The transition state is the position where O and R have the same configuration, $q^{\ddagger}$, where electron transfer only occurs according to Franck-Condon principle. This principle states that nuclear momenta and positions do not change on the time scale of electronic transitions therefore reactant and product share a common nuclear configuration at the moment of transfer.[51]

The free energy of activation for reduction of O can be written for homogeneous reactions by[51];

$$\Delta G_f^{\ddagger} = \lambda/4\ (1 + (\Delta G^0/\lambda))^2 \qquad (1.2)$$

Or for an electrode reaction;

$$\Delta G_f^{\ddagger} = \lambda/4\ (1 + (F(E - E^0)/\lambda))^2 \qquad (1.3)$$

Here, the term λ is the reorganization energy which is the energy required to structurally reorganize the nuclear geometry of the reactants and surrounding solvent molecules upon electron transfer and reflects nuclear configuration displacements from the reactant to the product state. This parameter is comprised of vibrational (λ_i for the inner-sphere barrier) and solvational (λ_o for the outer sphere barrier) components.[51, 67]

The inner-sphere reorganization energy (λ_i) is the free energy change associated with the nuclear bond length changes within the reactant molecules before and after the electron transfer.[51, 67] The outer-sphere reorganization energy (λ_o) is the free energy change associated with the polarization of the surrounding solvent molecules prior to electron transfer. λ_o depends on dielectric constants, separation of the redox sites and shape of the reactant molecules.[67] Figure 1.3 represents inner and outer-sphere reorganization change upon electrochemical reaction[68].

One of the most important predictions of the Marcus theory of electron transfer is that as the driving force of the electron transfer reaction increases, the electron transfer rate will initially increase, reach a maximum, and then decrease in the region where the driving force is larger than the reorganization energy ($-\Delta G^0 > \lambda$).[34, 63] This strongly exergonic regime is generally referred to as the Marcus inverted regime[67]. Figure 1.4 (using $\Delta E = E - E^0$ in place of $-\Delta G^0$) depicts three regions predicted by Marcus Theory:

(a and b) a "normal regime" for small driving forces ($\Delta E << \lambda$ or $\Delta E < \lambda$)

(c) an "activationless" point ($\Delta E = \lambda$)

(d) an "inverted regime" for strongly exergonic reactions ($\Delta E > \lambda$)

In Figure 1.4, the parabolic shape of the curve implies that the rate constant decreases as the driving force ($-\Delta G^0$ or ΔE) increases beyond the value at which it is equal to λ. Blue and black parabolas on the left in Figure 1.4 represent the reactant and product, respectively.[68] The red and green bars represent the ΔE and λ, respectively.[68]

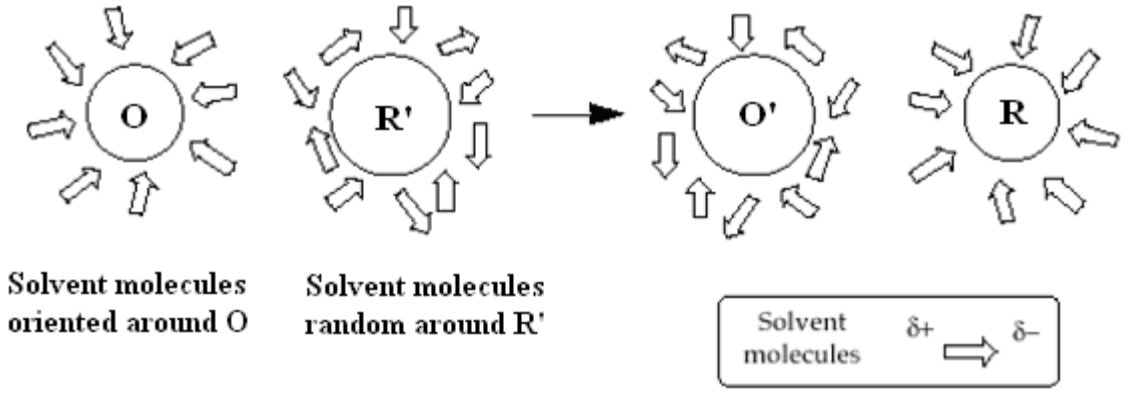

Figure 1.3 Visualization of the inner (depicted as a size change) and outer (depicted as the solvent reorganization) changes accompanying reaction.[68]

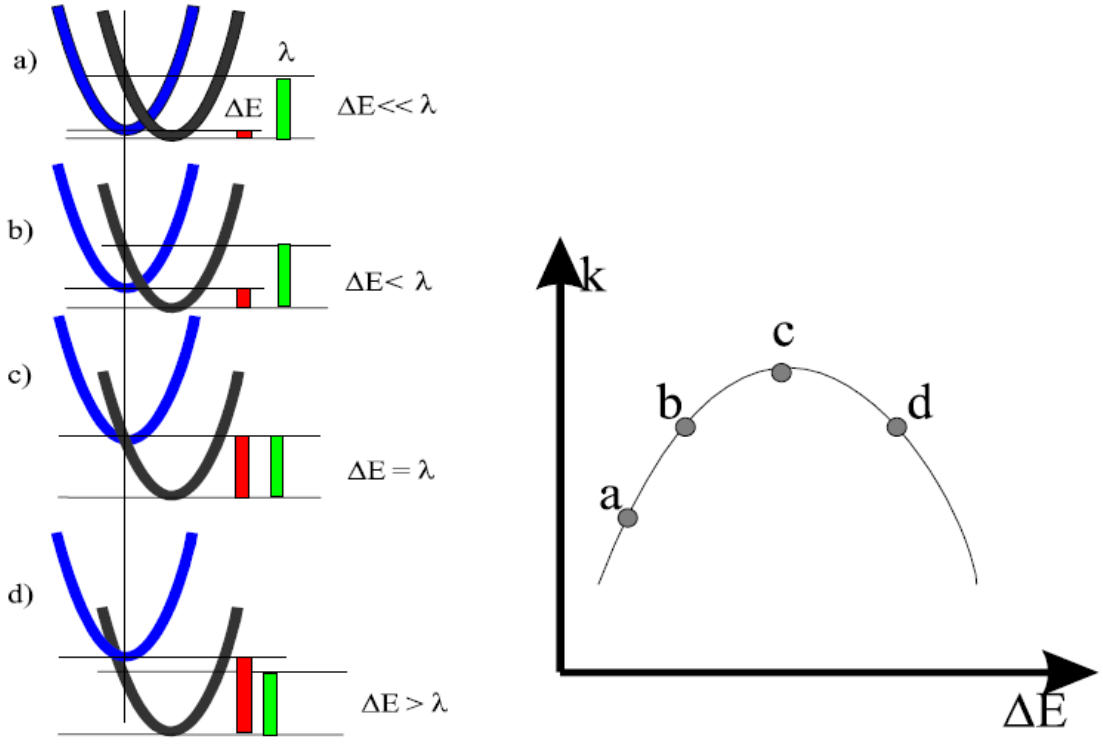

Figure 1.4 Marcus normal and inverted regions for charge transfer accompanied by reaction coordinates of reactant and product. The plot on the right shows rate constant as a function of ΔE of the reaction. Each point on the bell-shape parabola is represented on the left as reaction coordinates of the reactant and product in case of the following situations; a) $\Delta E << \lambda$, b) $\Delta E < \lambda$, c) $\Delta E = \lambda$, and d) $\Delta E > \lambda$.[68]

Marcus theory predicts that the rate of electron transfer is dependent exponentially on the distance between the redox center of the molecule (e.g. a metalloprotein) and the electrode surface.[69, 70] ET is usually considered as tunneling of the electron between states in the electrode and those in the reactant. Electron tunneling typically follows this expression:[71]

$$\text{Probability of tunneling} = C\exp(-\beta x) \qquad (1.4)$$

where C is a proportionality term, x is the distance over which tunneling occurs, and β is the factor that depends on the energy barrier height (work function of the electrode) and the nature of the medium.

Equation 1.4 can be written in terms of the effect of electron tunneling on the ET rate constant;[71]

$$k^0(x) = k^0(x = 0)\exp(-\beta x) \qquad (1.5)$$

Two examples of electron tunneling studies in which β is determined are : a) a blocking film on the electrode surface and electroactive molecules in solution, and b) an electroactive group tethered onto a self-assembled monolayer (SAM) of alkane thiols or oxide films attached to the electrode.[71] For the dissolved species such as in a), the rate constant reflects heterogeneous ET with units of cm/s and the rate is mass-transfer limited. However, for tethered electroactive species such as in b), the rate constant has a first-order reaction unit, s^{-1}.[71] Rate constants can be determined by voltammetric methods (e.g. potential-step chronoamperometry), in which current follows a exponential decay;[71]

$$i(t) = kQ\exp(-kt) \qquad (1.6)$$

where Q = nFAΓ, n is the number of electrons, A is the electrode area and Γ is the surface coverage of electroactive centers (mol/cm^2).[71] Also the rate constant can be measured as a function of the length of the alkyl chain in the SAM, and slope of the plot of ln(k_s) vs x allows determination of β.[51]

1.2.2 Laviron's Kinetic Method for Adsorbed Species

The rate of ET for an adsorbed or tethered species is generally much greater than the rate of the same species in solution since the diffusional aspect of the electrochemistry is eliminated.[49, 72] In this case, an alternative method for extracting kinetic information is necessary because traditional kinetic analysis is unsatisfactory for immobilized electroactive species.[49] A model based on cyclic voltammetry (CV) and Butler-Volmer kinetics was developed by Laviron[73] to calculate the ET rate constant, k_s, where the oxidized and reduced species are strongly adsorbed to the electrode. General expressions for a voltammogram of a diffusionless system are formulated by Laviron and the electron transfer rate constant is simply determined from the separation between the cathodic and anodic peak potentials and scan rate.[73] In this model, complications from adsorbate-adsorbate interactions or heterogeneous dispersion are excluded.[73, 74] The dimensionless variable *m* is defined as:

$$m = RTk/Fn\nu \qquad (1.7)$$

where k_s is the rate constant for the electrochemical reaction in s^{-1} and ν is the scan rate in V/sec.[74] The transfer coefficient, α, is a measure of the symmetry of the energy barrier to electron transfer. For adsorbed species, the relationship is given between nΔE and 1/*m*

where α is assumed to be 0.5 and peak potential separations are changing from 18 to 204 mV.[73, 74] Using an experimentally determined value of nΔE , the value of *m*, and therefore k, can be determined. It is important to note that Laviron incorporated several important assumptions into his model:[49, 73] 1) both the oxidized and reduced forms of the electroactive species are inherently stable and are strongly adsorbed to the electrode; 2) the system under consideration is completely diffusionless, and therefore diffusional aspects of the molecules can be excluded from the mathematical expression; and 3) a Langmuir adsorption isotherm is obeyed.

1.2.3 AC Impedance Technique

Electrochemical impedance spectroscopy (EIS) (sometimes also called AC impedance) is a technique in which a sinusoidal potential modulation of a small magnitude (~ 5 mV) is applied at various frequencies to a electrochemical cell.[71] To obtain an impedance spectrum, the current amplitude and phase resulting from the modulated potential are measured at various frequencies. To interpret the impedance data and describe the electrochemical reaction kinetics, circuit-based representations of the electrochemical cell (which is called an equivalent circuit model) are used.

In an ac impedance measurement the applied potential, E(t) varies with time according to:[75]

$$E(t) = \Delta E \sin(2\pi ft) \qquad (1.8)$$

where ΔE is the amplitude of the potential modulation, f is the frequency, t is the time.

The measured current:[75]

$$i(t) = \Delta i \sin(2\pi ft + \varphi) \quad (1.9)$$

where Δi is the amplitude of the current and φ is the phase angle.

Figure 1.5 shows the sinusoidal potential modulation and alternating current response of an electrochemical system separated by a phase angle, φ.[71] In this figure, the applied voltage at any time is represented as letter *e* which equals E(t) in Equation 1.8. A rotating vector or a phasor diagram which represents the relationship between the alternating current and voltage signals at frequency ω (equal to $2\pi f$) are also shown in Figure 1.5 on the left. *e* and i can be expressed in phasor notation as E' and I' respectively as it is in the phasor (Figure 1.5).

The impedance Z is determined by the derivative of potential over current:

$$Z = dE/di = Z' - jZ'' \quad (1.10)$$

where Z' is the real component of the impedance and Z'' is the imaginary component of the impedance. Components along the abscissa are real while components along the ordinate are imaginary and therefore are multiplied by j (square root of -1).[71]

The absolute magnitude of impedance is given by:

$$[Z] = (Z'^2 + Z''^2)^{1/2} \quad (1.11)$$

and the phase shift can be calculated from:

$$\tan(\varphi) = (Z''/Z') \quad (1.12)$$

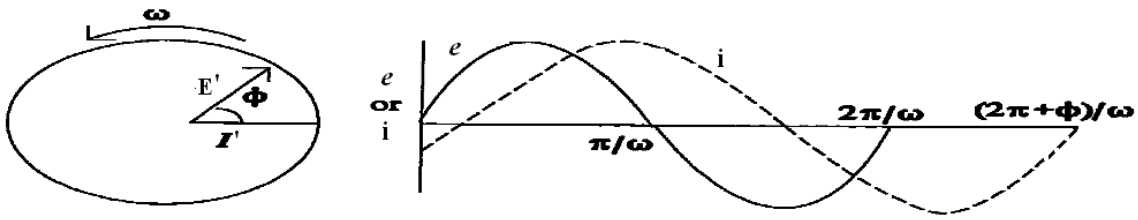

Figure 1.5 Phasor diagram for alternating current and voltage at frequency ω. Corresponding sinusoidal waves are shown on the right.

To describe the electrochemical behavior of an electrochemical cell, the impedance response should be acquired over a range of frequencies. There are basically three different formats which are commonly used to plot impedance data; i) Nyquist plot (also known as Cole-Cole plot or Complex plane plot), ii) Bode-magnitude plot, and iii) Bode-angle plot. Each one contains useful specific information for the chemical system that is under investigation. The imaginary part of impedance is plotted against real portion of impedance at different frequencies in a Nyquist plot. A typical Nyquist plot is shown in Figure 1.6 where the frequency is increasing from the right side of the plot to the left. From the interceptions of this plot with real axis, solution resistance and polarization resistance (charge transfer resistance)[76] can be determined.[75] The absolute value of impedance calculated from Equation 1.11 is plotted as a function of frequency in a Bode-magnitude plot and phase angle is plotted as a function of frequency in a Bode-angle plot. The Bode plots have more effective extrapolation of data in the high frequency region but will not be discussed here. Detailed explanations about impedance methods can be found in the literature[71, 77-79]

Our interest is to better understand heterogeneous charge transfer kinetics of surface confined redox active species and ac impedance techniques are powerful methods for this type of investigation. Studying ET kinetics of electroactive monolayers without electroactive species present in solution (e.g. alkylthiol modified electrodes with tethered electroactive groups) using impedance techniques is useful and has been described in the literature.[80-82]

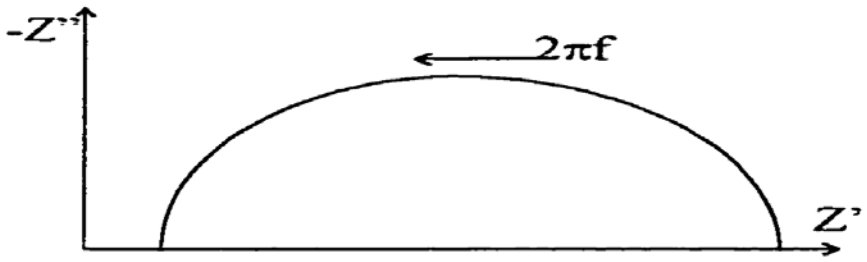

Figure 1.6 A typical Nyquist plot. Arrow indicates increase in frequency.

Ac impedance theory for the heterogeneous electron transfer kinetics of surface-confined redox centers has been developed by Laviron.[77] Figure 1.7 illustrates the circuit appropriate for modeling a redox-active monolayer on an electrode surface[73, 77, 80, 82, 83] where C_{dl} is the double-layer capacitance, C_{ads} is the adsorption capacitance, R_{ct} is the charge-transfer resistance and R_s is the solution resistance. In this case, the following relationships between the circuit elements and the parameters characterize the redox-active monolayer-coated electrode:[71, 82]

$$C_{ads} = (F^2 A\Gamma)/(4RT) \quad (1.13)$$

$$R_{ct} = (2RT)/(F^2 A\Gamma k) \quad (1.14)$$

where RT is the product of the gas constant, R, and absolute temperature, T. Γ_t and F represent the total surface coverage of the adsorbed layer and Faraday's constant (96485 C/mol e^-), respectively.

From these expressions, the rate constant can be obtained by:[71, 82]

$$k_s = 1/(2R_{ct}C_{ads}) \quad (1.15)$$

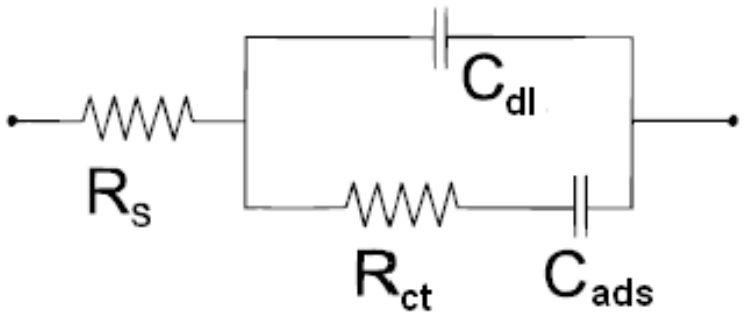

Figure 1.7 Equivalent circuit for an electrode coated with a redox-active monolayer film for impedance measurements.

1.3 Total Internal Reflection Phenomenon

The principles of total internal reflection have been described in great detail elsewhere[12, 13, 84-87] and a general overview of relevant topics will be provided here by using two basic concepts: 1) Total Internal Reflection and Snell's Law, 2) Evanescent Field Spectroscopy.

1.3.1 Total Internal Reflection and Snell's Law

When a light beam is incident on the interface between two media with refractive indices η_1 and η_2, light is transmitted through the interface (refraction) with an angle dependent on the refractive indices of the two media and the angle of incidence (the refractive index being defined as the speed of light in a vacuum versus the speed of light in the particular medium $(\eta = c / v)$). Snell's Law of Refraction relates the refractive indices to the angle of light propagation relative to the normal. If the incident medium has the larger refractive index, angle increases as light passes into the rarer medium (Figure 1.8a).

For an incident beam traveling from a higher index medium (η_2) to a lower index medium (η_1), there exists an angle of incidence which causes the transmitted beam to be refracted parallel to the interface between the two media (e.g. green light beam in Fig. 1.8b, $\theta_2 = 90^0$). Under these conditions, the interface acts as a perfect mirror and the incident beam is completely reflected back into the higher index medium. Incidence at this *critical* angle, or at any angle greater than the *critical* angle, results in complete

reflection of the incident beam (e.g. purple light beam in Fig. 1.8b); this phenomenon is known as total internal reflection (TIR).

If multiple reflections occur along the length of an IRE, it functions as a waveguide in which the totally internally reflected beam propagates within the IRE until it is outcoupled, absorbed, scattered, or otherwise extinguished.

a)

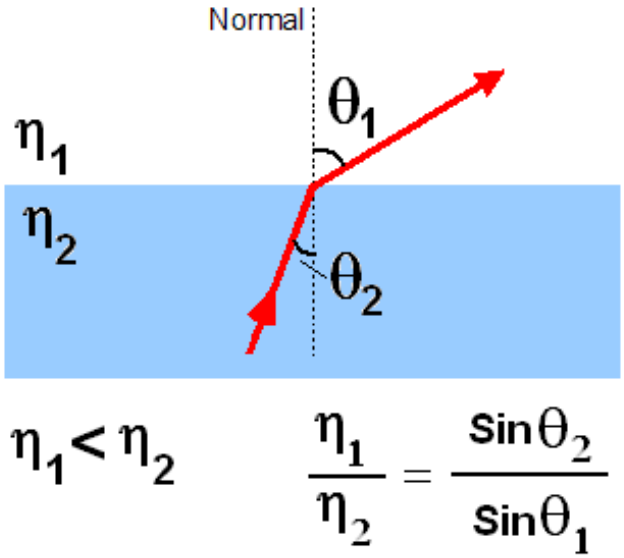

b)

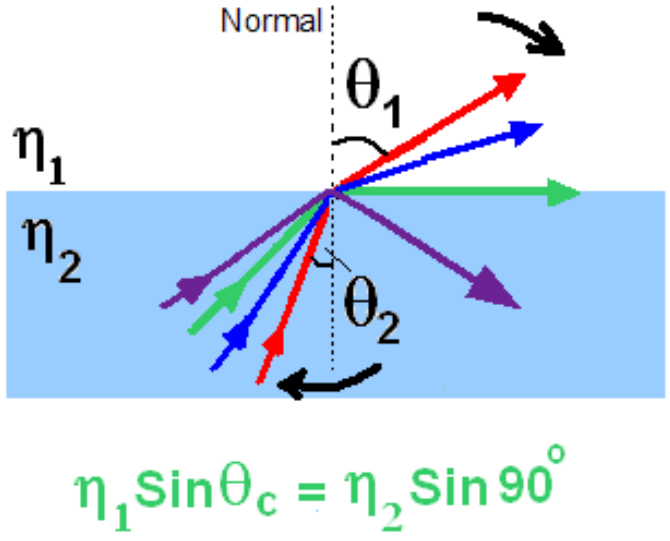

Figure 1.8 a) Snell's Law and refraction of light between two media of different refractive indices are shown. b) A schematic representation of total internal reflection is shown. The angle of incidence is increasing from the red light beam to the purple light beam. The green light beam shows the threshold condition for total internal reflection. The purple light beam represents total internal reflection. θ_c in the equation represents incident angle which is called '*critical* angle' in the case of green light beam.

1.3.2 Evanescent Field Spectroscopy

At an interface at which TIR occurs, an extension of electromagnetic radiation, known as an evanescent field, penetrates into the rarer medium perpendicular to the plane of the interface. The evanescent field decays exponentially with distance and therefore TIR spectroscopy selectively probes only the region adjacent to the IRE (Figure 1.9). Typical penetration depths in the visible region of the spectrum are from 100-500 nm, and are dependent on parameters such as the wavelength of light, the refractive indices of the two media, the IRE material, and the internal reflection angle, θ.[11]

Evanescent field energy can be absorbed by molecules within the evanescent volume which will cause attenuation of the propagating beam after each reflection. Attenuated total reflectance (ATR) spectroscopy is based on this phenomenon. The surface selective nature of internal reflection methods is ideally suited for the study of thin films on an IRE surface, since the energy of the evanescent field is localized within the film.[88]

The absorption of evanescent energy for a molecule, in the superstrate adjacent to an IRE, per internal reflection, can be defined as:[89]

$$\frac{A_b}{N} = \varepsilon_b c_b \left(\frac{I_e}{I_i} \right) d_p \qquad (1.16)$$

where A represents the absorbance, (I_e/I_i) represents the interfacial transmitted intensity per unit incident beam intensity, d_p is penetration depth, N is the number of internal reflections, and ε and C are the molar absorptivity and concentration of the molecule,

respectively. The subscript *b* denotes the bulk solution in which a homogeneous distribution of the molecule throughout the evanescent volume is assumed.[89]

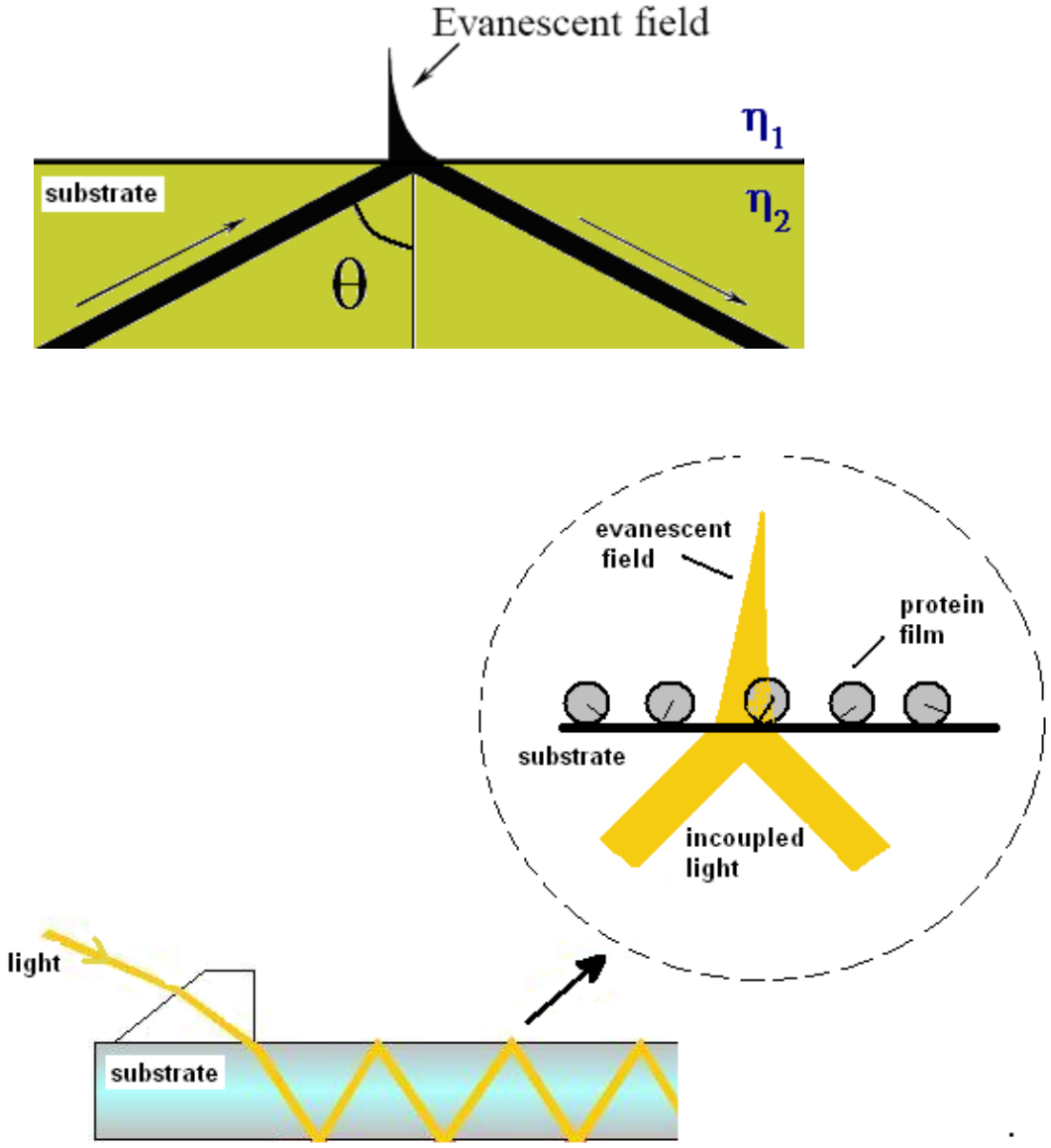

Figure 1.9 Schematic diagrams illustrating the evanescent field and its use for surface spectroscopy and chemical sensing of thin films (protein film in this case). The evanescent field induced at the point of reflection extends into the optically rarer medium to a distance dependent on the refractive index contrast between the two media, the wavelength of light, and θ.

1.4 Potential Modulated Spectroelectrochemical Techniques to Study Charge Transfer Kinetics

Determining rates of electron transfer through molecular films is central to a wide range of chemical, physical, and biological processes and consequently has important applications in sensors and organic electronic devices.[30-33, 90] An electroreflectance (ER) technique that combines spectroscopy and electrochemical impedance methods has been developed by Niki and Sagara,[91-93] and has been used extensively to study electron transfer processes and rates for molecular adlayers at reflective electrode surfaces, such as alkanethiol-modified gold.

Many ER studies reported to date have used external reflection and surface plasmon resonance geometries to monitor changes in film optical properties. Alkanethiolated gold has been used to study optical-switching and electron transfer kinetics of porphyrins[94, 95] and adsorbed protein films, such as azurin[96] and cytochrome *c*,[70, 97-100] using ER spectroelectrochemistry. Also, UV-VIS ER spectroscopy has been applied to small molecular adsorbates such as hemin and Nile blue to study electron transfer rates on different electrode surfaces such as glassy carbon electrode and highly oriented pyrolytic graphite.[92, 93, 101]

Fujishima and coworkers[102-105] utilized this approach in a transmission geometry to differentiate kinetically heterogeneous processes in polypyrrole films on SnO_2 electrodes. In these works, the measured optical response is a change in transmittance rather than reflectance. Several other examples of transmission spectroelectrochemistry using the ER approach can be found in the literature.[106-108]

Doherty et al.[109] reported the first implementation of ER in multiple reflection ATR spectroscopy and its application to study electro-optical transition kinetics in molecular adlayers. In this work, the theoretical framework developed by Niki and Sagara[91-93] was used to extract an apparent heterogeneous charge transfer rate, or rate of spectroelectrochemical switching (k_s), for thin films of poly(3,4 ethylenedioxythiophene) (PEDOT) and poly(3,4-ethylenedioxythiophene methanol) (PEDTM).

An overview of theoretical aspects of ER spectroscopy is presented in the following section.

1.4.1 The Basic Principles of ER Spectroscopy

In ER spectroscopy, an ac potential modulation is applied to the electrode, while the change in light intensity reflected at (or transmitted through) the electrode surface is monitored simultaneously. Changes in the reflectivity represent changes in the optical constants of the film which can be caused by changes in oxidation state, charge density, and/or molecular conformation. Optical changes in the film as a function of the modulation frequency and amplitude can provide kinetic information about rates of electron transfer and the rate at which the optical properties of the molecular film can be "switched", or cycled, between the reduced and oxidized forms (electro-optical switching rate).

The following expressions represent the relationship between the applied modulated potential and the electroreflectance signal in ER spectroscopy.

$$E = E_{dc} + E_{ac} \sin \omega t \tag{1.17a}$$

$$\mathcal{R} = \mathcal{R}_{dc} + \mathcal{R}_{ac} \sin(\omega t - \theta) \tag{1.17b}$$

In these expressions, E represents the overall potential applied to the electrode, E_{dc} is the time-average potential, and E_{ac} is the amplitude of the potential modulation. Analogously, R represents the overall reflectance of the probe beam, R_{dc} is the time-average reflectance, R_{ac} is the amplitude of the modulated reflectance induced by E_{ac}, ω is the modulation frequency in radians, θ is the phase angle between E_{ac} and R_{ac}, and t is time.

1.4.2 Electron Transfer Rate from ER Spectroscopy

Traditional electrochemical techniques used to evaluate the electrode reaction rate constant, k_s (the turnover rate constant), of a species adsorbed on an electrode include dc cyclic voltammetry, ac impedance spectroscopy and ac voltammetry. These techniques have been discussed in great detail in the literature.[73, 77, 110, 111] Briefly, when the dc voltammetric peak potential is measured as a function of scan rate without the influence of ohmic drop, the formula derived by Laviron et al.[73, 112] is applicable to evaluate k_s.[92] Based on the formula, the electron transfer rate can be calculated from the anodic and cathodic peak separation at a known scan rate.[73, 112] However, determination of k_s by traditional electrochemical techniques is difficult when there is large double-layer

capacitance, large solution resistance, and/or irreversibly adsorbed redox species on electrode surface.

In UV-VIS ER spectroscopy, the ac reflectance of the electrode surface is measured instead of the ac current response.[92, 93, 113] The ac reflectance response (ER response) measured in the vicinity of the formal potential E^0 of an adsorbed redox-active species originates from its redox reaction.[114] Therefore, a change in the fractions of oxidized and reduced forms of the species present at the electrode surface is expected to produce a corresponding change in the ER response, assuming the molar absorptivities of the oxidized and reduced forms are different.[92] It is important to note that the amplitude of the ac reflectance response is proportional to the amount of the redox species interconverted between oxidized and reduced forms in response to the potential modulation.[93]

Theoretical derivations of electroreflectance parameters and derivation of expressions for reflectivity have been well-explained in detail elsewhere.[89] Here, extraction of kinetic information from ER response will be described briefly.

The equivalent circuit which represents the electrochemical impedance response of an electrochemical cell consisting of an ITO electrode, an electroactive adlayer, and the electrolyte, shown in Figure 1.7 (in Section 1.2.3) is redesigned here as Figure 1.10 to include the necessary parameters to explain the processes that occur in this system.[89] Faradaic electron transfer processes between the adlayer and the electrode require additional capacitance (C_a) and charge transfer resistance (R_{ct}) terms to adequately simulate the overall electrochemical response.[115, 116]

In Figure 1.10, an ac voltage (E_{ac}) is applied across the entire cell. A fraction of this voltage is dropped across the resistance of the solution (R_s), leaving $E_{ac}{}^{F}$ across the Faradic component of the circuit (C_a and R_{ct}). The current flow in the Faradic portion of the cell is related to the amount of redox activity in the adlayer film. Note that $E_{ac}{}^{F}$ is also applied across the double-layer capacitance (C_{dl}). The total current flowing through the cell is denoted i_{ac}; it passes directly through R_s and is then divided across the Faradaic and double-layer capacitive portions of the cell, denoted $i_{ac}{}^{F}$ and $i_{ac}{}^{dl}$, respectively. Note that the i_{ac} can be further defined as the sum of $i_{ac}{}^{F}$ and $i_{ac}{}^{dl}$, according to Kirchhoff's Laws.[89]

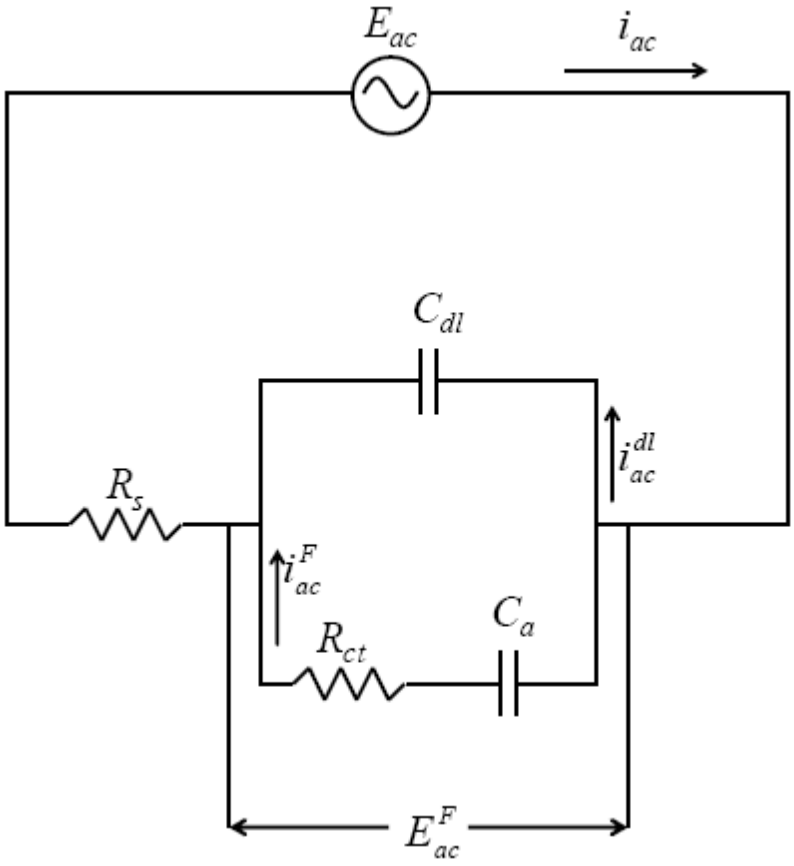

Figure 1.10 The equivalent circuit diagram representing the electrochemical cell consisting of an ITO electrode, an electroactive adlayer, and the electrolyte solution. E_{ac} represents applied ac potential to the circuit. R_s and C_{dl} represent the solution resistance and double layer capacitance of the cell. R_{ct} and C_a comprise the Faradaic portion of the circuit, representing the charge transfer resistance and the adlayer capacitance, respectively. $E_{ac}{}^{F}$ is the potential applied across the Faradaic portion of the cell. The total cell current, i_{ac}, is divided across the Faradaic cell ($i_{ac}{}^{F}$) and the C_{dl} ($i_{ac}{}^{dl}$).[89]

Equations derived by Laviron[77, 111] enable the extraction of the electrode rate constant, k_S, from experimental values of R_{ct} and C_a by Equations 1.13 and 1.14 in Section 1.2.3. Combining Equations 1.13 and 1.14 gives an expression for k_s (recall Equation 1.15).

The optical switching rate, k_S, can also be determined graphically. A plot of real Re(R_{ac}) versus imaginary Im(R_{ac}) components of the reflectance signal at varying frequencies of E_{ac} results in a hemispherical plot, or complex plane plot (analogous to a Cole-Cole plot in impedance spectroscopy). It has been shown by Niki et al.[92] that the complex plane crosses the origin, where $R_e(R_{ac}) = 0$, at one specific frequency (ω) which is called the optical switching frequency. The optical switching frequency can be used to determine k_S. After derivations of expressions for reflectivity and making some assumptions, an expression for k_S can be written as follows:[89]

$$\omega = \left(\frac{2k_s}{R_s C_{dl}} \right)^{1/2} \quad \text{or} \quad k_s = \frac{\omega^2}{2} R_s C_{dl} \tag{1.19}$$

Thus, k_S can be determined if R_s and C_{dl} (which can easily be measured using classical impedance techniques) for the electrode ensemble are known.

1.5 Overview of Experiments

The research described in this dissertation is focused on spectroelectrochemical characterization of electron transfer processes occurring at the electrode – electroactive

thin film interface. Using a novel form of electroreflectance spectroscopy, potential-modulated ATR, various thin films (a protein film, a conducting polymer film and a semiconductor nanoparticle film, etc.) have been evaluated to study charge transfer kinetics. In this research, the following points were investigated and achieved for *the first time* using this novel technique:

i) Determination and comparison of apparent electron transfer rate of Prussian blue on an ITO electrode obtained using this novel method and conventional cyclic voltammetry. (Chapter 2)

ii) The correlation between a distribution of molecular orientations and a distribution of apparent electron transfer rates in a redox-active protein film using s- and p-polarized light. (Chapter 3)

iii) Effects of a surface modifier and electrode surface treatments on charge transfer kinetics for conducting polymer films on ITO. This measurement is difficult to perform by conventional electrochemical methods due to polymer's high non-Faradaic background. (Chapter 4)

iv) Characterization of reversible electron injection into sub-monolayer coverages of surface-tethered semiconductor nanoparticles and estimation of energy band gaps. (Chapter 5)

2. POTENTIAL MODULATED ATTENUATED TOTAL REFLECTANCE SPECTROSCOPY OF PRUSSIAN BLUE ON INDIUM TIN OXIDE ELECTRODES

2.1 Introduction

Prussian blue (iron (III) hexacyanoferrate (II), PB) has been extensively used as a pigment in the formulation of paints, lacquers, and printing inks.[117] Prussian blue (PB) is a mixed valence compound with a cubic structure in the solid state, shown in Figure 2.1, with a lattice dimension of 10.16 Å, in which corner sites are occupied by alternating ferrous and ferric ions and cyano ligands lie along the edges.[118] The remaining charge is balanced either by potassium ions, as in so-called "soluble" PB ($KFe^{III}[Fe^{II}(CN)_6]$), or by ferric ions, as in "insoluble" PB ($Fe_4^{III}[Fe^{II}(CN)_6]_3$).[119] Both compounds are actually water-insoluble ($K_{sp} = 10^{-40}$) and the term "soluble" refers to the ease with which the potassium salt can be peptized and the ability of material to form an aqueous suspension.[119]

PB can be electrochemically deposited onto electrode surfaces.[120-133] The electrochemical properties of PB films have been well characterized in the literature.[118, 120-134] PB-modified electrodes have found applications in biosensing[128] and electrocatalysis.[129] The molar absorptivity of PB in the visible spectrum varies with changes in its oxidation state.[127] Based in part on these properties, PB has been chosen as a model system in this work to assess the utility of PM-ATR spectroscopy for studies of

charge transfer kinetics in thin molecular films. This data is presented in Section 2.3, after a brief survey of electrochemical and spectroscopic properties of PB.

2.1.1 Electrochemical Studies of Prussian Blue

Since Neff[130] reported for the first time the electrochemical behavior and the successful deposition of a thin layer of Prussian blue on a platinum foil, the electrochemistry of PB has been fully investigated by various researchers.[118, 120-134]

A colorless compound known as Everitt's Salt (ES) or Prussian white (PW) is obtained by reduction of PB, while the yellow form, Prussian yellow (PY) or Berlin green (BG) is obtained when PB is oxidized.[135] A representative cyclic voltammogram is shown in Figure 2.2.[136] Cyclic voltammetry experiments showed that the oxidation and reduction of PB/PW couple was more reversible than that of the PB/PY couple.[137] Thus studies described in this thesis focused exclusively on the PB/PW redox couple.

According to Itaya et al.[127], reduction of PB is described by

$$\underset{\text{(PB)}}{Fe_4^{III}[Fe^{II}(CN)_6]_3} + 4K^+ + 4e^- \leftrightarrows \underset{\text{(PW)}}{K_4Fe_4^{II}[Fe^{II}(CN)_6]_3}$$

As mentioned above, PB is reported to exist in two forms, insoluble PB and soluble PB.[119, 123] When the potential of a PB film is cycled several times in an electrolyte containing potassium, the lattice structure is converted to the soluble form.[119, 122] After this cycling process, the reactions above can be re-written as:[131, 133]

$$KFe^{III}[Fe^{II}(CN)_6] + K^+ + e^- \leftrightarrows K_2Fe^{II}[Fe^{II}(CN)_6]$$

(PB) (PW)

2.1.2 Spectroscopic Studies of PB

Spectroscopic characterization of Prussian blue films (under potential control) has been done by various groups by different methods such as UV-VIS absorption,[127, 132, 134, 137-139] Raman scattering,[137] colorimetry,[117] surface plasmon resonance,[140] infrared,[141] electrochemical impedance,[142] etc.

Absorption spectra of PB films have been measured on SnO_2[127, 138] and Au[143] (semitransparent) electrodes at various electrode potentials. At an electrode potential of 0.6 V, the spectrum was assigned to PB with a peak wavelength of 700 nm.[127] Changes in the absorption spectra of PB obtained at different electrode potentials are reversible which suggests the use of PB as a material for an electrooptical signal modulator.[138]

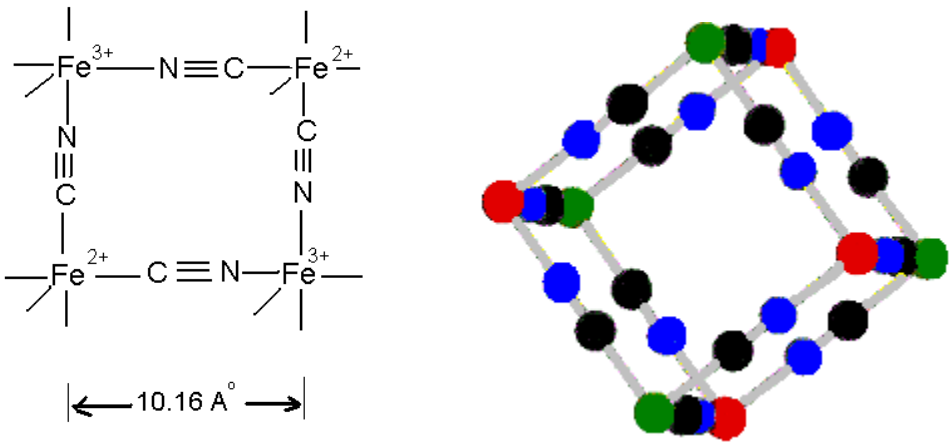

Figure 2.1 Crystal structure of Prussian blue. The figure on the right represents ferric ions (red), ferrous ions (green), carbon (black), nitrogen (blue).

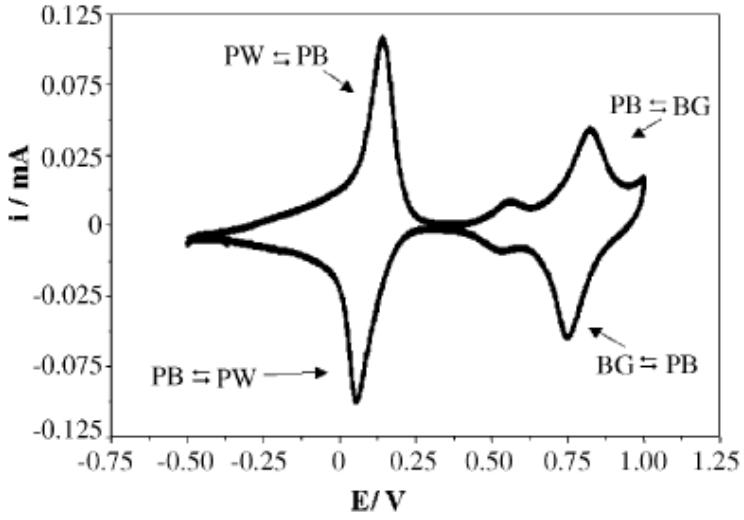

Figure 2.2 Cyclic voltammogram of a PB-modified gold electrode showing the oxidation and reduction peaks of Prussian blue.[136]

2.2 Experimental Methods

2.2.1 Cleaning of ITO Substrate

The ITO-coated planar electrodes used in these studies were obtained from Colorado Concept Coatings Limited, with a sheet resistance of ca. 13 Ω / cm.[2] They were cleaned by scrubbing with a 1% Alconox solution for 1 min and then sonicating for 15 min each in 1% Alconox, water, and ethanol, followed by low temperature air plasma cleaning (Harrick model PDC-3XG) for 15 min[144] at 30 W.

2.2.2 Formation of Prussian Blue Films

$FeCl_3$ (Aldrich), $K_3Fe(CN)_6$ (Mallinckrodt), KCl (Aldrich), and HCl (Mallinckrodt) were used for the synthesis of the PB film. Barnstead Nanopure (18 MΩ–cm) water was used for any required dilutions.

PB films were deposited galvanostatically using the method described by Garcia-Jareno and coworkers.[115] Briefly, the cleaned ITO electrode was immersed in a solution composed of 0.02 M $K_3Fe(CN)_6$, 0.02 M $FeCl_3$ and 0.01 M HCl and a controlled cathodic current of 40 μA/cm^2 was passed through the circuit, which contained a Ag/AgCl reference electrode (Bioanalytical Systems) and a Pt wire counter electrode. Unless otherwise stated, the deposition time for PB was 10 sec. After deposition, the cell was rinsed several times with electrolyte (1 M KCl adjusted to pH 4 with HCl). To obtain a stable electrochemical response from the film, the cell was then filled with electrolyte and the potential was scanned from -400 mV to +700 mV several times[115, 122, 145]

2.2.3 Cyclic Voltammetry

Cyclic voltammetry (CV) was carried out using a typical three-electrode cell in which the PB-coated ITO was used as the working electrode, with the reference and counter electrodes as described above. Two different cells were used: a standard teflon electrochemical cell (electrode area = 0.785 cm^2) and a spectroelectrochemical ATR cell (electrode area = 2.1 cm^2). All electrochemical measurements were performed on an EG&G Princeton Applied Research Model 263A potentiostat/galvanostat. Cyclic voltammograms were obtained at a scan rate of 100 mV/sec (except where noted) and a potential range of -400 to +700 mV.

2.2.4 Impedance Spectroscopy

Electrochemical impedance spectroscopy (EIS) was also carried out using the same three-electrode cell used in CV experiments, in which the PB-coated ITO was used as the working electrode. Impedance measurements were obtained with an EG&G Princeton Applied Research Model 1025 Frequency Response Detector operated with PowerSuite 2.00.5 software.

2.2.5 PM-ATR Theory

A complete description of PM-ATR is provided elsewhere[109] but here the principle of the method is described briefly. The theory used to interpret PM-ATR spectroscopy data is analogous to that used with electroreflectance (ER) spectroscopy performed in an external reflectance geometry,[91-93] described in Section 1.4.1. In PM-

ATR, changes in the electroreflectance signal, R_{ac}, are referenced to the frequency of the ac potential, E_{ac}, applied to the electrode. The ac potential is centered around E_{dc}, which is typically the formal reduction potential of the molecular film. The portions of R_{ac} that are in- and out-of-phase with the reference signal (X and Y, respectively) are monitored and used to determine R_{ac} ($=\sqrt{X^2 + Y^2}$) and the phase shift ($\theta = \tan^{-1}\left(Y/X\right)$) between R_{ac} and the applied ac potential.

At low modulation frequencies (relative to the rate of electron transfer of the adsorbed film), R_{ac} is mostly in phase with the reference signal. As the frequency is increased relative to the rate of electron transfer, θ increases as the out-of-phase portion of R_{ac} increases. From the optical switching frequency, where the in-phase portion of the signal becomes zero, the rate of electron transfer can be determined by equation 1.19 as described in Section 1.4.2.

2.2.6 PM-ATR Setup

A schematic diagram of the broadband ATR spectroelectrochemical apparatus and the ATR cell is presented in Figure 2.3.[146] Briefly, white light is directed through an optical fiber, prism-coupled into an ITO-coated glass IRE, totally internally reflected down the length of the substrate, and out-coupled via a second prism. The outcoupled light is detected using a dispersion grating and CCD camera. Absorbing molecules present within the evanescent volume near the ITO surface cause attenuation of the incident beam. Simultaneous acquisition of electrochemical information is facilitated through a counter electrode (CE), a Ag/AgCl reference electrode (RE), and the ITO layer,

which serves as a working electrode (WE).[146] To ensure homogeneous current density across the electrode area, the platinum wire (CE) was arranged parallel to the ITO surface, such that all areas of the ITO were approximately equidistant (~ 1 mm) from the Pt wire. The ITO electrode surface dimensions were 71.5 mm x 3 mm, with the ATR beam propagating along the long axis, at an internal reflection angle of 63^{o} to 64^{o}. Coupling prisms were positioned 40 mm apart, affording approximately 10 internal reflections along the length of the ITO electrode. This geometry is approximately 35-fold more sensitive than a transmission geometry.[147] Detailed ray-optics diagrams of prism coupling, and schematic illustrations of the ATR spectroelectrochemical cell can be found elsewhere.[89]

Figure 2.4 shows a schematic diagram of the PM-ATR electrical setup.[109] The electrochemical ATR apparatus has been described above. To drive the potential modulation at the ITO electrode, a function generator (FG) (Krohn-Hite Model 5200) was used to supply a 5 V peak-to-peak square wave external reference to the lock-in amplifier (LIA) (Stanford Research Systems Model SR830). The amplitude of the reference output of the LIA was adjusted to the desired modulation amplitude and coupled to the external input of the potentiostat. The cell potential (E_{dc}) was set using the potentiostat at 185±5 mV. This arrangement provides a sinusoidally modulated voltage (E_{ac}) applied to the ITO electrode about E_{dc}, which also serves as the reference signal for lock-in detection of the optical response. Unless otherwise stated, E_{ac} was set to 20 or 22 mV rms (0.028 V or 0.031 V peak-to-peak). The frequency of E_{ac} was set at the function generator and monitored on the LIA with an analog oscilloscope (OS).

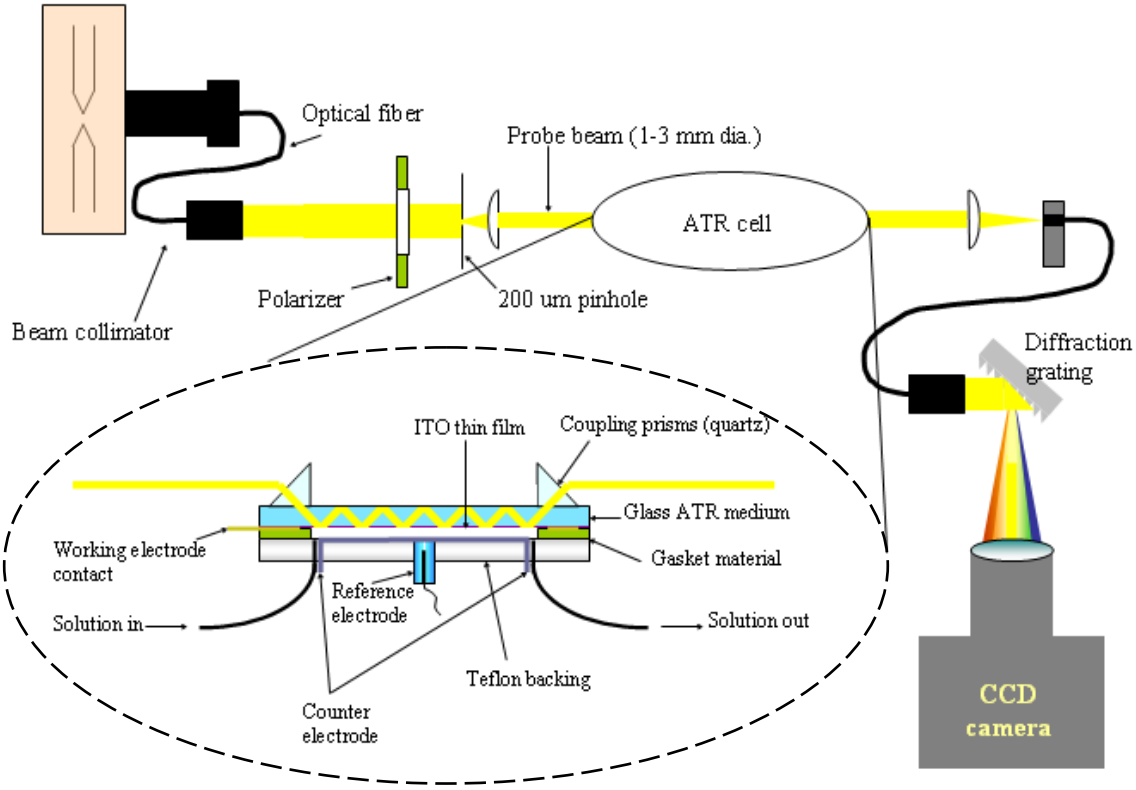

Figure 2.3 Optical arrangements of the ATR apparatus and a cross-section of the spectroelectrochemical ATR cell is shown.[146]

.

To monitor the optical response of the PB film, the outcoupled beam was filtered with a 660 nm bandpass filter (FWHM 20 nm), then measured with a photomultiplier tube (PMT), the output of which was monitored on the OS and fed into the input channel of the LIA. A LabView program was written to record the signal intensities of the in-phase (X) and 90^{o} out-of-phase (Y) components using a 60 sec integration time.[109] Broadband ATR spectra, measured as a function of applied potential, were acquired using a CCD array in place of the bandpass filter and PMT, as described by Doherty et al.[146]

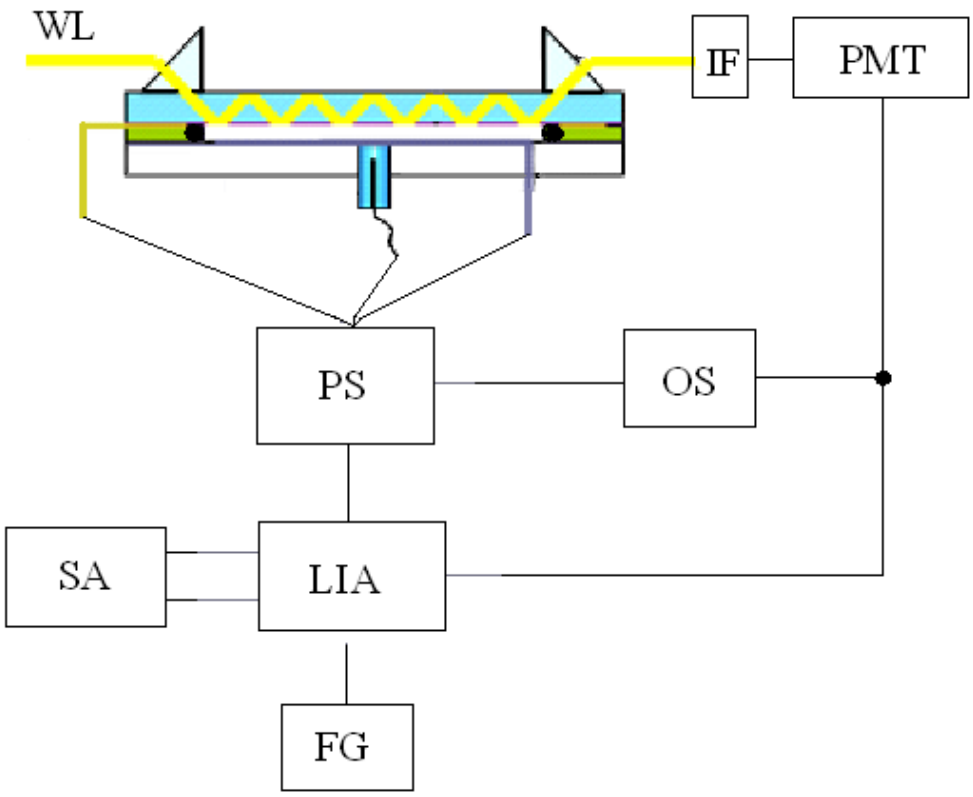

Figure 2.4 Schematic of electrical setup for PM-ATR. White light (WL) is incoupled and internally reflected down the length of an ITO-coated glass microscope slide. The steady-state potential (E_{dc}) is set at the potentiostat (PS) and modulated by applying a sinusoidal reference voltage from a lock-in amplifier (LIA) to the external input of the PS. The modulation frequency is set at the function generator (FG) which supplies a 5 $V_{p\text{-}p}$ external reference signal to the LIA. The optical signal, i.e. the intensity of the outcoupled beam, is monitored at a photomultiplier tube (PMT) after passing through a 660 nm bandpass filter (IF). Both the reference voltage and PMT output are monitored with an oscilloscope (OS), and the PMT output is coupled to the LIA input. Both the in-phase ($Re(R_{ac})$) and 90^{o} out-of-phase ($Im(R_{ac})$) components are recorded using computer running a LabView signal averaging (SA) program.[109]

2.3 Results and Discussion

2.3.1 Thickness and Stability of PB Films

Prior to performing PM-ATR studies on PB films, appropriate conditions for the formation of stable, thin films of PB were established. PB films of varying thickness were made by varying the deposition time. As can be seen in Figure 2.5a, the cathodic current of the film also increases as the deposition time is lengthened. The current can be related to the film thickness by:[126, 148]

$$l = \left(Q \big/ nFA\right)\left(d^3 NA \big/ 4\right) \tag{2.1}$$

where l is the film thickness, Q is the electric charge, A is the electrode area, F is Faraday's constant, n is the number of electrons, d is the length of the unit cell (10.16 Å) and NA is Avogadro's number. The value 4 appears in Eq 2.1 because there are four iron atoms per unit cell. The estimated film thickness for a PB film formed using a 10 sec deposition time is 22 nm. Controlling the film thickness is important because of the sensitivity of the ATR technique. Films deposited for > 30 sec were too highly absorbing to perform ATR measurements. A 10 sec deposition time was chosen for further experiments because the absorbance of these films was well within the linear dynamic range of the ATR instrument.

Other groups have shown that cycling the potential several times between oxidized and reduced forms of PB leads to highly stable films on electrode surfaces.[122,

[126, 132, 136, 145] This cycling stability is dependent on the pH of the electrolyte, especially for the PB/PW couple.[149] It has been demonstrated that PB film is unstable (dissolves from surface) in neutral and alkaline solutions.[149] In this work, adequate results for electrochemical measurements were obtained by cycling the potential ten times between –400 mV and +700 mV in electrolyte (pH 4), then allowing the film to sit in electrolyte for 15 min. Representative voltammograms are shown in Figure 2.5b. Peak separation and current increased slightly (10-20%) during the 15 min incubation; thereafter (up to 45 min), only very minor variations were observed (1-2%). However, CV measurements performed before and after PM-ATR experiments, which required 2-4 hours, did show some further increases in current (up to 750 $\mu A/cm^2$) and somewhat greater peak separation (up to 48 mV). Despite this variability, consistent kinetic results were obtained (see below).

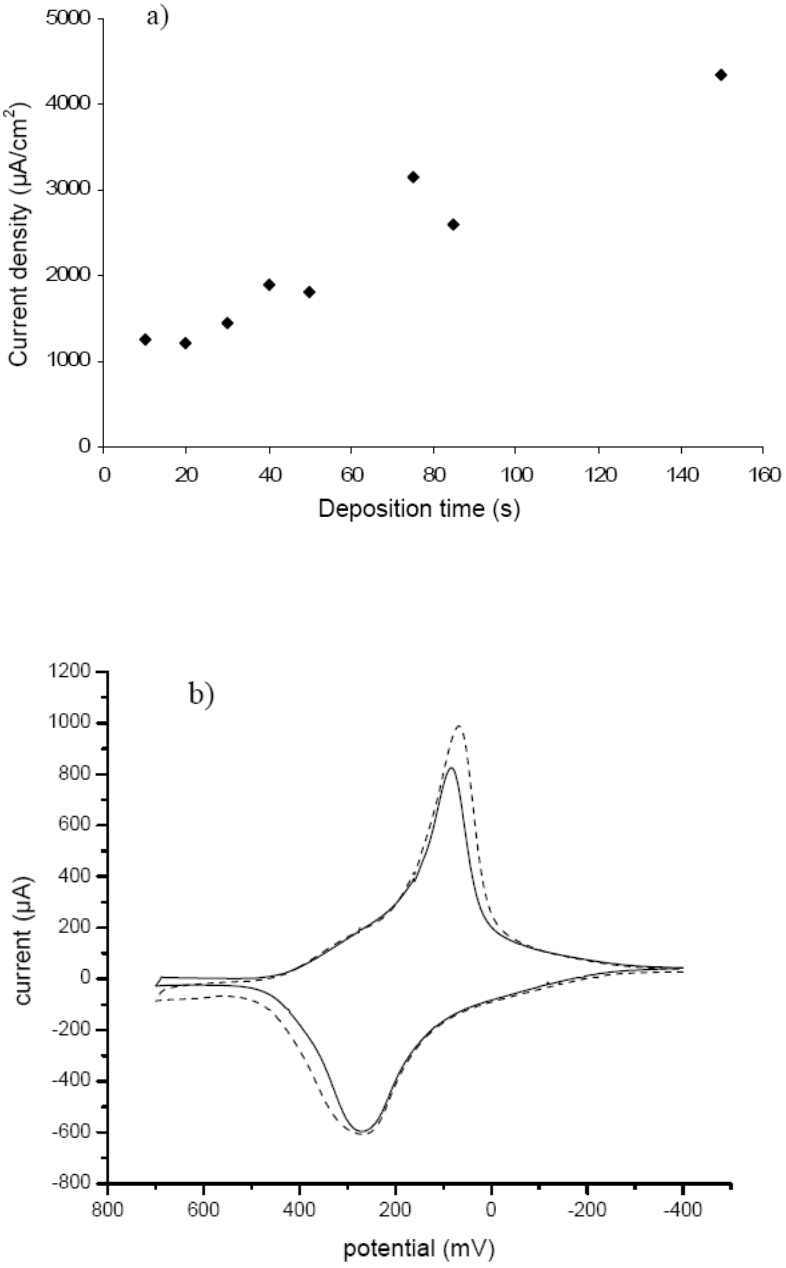

Figure 2.5 a) Cathodic current density, obtained from cyclic voltammograms of PB films, versus film deposition time. b) Cyclic voltammograms of a PB film deposited on an ITO electrode at a current density of 40 μA/cm^2 for 10 sec: after cycling the potential ten times between –400 mV and +700 mV at a scan rate of 100 mV/sec (solid line) and 15 min later (dashed line).

2.3.2 Spectroelectrochemical Results

Potential controlled ATR spectra of PB films were acquired to determine the wavelength region and optical switching potential (E_{dc}) for PM-ATR experiments. As shown in Figure 2.6, large changes in PB/PW molar absorptivity occur between 650 and 770 nm. The observed blue shift in λ_{max} at more positive potentials is similar to previous data reported in the literature.[127] Based on these spectra, 660 nm was selected for PM-ATR measurements.

Figure 2.7 shows a representative optically detected voltammogram of a PB film. It was acquired by scanning the potential between +700 mV and -400 mV at 2 mV/s while applying an ac potential modulation of 8 mV at a frequency of 1 Hz. A relatively low combination of frequency and scan rate was used so that relatively slow optical changes in the film, if they occurred, would be detected. Changes in the molar absorptivity accompany oxidation and reduction of the PB film, which causes R_{ac} to vary. R_{ac} reaches a maximum when the change in molar absorptivity also reaches a maximum; this occurs at approximately 184 mV, which is close to the formal potential (E^o = 172 mV) of the PB/PW redox couple, as determined by cyclic voltammetry. Optically detected voltammograms were measured for all PB films, and E_{dc} was selected for subsequent PM-ATR experiments based on these data. Most E_{dc} values were in the range of 180-190 mV.

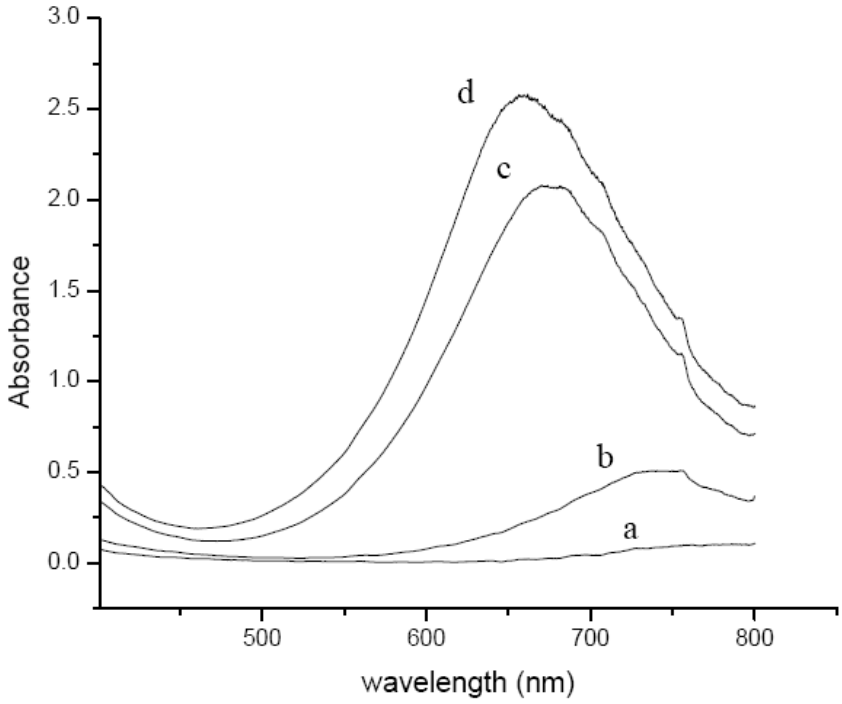

Figure 2.6 ATR spectra of a PB film at different applied dc potentials: -100 mV (a), +100 mV (b), +300 mV (c), and +600 mV (d). The blank was measured with 1 M KCl, pH 4 electrolyte in the ATR cell.

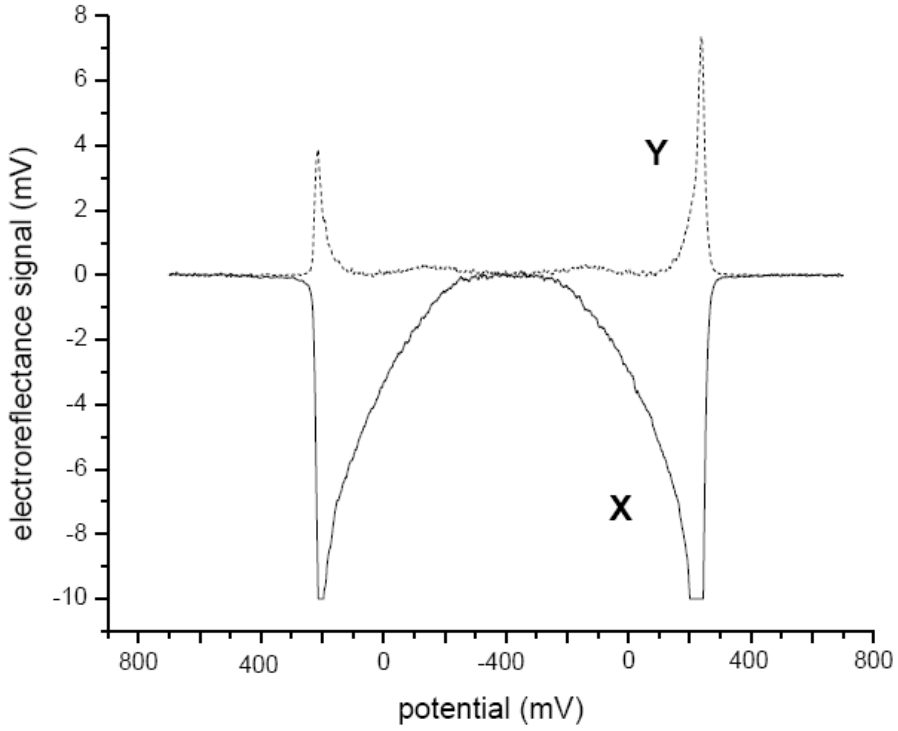

Figure 2.7 Optically detected cyclic voltammogram of a PB film on ITO, measured in the ATR configuration described in the text. The dc potential of the ITO electrode was scanned from +700 mV to -400 mV and back to +700 mV at a rate of 2 mV/sec. A modulation amplitude of 8 mV was applied to the dc potential at a frequency of 1 Hz. The intensities of the in-phase (X, solid line) and out-of-phase (Y, dashed line) signals are plotted.

The modulation amplitude (E_{ac}) used in PM-ATR experiments was selected by monitoring R_{ac} over a range of modulation amplitudes (4 mV to 30 mV) centered around E_{dc} at a fixed frequency of 1 Hz. The in- and out-of-phase portions of R_{ac} are plotted in Figure 2.8 as a function of modulation amplitude. An approximately linear response for X and Y was observed over the entire range of modulation amplitudes. Based on these data, E_{ac} = 22 mV was selected for PM-ATR experiments.

Shown in Figure 2.9 are representative results from a PM-ATR experiment in which the modulation frequency was gradually increased from 0.1 Hz to 250 Hz with E_{dc} = 185 ± 5 mV and E_{ac} = 22 mV. The in- (X) and out-of-phase (Y) portions of R_{ac} were measured at each frequency, then values of R_{ac} normalized to one (R_{norm}) and θ normalized to zero (θ_{norm}) were calculated. X_{norm} and Y_{norm} values were calculated from R_{norm} and θ_{norm} values. In Figure 2.9a, log R is plotted vs. log frequency; in Figure 2.9b, pairs of X_{norm},Y_{norm} values at different frequencies are plotted.

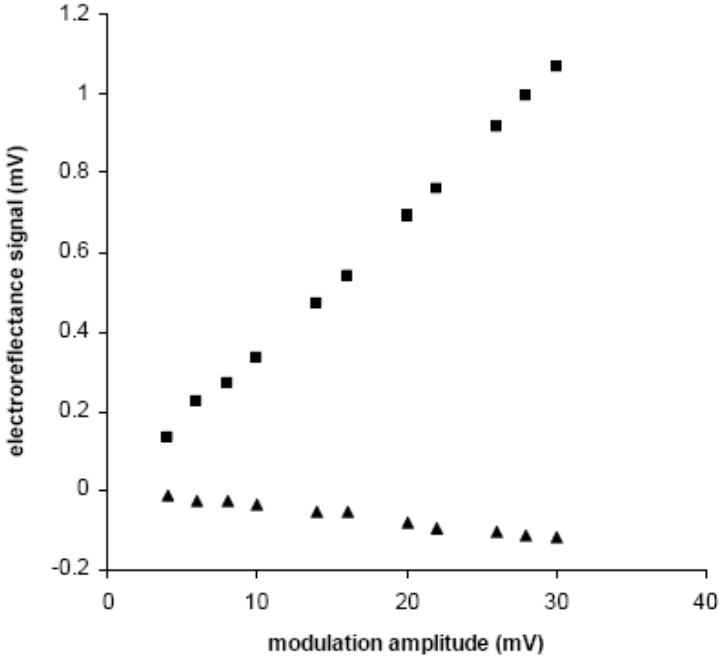

Figure 2.8 The intensities of the in-phase (squares) and out-of-phase (triangles) portions of R_{ac}, measured as a function of modulation amplitude over a range of 4 mV to 30 mV. The E_{dc} was 185 mV and the frequency was 1 Hz.

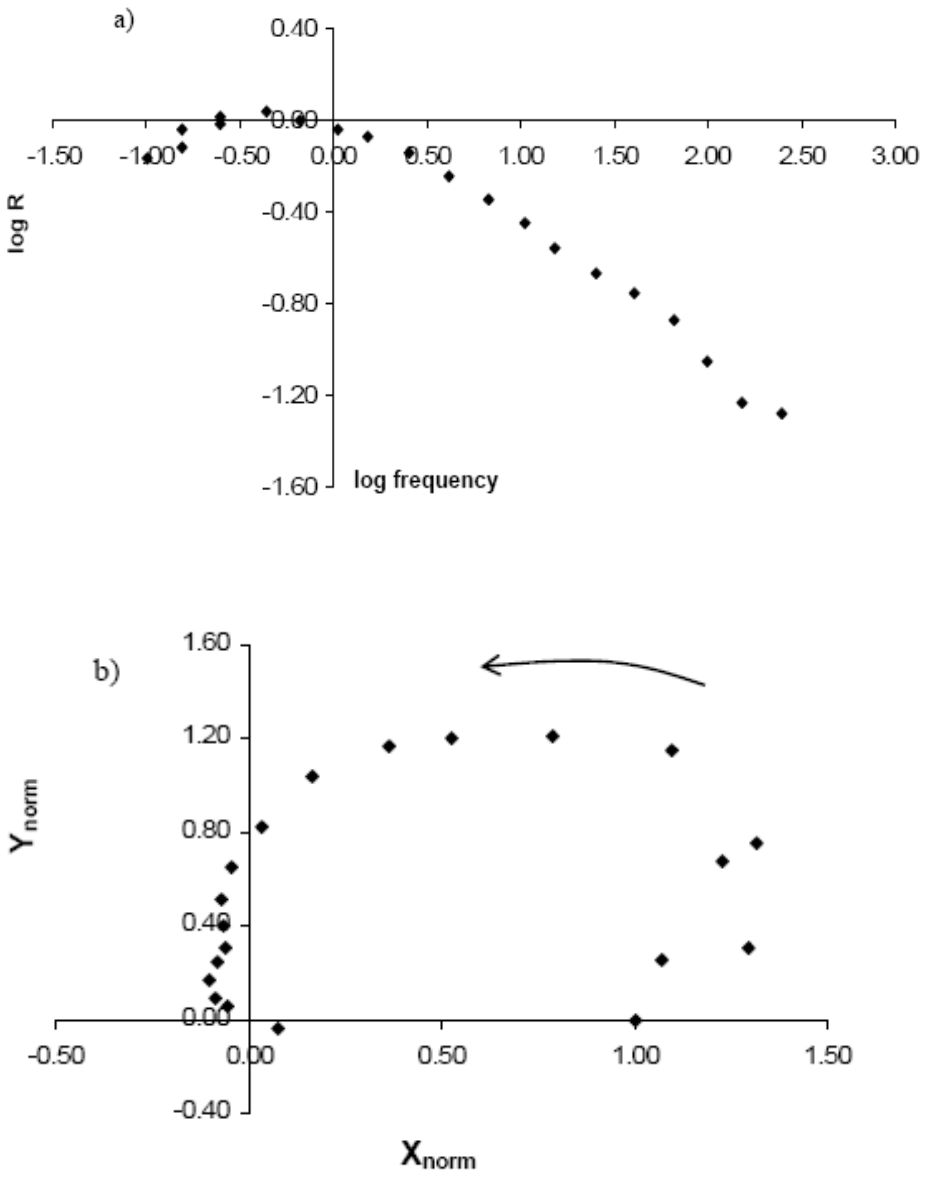

Figure 2.9 a) Log of the electroreflectance signal (log R) vs. log of the modulation frequency. b) Complex plane plot of the electroreflectance response, composed of pairs of X_{norm},Y_{norm} values at different modulation frequencies. The frequency range is 0.1 Hz - 250 Hz (the arrow indicates the direction of increasing frequency).

Three independently prepared PB films were evaluated using PM-ATR. The frequency (ω) at which X_{norm} was zero was in the range of 15.8 – 42.6 Hz for these films. The double layer capacitance and uncompensated solution resistance were determined on independently prepared films using impedance spectroscopy and found to be 0.00502 F/cm^2 and 9.91 $\Omega.cm^2$, respectively. Using Equation (1.19) and these data, the apparent rate constant of electron transfer was calculated to be 13.1 ± 5.4 s^{-1} (n = 3)

Comparative measurements were made on the same three PB films using cyclic voltammetry. Following the method of Laviron (and assuming a transfer coefficient, α, of 0.5 and no influence from ohmic drop),[73, 112] the electron transfer rate was calculated from the anodic and cathodic peak separation and scan rate, yielding an apparent rate constant of 1.09 ± 0.45 s^{-1}. Combining these data with CV measurements on an additional seven films yielded 0.71 ± 0.37 s^{-1}.

The apparent rate constants for PB that are obtained by PM-ATR are about an order of magnitude higher than the results obtained by conventional cyclic voltammetry following Laviron's model.[73, 74]

This is not the first time that this kind of discrepancy in values of apparent rate constant determined by these two methods has been observed. Literature reports on molecular thin films generally show that electroreflectance measurements give higher rate constants compared with those measured by cyclic voltammetry. In one of the earliest applications of ER to heterogeneous electron transfer, the rate coefficients for Nile Blue A adsorbed on pyrolytic graphite[93] were determined to be 5 s^{-1} and 63-78 s^{-1} by Laviron's method and ER techniques, respectively. The heterogeneous ET rate constant

for cytochrome *c* immobilized on gold electrodes coated with long chain alkanethiols ($HS(CH_2)_9COOH$) by Feng et. al[97] is found to be 320 s^{-1} by ER measurements. It was reported by Feng et. al[97] that the anodic and cathodic peak potential separation (from which the rate constant is calculated using Laviron's method) remains the same for cytochrome *c* immobilized on shorter chain alkanethiol monolayers ($n < 9$). It is reported that the heterogeneous rate constant of this protein on shorter chain alkanethiol monolayers ($n < 9$) is so rapid that the ET rate cannot be measured by traditional voltammetric techniques.[97] In another paper, Ruzgas et. al[99] interpreted the value of an apparent rate constant of 20-30 s^{-1} from Feng's[97] reported CV data. Similarly, Gaigalas et. al[96] reported a large discrepancy in ET rate constants (from CV, k_S = 4-12 s^{-1}, and from ER, k_S = 50-200 s^{-1}) for azurin immobilized on 1-hexanethiol-modified gold electrodes.

As explained in Section 1.2.2, in Laviron's model, there are some assumptions which may be introducing some uncertainty to the results. For example, in this model complications from adsorbate-adsorbate interactions and heterogeneous dispersion are excluded.[73, 74] Determination of peak separation for broader peaks is also imprecise and can introduce some errors. For traditional electrochemical techniques, the charging current of the electrical double layer at the electrode interface limits the measurable ET rate[70] and estimation of the rate constant from Laviron's equation is, therefore, hampered by this charging current.[95] Also, when the overlapping redox current is relatively small as compared with the charging current, one cannot clearly distinguish the peak positions and thus the estimation of the rate constant may include some uncertainty.[95] The potential-

modulated ER technique, on the other hand, enables measurement of electrode reaction rates up to 10^4 s^{-1} because the nonfaradaic current, e.g. effect of double layer charging, can be minimized.[70, 92] One of the advantageous features of ER method is that faradaic processes can be selectively observed[92] which may lead to more accurate results.

It is also important to mention another experiment where a combination of three techniques, electrical charge, mass, and color impedance spectroscopy, was evaluated.[150, 151] It was reported that all three signals (current, mass, and color) are not synchronized, i.e., the rates for the electron motion through the electrode (electron hopping between neighboring centers), mass changes associated with the charge balance (ion exchange), and color changes (electron configuration changes due to the electrochemical reactions of a chromophore center) are different for a PB film on a high-reflectance, gold-quartz crystal electrode.[150] The color changes were faster than the electrical charge movement through the electrode, which must be balanced by movement of counterions.[150] The authors have proposed following steps for PB electrochemical behavior from these measurements:[150] i) firstly, an electron configuration change associated with changes of absorbance at 690 nm takes place, ii) then, the electron moves to a neighboring center (electron conduction), iii) lastly, cations reach or leave their site in the PB structure to balance the electrical charge movement. The electrochemical reaction is proposed to take place by exchange of different counterions (potassium, proton and hydrated proton)[150, 152] and therefore counterion movement and insertion at different sites within the PB film may cause the delay between the optical and electrochemical responses.

In summary, discrepancy between the rate constants from CV and PM-ATR measurements is not surprising and may be introduced from uncertainty from some of the parameters in Laviron's model at slow scan rates, effect of charging current on CV measurements, and/or slow counter ion movement within the film. Therefore conventional voltammetric methods that use Laviron's model may not be suitable for measuring electron transfer rate constants for some types of electroactive films.

2.4 Conclusion

PM-ATR is a novel spectroelectrochemical method in which film absorbance is monitored using a probe beam that is internally reflected in a planar waveguide electrode. Charge transfer kinetics are determined by measuring the optical response as a function of the frequency of potential modulation applied to the electrode. Using electrodeposited PB films as a test system, electron transfer rate constants were determined with PM-ATR and conventional cyclic voltammetry. Higher rate constants were obtained using PM-ATR. The PM-ATR technique may be a better option to use for electroactive films where there is a large non-Faradaic background current that can easily be eliminated by the method, and for films where the counterion movement may limit the charge transfer rate.

The enhanced sensitivity of ATR geometry relative to single external reflection and transmission geometries makes PM-ATR useful for studying weakly absorbing or very thin molecular films. The estimated minimum PB film thickness that could be measured by this method is about 1 nm, assuming a linear dependence of electroreflectance signal on film thickness (see Fig. 2.7). Even greater sensitivity could

be achieved by using a thinner waveguide, such as an electrochemically-active integrated optical waveguide (EA-IOW), for which pathlength enhancements of 10^3-10^4 relative to a transmission geometry have been reported.[18]

An additional advantage of an internal reflection geometry (as opposed to external reflection) is that both *s*- and *p*-polarized light can be used to probe the adsorbed film. The availability of two orthogonal polarizations allows orientation parameters of the molecules in the film to be determined. Combining this capability with the PM-ATR method suggests that electron transfer rates for oriented subpopulations of molecules in the film can be determined. A PB film is not a good candidate for orientation studies because its molecular structure is expected to be isotropic. In Chapter 3, relationships between molecular orientation and electron transfer kinetics in thin films of cytochrome *c*, for which some degree of structural anisotropy is expected, are investigated.

3. CORRELATING MOLECULAR ORIENTATION DISTRIBUTIONS AND ELECTROCHEMICAL KINETICS IN SUBPOPULATIONS OF AN IMMOBILIZED PROTEIN FILM

3.1 Introduction to Cytochrome *c* (Cyt *c*)

Cytochrome *c* (cyt *c*) acts as an electron carrier in the respiratory chain of aerobic organisms.[153] It transfers electrons between the enzyme complexes in the mitochondrial membrane and thus plays a crucial role in the redox chain of mitochondria.

Cyt *c* is one of the most thoroughly physicochemically characterized and widely studied redox-active metalloproteins.[153, 154] One of the reasons for its widespread popularity is that cyt *c* is a small, stable protein that can reversibly withstand rather extreme conditions and therefore is suitable for testing mechanisms of protein behavior.[153] Also, cyt *c* includes a large prosthetic group, the heme, which is in contact with many amino acid residues and allows changes in the structure of protein to be detected and followed by variety of spectroscopic techniques.[153]

Figure 3.1 presents the folded state structure (Fig. 3.1a) and color coded X-ray image (Fig. 3.1b) of horse heart cyt *c*, which is used in the research presented here. It has 104 amino acid residues (MW 12,384) and a charge of +9 at pH 7. The redox-active prosthetic heme group, in which iron is coordinated, is slightly non-planar and is located in a groove of the folded polypeptide, almost completely buried inside the protein.[154]

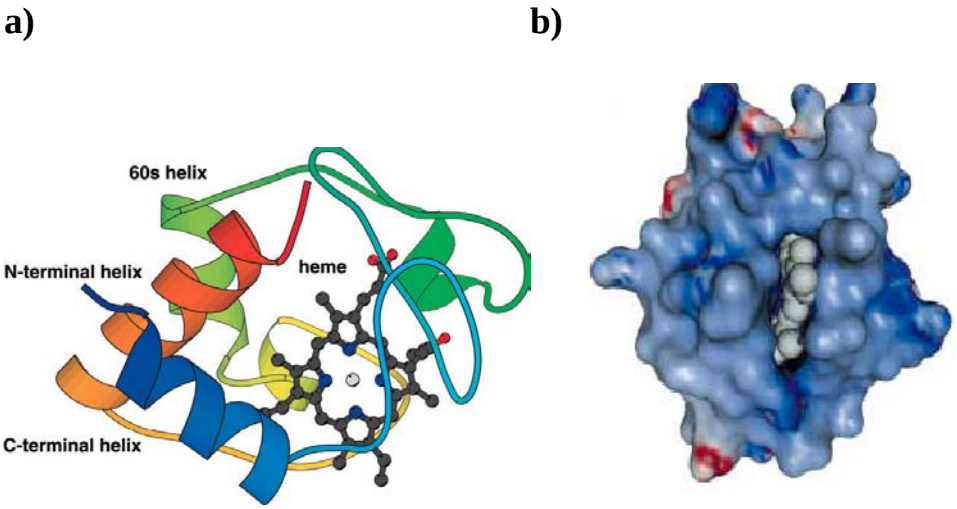

Figure 3.1 a) Structure of cytochrome c showing the prosthetic heme group.[155]

b) Color coded X-ray image of horse heart cyt *c* (red = negative charges, blue = positive charges).[156]

3.1.1 Electrochemical Studies of Cyt c Films

Electron transfer reactions play a central role in biological processes such as photosynthesis and respiration. In addition, electron transfer processes are crucial to the development and operation of many biosensors and biocatalytic devices.[157] Since the biological function of cytochrome *c* is to carry out oxidation-reduction reactions, measurements of redox potentials and associated electron transfer kinetics of cytochrome *c* are central to this protein and can be well addressed by electrochemical techniques.[153] The electrochemistry of cyt *c* films has been investigated in solution and on electrode surfaces by many groups.[154, 156-162]

Usually, electron transfer proteins adsorbed directly on bare electrode surfaces do not exhibit a reversible electron transfer reaction and, in many cases, inhibit the redox reaction of the proteins in the solution phase.[163] For example, the electrochemistry of cyt *c* adsorbed to bare gold and silver has been found to be unstable because the structure of the protein changes upon adsorption to a form that is not electroactive.[164, 165] To establish reversible electron transfer reactions at the electrode interface, surface modifiers are often used. Cyt *c* exhibits a quasi-reversible redox reaction of its ferri/ferro heme couple at appropriately modified electrode surfaces.[166] A variety of surface modifiers have been investigated and are often referred as electron transfer promoters.[163] Examples of promoters include a self-assembled monolayer (SAM), e.g. carboxylate-terminated alkanethiol,[81, 167] adsorbed layers of 4-pyridyl derivatives,[93, 168, 169] and others.[170]

Figure 3.2a presents one possible method for immobilization of cyt *c* on COOH-SAM-coated electrodes.[169] Most studies on cyt *c* electrochemistry use an anionic surface (typically carboxylate moieties such as -COOH SAMs) that electrostatically binds the positively charged surface of the protein (Fig. 3.2a). Under these conditions, the electron transfer between the protein and the electrode displays an unusual dependence on the protein-electrode distance.[70, 169] For alkanethiols with alkyl chain lengths of 10 or more methylene units, the rate of electron transfer decreases exponentially as the length of the alkanethiol chain increases and exhibits an overpotential dependence which is consistent with an electron tunneling model for electron transfer.[169] At shorter chain lengths, the rate is independent of chain length and overpotential.[171] These observations have been explained by a conformationally gated mechanism which states that the rate is limited by conformational changes and rearrangements in the protein necessary to undergo electron transfer.[70, 169]

Figure 3.2b shows an alternative immobilization scheme that uses alkanethiols with a nitrogen containing terminal group (e.g., pyridine) that displaces the native methionine ligand in cyt *c* and "wires" the Fe in the heme to the metal electrode.[157] The distance dependence of the electron transfer rate for this scheme is qualitatively similar to that of the electrostatic immobilization scheme, except that the transition between long-range and short-range mechanisms occurs at a methylene chain length of 12 rather than 9.[169] This difference results from a change in the dominant electron tunneling pathway for these two schemes[169] and there are detailed studies on this subject.[157, 172, 173]

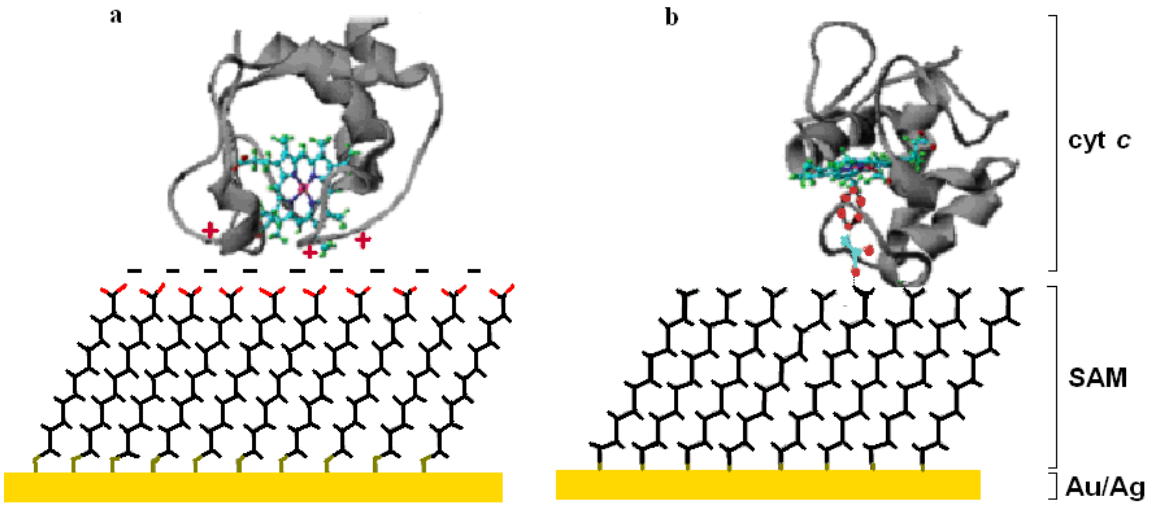

Figure 3.2 Immobilization of cyt *c* on SAM-coated electrodes: a) electrostatic adsorption of cyt *c* on ω-carboxylalkanethiols; b) coordinative binding of cyt *c* to pyridine-terminated alkanethiols.[169]

It has been shown that cyt *c* adsorbs strongly on tin oxide electrodes in neutral pH, low ionic strength solutions with retention of its native redox potential.[174-176] The electron transfer is quasi-reversible with typical rate constants of 1-10 s^{-1}.[175, 176] Unlike unmodified gold and silver electrodes, cyt *c* electrochemistry on bare tin oxide electrode is very stable. More studies related to electrochemistry of cyt *c* on ITO electrodes can be found in the literature.[158, 177-179]

The electrode used in this work is ITO, a semiconductor at which adsorbed cyt *c* can also undergo stable, quasi-reversible electron transfer without a modifying layer.[175, 179] It has been hypothesized that cyt *c* is adsorbed onto ITO through electrostatic interactions with basic residues on the surface of the protein, forming an electroactive protein submonolayer at pH 7 at which the ITO surface is negatively charged.[179]

3.1.2 Spectroscopic Studies of Cyt c Films

Cyt *c* is widely used as a model protein to investigate the structural properties of immobilized protein films. There are several reasons for cytochromes *c* to be popular for these studies such as easy isolation from any tissue or organ and straightforward purification by ion-exchange chromatography because of its high positive charge and high stability.[153] More importantly, the prosthetic heme group is a useful spectroscopic probe of the structure of cyt *c* because it absorbs strongly in the ultraviolet and visible regions. Figure 3.3a shows the position of the heme plane in cyt *c* in relation to the overall dipole moment of the protein; the structure of the prosthetic heme group of cyt *c* is shown in Figure 3.3b.[180] Because of this large dipole moment, it is thought that

electrostatic interactions between cyt *c* and redox-active transmembrane proteins results in oriented binding, with the heme pocket facing the negatively charged surface of the binding partner. Upon oxidation and reduction, the molar absorptivity of cyt *c* changes[181] (Fig. 3.4) which makes this protein a suitable model system for UV-VIS spectroelectrochemical studies.[182, 183]

A wide variety of other spectroscopic techniques have been used to study surface immobilized cyt *c*. Hildebrandt and Stockburger have demonstrated that the spin-state of cyt *c* changes when it is adsorbed on a silver electrode surface by using SERRS (surface enhanced resonance Raman scattering spectroscopy) measurements.[184] Time-resolved SERRS (sensitive to the heme group) has been used to study the rate of electron transfer for cyt *c* films on alkanethiol modified silver electrodes.[153, 185, 186] It has been found that with alkanethiol chains shorter than 19 Å, the electron transfer rate does not vary with chain length because of the effect of an increased electric field closer to the electrode, which increases the activation energy for electron transfer.[186]

Sagara and Niki[163] have investigated the redox reaction of cyt *c* at a gold electrode in the presence of a surface modifier, (4,4'-bipyridyl), using ER spectroscopy. It was found that the electronic structure of cyt *c* co-adsorbed with 4-bpy is different from that of the native cyt *c*.

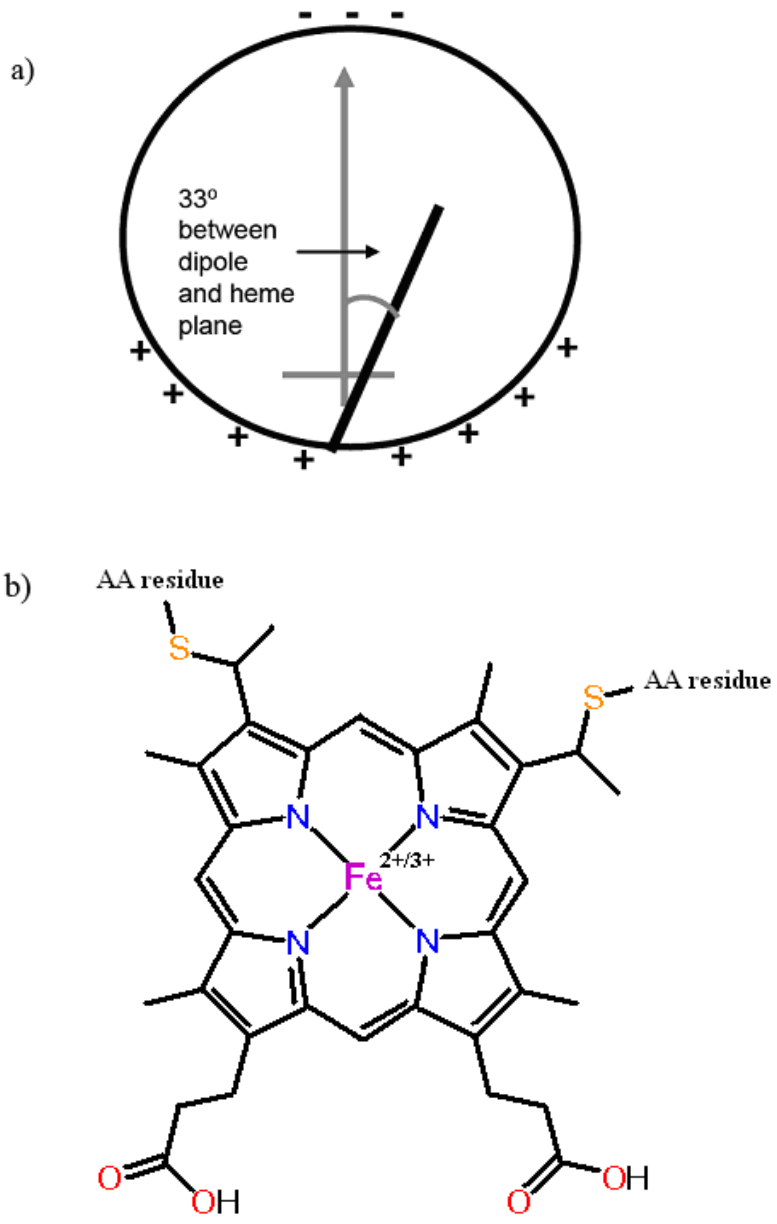

Figure 3.3 a) Schematic of cyt *c* structure showing position of heme plane (side view) relative to the dipole moment of the protein and the distribution of positive and negative charges. b) Structure of prosthetic heme group of cyt *c*.

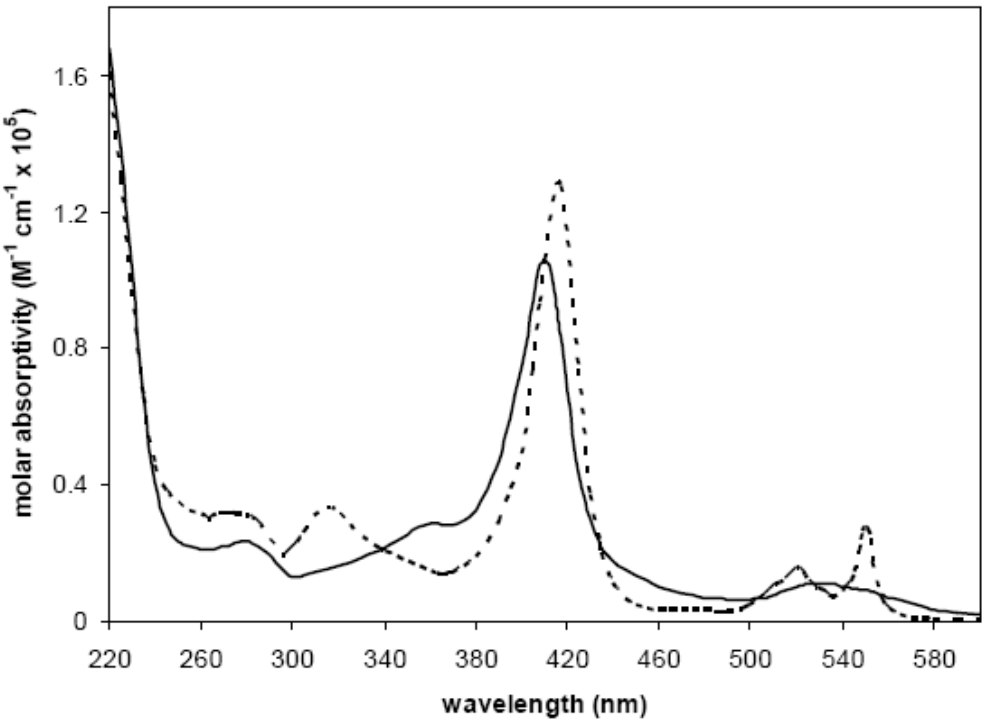

Figure 3.4 Absorbance spectra of ferricyt *c* (solid line) and ferrocyt *c* (dashed line)[181]

Recently, Yue and coworkers[169] have investigated the mechanism of heterogeneous electron transfer of immobilized cyt *c* by cyclic voltammetry and time-resolved surface enhanced Raman spectroelectrochemistry. In their work, cyt *c* is coordinatively bound to SAMs of pyridine-terminated alkenethiols on Au and Ag electrodes. It was found that the temperature, distance and overpotential dependencies of the electron transfer rates indicate a change of mechanism, from a tunneling controlled reaction at long distances (thicker films) to a solvent/protein friction controlled reaction at shorter distances (thinner films).[169] They suggested that the mechanism change is linked to the increase in electronic coupling and the slowing of the polarization relaxation with the decreasing film thickness.

ATR spectroscopy is sensitive enough to detect monolayer and submonolayer molecular films of cyt *c* absorbed to transparent substrates. For example, the denaturation of the cyt *c* adsorbed to glass has been followed using ATR UV-VIS spectroscopy to monitor the Söret band of the protein,[187] analogous to the many denaturation studies on cyt *c* in solution.[153] It was found that adsorbed cyt *c* is less stable since it is unfolded at a slightly higher pH than dissolved cyt *c*.

Brusatori et al. has investigated adsorption of cyt *c* onto an ITO-coated optical waveguide as a function of surface potential[188] using optical waveguide lightmode spectroscopy. They found that the rate of adsorption was increased by increasing the voltage applied to the electrode surface. It has been suggested that the electric field leads to more oriented and efficiently packed adsorbed molecules and, in case of high voltage, to multilayer formation.

3.1.3 Orientation Distribution Studies of Molecular Films

Understanding the orientation and conformation of proteins adsorbed on solid surfaces is important in design of biomaterials, biosensors, and bioanalytical systems.[170] The rate of electron transfer reaction of proteins in biological and electrochemical systems appears to depend on the orientation of the molecules during the reaction and on the period of time that a given orientation is maintained.[159, 189] Optimization of the orientation is required not only to achieve a fast electron transfer process between the protein active center and the electrode but also to facilitate the access of a binding partner protein or substrate from the solution phase to the immobilized protein.[166]

A variety of methods have been applied to probe the orientation of proteins at the electrode/electrolyte interface for over 20 years. Many of them have been used for cyt *c* at surface-modified electrodes in the absence of an electron transfer mediator.[166]

The orientation of cyt *c* immobilized on electrode surfaces has been simulated by computational methods, speculated on the basis of interfacial electron transfer kinetic data, and experimentally estimated using the results of spectroelectrochemical measurements.[166] It has been found from simulations that the large electric dipole moment of cyt *c* is the key factor that orients the molecule on negatively charged surfaces, with the heme crevice facing the surface, with a near upright heme plane orientation.[190] On a carboxy-terminated SAM, the positively charged Lys residues surrounding the heme crevice eletrostatically interact with the carboxylates, aiding the molecular orientation.[190]

In the electrochemical kinetic studies, it is generally accepted that when a reversible or quasi-reversible redox response is observed, the adsorbed cyt *c* molecules assume an orientation in agreement with the above-mentioned simulation results.[166] It has been suggested that in this orientation, the closest approach of the heme to the underlying electrode surface is attained, maximizing the electron transfer rate.[166] Kinetic studies on surface-site-modified cyt *c* molecules (site-directed mutants) on an Au electrode have been reported by Niki[191] and Imabayashi[192]. For the former study, they showed that the substitution of a lysine residue with alanine at position 13 in recombinant rat cyt *c* (RC9-K13A) lowers the interfacial electron transfer rate more than 5 orders of magnitude. They proposed that lysine 13 facilitates the most efficient electron transfer pathway to the SAM carboxylate terminal. In the latter study, it was shown that the dipole moment of cyt *c* determines its orientation of adsorption on the SAM and affects the rate of the electron transfer. Both of these results strongly suggest that the orientation of the cyt *c* molecule is in fact the predominant factor in determining its electron transfer kinetics. It was also shown that when the modifier layer does not have the ability to bind to cyt *c* in the right orientation, its electrochemistry appears sluggish.[193]

In order to estimate electron transfer rates with respect to orientation of proteins on electrode surfaces, attempts have been made to fix the protein on the electrode surface in a specific orientation. The firm attachment and exact orientation is thought to be due to the interaction of local protein charges with charged groups of the modifier attached to the electrode surface.[159, 167] Different chemical methods have been used to fix cyt *c* molecule on electrode surfaces, including electrostatic adsorption on ω-

carboxylalkanethiols[169] and coordinative binding to pyridine-terminated alkanethiols[169] on Au/Ag surfaces, and covalent attachment using a carbodiimide under an applied potential[159] on a glassy carbon electrode.

The orientation of cyt *c* has been directly probed at various dielectric and electrode surfaces using several spectroscopic and spectroelectrochemical techniques. The breadth of these studies is remarkable and details can be found in literature: Edmiston et al. performed waveguide ATR and total internal reflection fluorescence (TIRF) anisotropy measurements (the latter using Zn-substituted cyt *c*) to investigate molecular orientation of adsorbed cyt *c* films.[194] The results show that an adsorbed cyt *c* film with a narrow orientation distribution can be produced when a single, high-affinity type of non-covalent binding occurs between the surface of the protein and the substrate surface.

In films where there are more types of interactions between the surface and cyt *c*, there is a broader distribution of heme dipole orientations present than those which have one dominant interaction, such as an electrostatic interaction.[194] Ataka and Heberle have measured potential-induced difference IR spectra of the electron transfer reaction taking place between a monolayer of cyt *c* and a Au electrode modified by carboxyl, hydroxyl, zwitterionic, and pyridine-terminated SAMs.[195] They found that the frequencies of the vibrational bands are identical for the various surface modifiers, but the relative peak intensities differ. Therefore they claimed that the functionality of cyt *c* is fully preserved independent of the surface modification, while the difference in peak intensities was attributed to the differences in surface structure, i.e., the orientation and the relative

distance of cyt *c* from the surface. Dick and co-workers used SERRS to probe the orientation of ferrocyt *c* on a nanosphere (AgFON) electrode modified with carboxylate-terminated alkanethiols of various chain lengths.[196] They showed that the electrostatic binding of ferrocyt *c* to AgFON/S$(CH_2)_x$COOH surfaces yields a highly oriented redox system with the heme edge directed toward the electrode surface.

ATR and TIRF techniques have been developed in terms of optical models and order parameter elucidation and applied to cyt *c* adsorbed on glass and ITO substrates by Runge et al.[179, 197, 198] The orientation distribution of the heme groups on ITO was found to be very broad, centered at around 50^0 but nearly isotropic. These studies are closely related to this project and will be discussed further in Section 3.3.3.

3.1.4 Motivation

It is well recognized that immobilization of a metalloprotein may affect its electron transfer activity, because of an "un-optimized/incorrect" molecular orientation and/or altered conformation relative to the native state.[70, 81, 166, 194, 196, 199-201] Horse heart cyt *c* has been frequently used as a model to study these effects.[166, 194, 196] The influence of electrode-protein separation distance on the electron transfer rate constant (k_s) of immobilized cyt *c* has been thoroughly investigated.[70, 81, 200, 201] Orientation is also predicted to play a significant role because the heme is not located at the center of the protein.[80, 179, 196, 202] Thus a distribution of molecular orientations will generate a distribution of heme-electrode separation distances and electron-tunneling pathways, producing a distribution of k_s values. This concept has been invoked to explain the

nonideal voltammetry of immobilized cyt *c* films,[202] but has not been experimentally verified. The difficulty lies in measuring the molecular orientation distribution of a cyt *c* film, measuring a distribution of k_s values on that film, and establishing a correlation between the distributions. Dick et al.[196] demonstrated that a more oriented cyt *c* film is more electrochemically reversible but their work did not address *distributions* of orientations and k_s values.

Herein PM-ATR technique that allows measurements of k_s values for differently oriented subpopulations of the electroactive molecules in an immobilized cyt *c* film was used, without interference from the nonelectroactive subpopulation. This measurement cannot be done by conventional electrochemical methods because only about half of the film is electroactive (see Sections 3.3.1 and 3.3.3 for detailed explanation). Using PM-ATR, measurements can be made in both transverse electric (TE) and transverse magnetic (TM) polarizations, which can provide information about molecular orientation.

3.2 Experimental

3.2.1 Substrate Preparation

To increase sensitivity, glass substrates thinner than the 1 mm thick substrates employed in prior work were used here. Decreasing the thickness of the ATR element increases the number of reflections and therefore the sensitivity. ITO was sputtered onto glass coverslips (150 μm) by Mike Brumbach in the Armstrong group at the University of Arizona. It had a nominal thickness of ~ 80 nm, sheet resistance of ~70 Ω and surface roughness of less than 1 nm over a 1 x 1 μm scan area. ITO-coated planar electrodes were

cleaned as described in Section 2.2.1. Briefly, they were cleaned by scrubbing with a 1% Alconox solution for 1 min and then sonicating for 15 min each in 1% Alconox, water, and ethanol, followed by low temperature air plasma cleaning (Harrick model PDC-3XG) for 15 minutes.[144]

3.2.2 Formation of Cyt c Films on Coverslip ITO

Horse heart cyt *c* obtained from Sigma was used without further purification. Cyt *c* was prepared and adsorbed on ITO from pH 7 phosphate buffer, as described previously,[179] to produce films of near monolayer surface coverage. Briefly, cyt *c* films adsorbed on ITO-coated coverslips were made by injecting a 10 μM cyt *c* solution into the electrochemical cell or ATR flow cell, followed by a 15 minute static incubation period, then rinsing the cell with 10 mL of 10 mM (pH 7) phosphate buffer[179]. The cell was then filled with phosphate buffer for cyclic voltammetry and ATR experiments. The electroactive surface coverage, measured by cyclic voltammetry, was 7.9 pmol/cm^2. This value differs from previous measurements[179, 203, 204] which is likely due to differences in the properties of ITO obtained from different sources.

3.2.3 PM-ATR Experimental

Complete descriptions of PM-ATR theory and instrumentation are given in Chapter 2 and elsewhere.[109, 205] Briefly, the potential at the ITO electrode was set using the potentiostat while the lock-in amplifier was used to monitor both the modulating potential and modulated spectroscopic signal. Labview software was used to record the

in- and out-of-phase portions of the electroreflectance signal. Here a polarizer and a 417 nm bandpass filter (3 nm fwhm) were placed between the light source and ATR cell to control polarization and spectral bandwidth, respectively.

3.3 Results and Discussion

3.3.1 Surface Coverage of Cyt c Films

The detailed studies that have been done to calculate total and electroactive surface coverages of cyt *c* films adsorbed on ITO electrodes can be found in literature.[179, 197, 204] The electroactive surface coverage was determined using voltammetry.[170, 203] Integrating the cathodic peak of cyclic voltammograms yielded a value of 9.5 ± 0.5 pmol/cm^2 [204].

The ratio of the electroactive surface coverage to the total surface coverage determines the percentage of 'active' proteins in the film.The total surface coverage was measured spectroscopically using ATR linear dichroism technique by Runge at al., from which a value of one full monolayer of cyt *c*, 22 pmol/cm^2 was determined.[179, 197] Thus cyt *c* films on ITO are about 43% electroactive (9.5 pmol/cm^2 / 22 pmol/cm^2).[197] The low percent electroactivity could be due to the heterogeneous surface of ITO,[206] which is composed of conducting and insulating regions.[207] It could be also due to conformational changes, induced by adsorption, that yield inactive proteins. Another possibility is that a subpopulation of the adsorbed cyt *c* molecules is adsorbed in an orientation that places their heme groups too far from the surface to efficiently exchange electrons with the ITO surface.[197] Since electrochemistry probes only the electroactive portion of the film and

spectroscopy probes the entire film, making a correlation between charge transfer and orientation of molecules is challenging because only about half of the film is electroactive. However, PM-ATR provides a unique approach to this problem because it allows only the electroactive portion of molecular film to be probed spectroscopically.

3.3.2 Spectroelectrochemical Results

Sinusoidally modulating the electrode potential over a small range near the midpoint between the oxidation and reduction potentials of the cyt *c* film produces a modulated change in the electroreflectance (R, which is proportional to the intensity of light outcoupled from the waveguide) at the same frequency, due to the difference in molar absorptivities of ferro- and ferricyt *c*. Only electroactive molecules contribute to the modulated component of R.

Figure 3.5 shows a representative optically detected voltammogram of a cyt *c* film adsorbed on an ITO-coated waveguide electrode recorded in TM polarization.[208] It was acquired by scanning the potential between -250 mV and +250 mV at 1 mV/s while applying a potential modulation of ±8 mV at a frequency of 1 Hz. A relatively slow scan rate and slow modulation frequency were used so that relatively slow optical changes in the film, if they occurred, could be detected. The largest change in R (corresponding to the minimum in-phase (*X*) signal) occurs at approximately -12 mV (most E_{dc} values were in the range of -12 to 12 mV for independently prepared films) vs Ag/AgCl which is close to the midpoint (5 mV) between the anodic and cathodic peaks in the cyclic

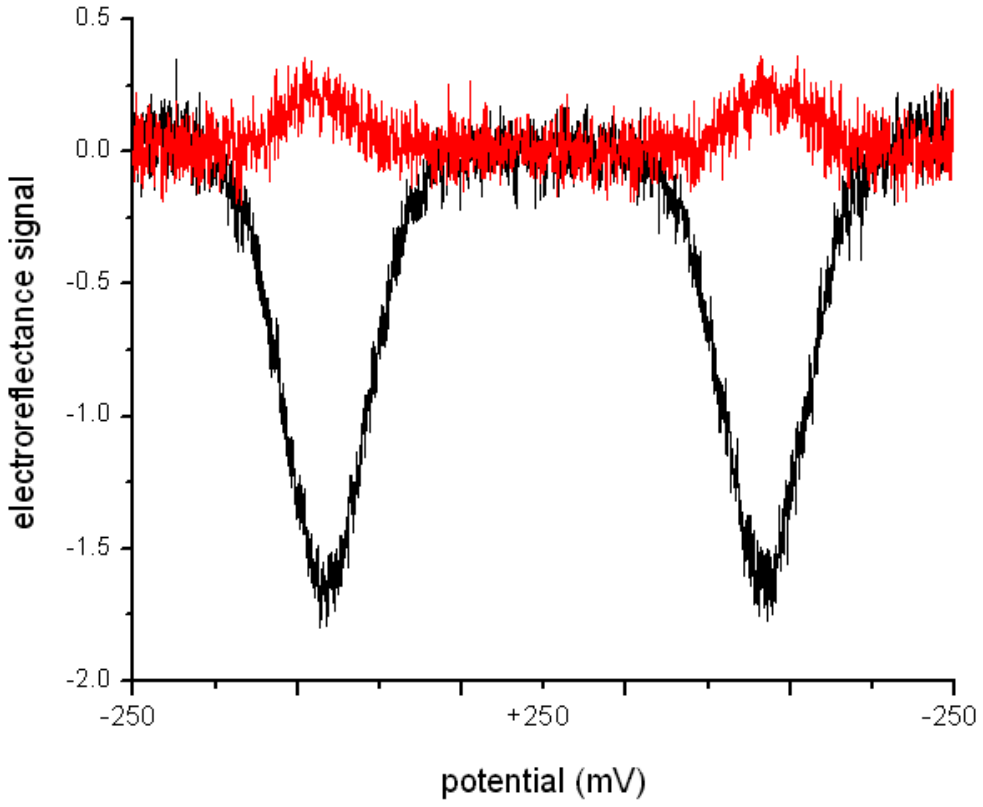

Figure 3.5 Optically detected voltammogram for a cyt *c* film recorded using TM polarized light. The in-phase (*X*) and out-of-phase (*Y*) components of the electroreflectance (R) are shown in black and red, respectively. An AC potential modulation of 8 mV at a frequency of 1 Hz was applied during the scan, producing a modulation in R at the same frequency.

voltammogram of the cyt *c* film. On the basis of these data, the midpoint potential (E_{dc}) was selected for subsequent PM-ATR experiments on the same film.

To select the modulation amplitude (E_{ac}) used in a PM-ATR experiment, the electroreflectance was measured over a range of amplitudes (4 to 50 mV) centered at E_{dc} and using a modulation frequency of 1 Hz. A typical result is shown in Figure 3.6. Approximately linear response for X and Y was observed approximately over the entire range of modulation amplitudes. E_{ac} = 22 mV was selected as the modulation amplitude because it is well within the linear response ranges and provides adequate sensitivity.

Figure 3.7 is a representative result from a PM-ATR experiment. The real (in-phase, *X*) and imaginary (out-of-phase, *Y*) portions of R were measured over a modulation frequency range of 0.1-250 Hz. To enable comparison of results from different films, normalized values of *X* and *Y* were calculated as described previously.[109, 205] X_{norm}, Y_{norm} curves were fit to a polynomial function to determine the frequency (ω) at which $X_{norm} = 0$. Electron transfer rate constants were then calculated from $k_S = 0.5\omega^2 R_s C_{dl}$ (Equation 1.19, Section 1.4.2).

The double layer capacitance (C_{dl}) and uncompensated solution resistance (R_s) were determined on independently prepared films using electrochemical impedance spectroscopy and found to be 9.1 μF/cm^2 and 1.1 kΩ.cm^2, respectively.[208] The time constant of the electrochemical cell with a bare ITO electrode was 4.9 ms.[208]

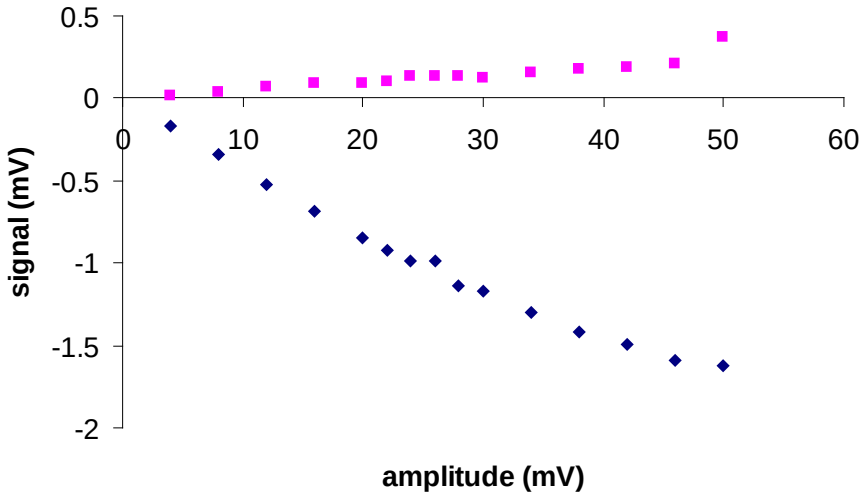

Figure 3.6 Electroreflectance of a cyt *c* film adsorbed on an ITO-coated waveguide measured as a function of modulation amplitude using TM polarized light: in-phase (*X*) signal, blue squares; out-of-phase signal (*Y*), pink squares. The E_{dc} was 2 mV vs Ag/AgCl and the frequency was 1 Hz.[208]

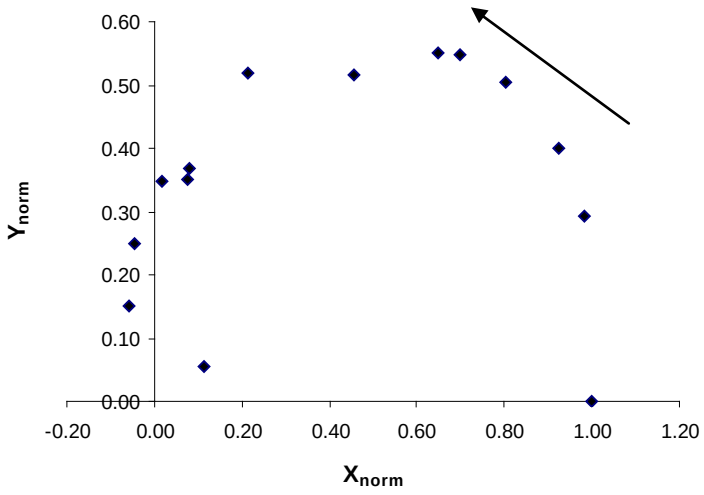

Figure 3.7 Complex plane plot composed of pairs of *X*norm,*Y*norm values measured on a cyt *c* film adsorbed to ITO over a frequency range of 0.1- 250 Hz using TM polarized light and E_{dc} = 5 mV. The arrow indicates the direction of increasing frequency.[208]

Data were acquired in both TM and TE polarizations on each cyt *c* film, yielding $k_{S,TM} = 158 \pm 30\ s^{-1}$ ($n = 3$) and $k_{S,TE} = 47 \pm 11\ s^{-1}$ ($n = 3$), respectively. On the same cyt *c* films, conventional cyclic voltammetry was performed, from which $k_{S,CV}$ was calculated from the anodic and cathodic peak separation.[203, 204] The result, $3.1 \pm 0.3\ s^{-1}$, represents the electrochemically obtained rate constant for the entire electroactive portion of the cyt *c* film. A graphical representation of these results is presented in Figure 3.8. Relatively faster rate constants obtained optically with PM-ATR compared to conventional electrochemistry. We have obtained similar discrepancy between the rate constants measured by PM-ATR and CV for PB films that are reported in Chapter 2. As explained in Section 2.3.2 in detail, literature reports on molecular thin films generally show that electroreflectance measurements give higher rate constants compared with those measured by cyclic voltammetry.[93, 96, 97] Similar trend has obtained for cyt *c* immobilized on gold electrodes coated with long chain alkanethiols $HS(CH_2)_9COOH$ by Feng et. al[97] and for another protein molecule, azurin immobilized on 1-hexanethiol-modified gold electrodes by Gaigalas et. al[96].

Here, the discrepancy between the observed rate constants may be due to the following reasons: i) estimation of the rate constant from Laviron's equation is hampered by non-Faradaic current (charging current),[95] on the other hand, ER method enables measurements of Faradaic processes selectively[92] and minimizes the effect of double layer charging which may lead to more accurate results, ii) the assumptions that are made in Laviron's model[73, 74] may introduce some uncertainty to the results, iii) for

conventional CV, difficulty in determination of peak positions for broader peaks and therefore estimation of rate constant may include some errors.

- **In TE, $k_S = 47 \pm 11\ s^{-1}$**

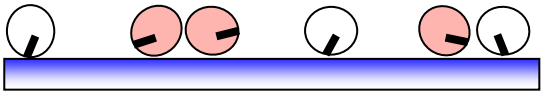

- **In TM, $k_S = 158 \pm 30\ s^{-1}$**

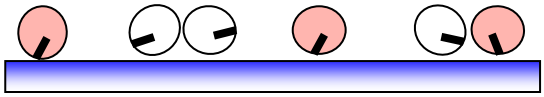

- **Average $k_S = 3.1 \pm 0.3\ s^{-1}$, based on cyclic voltammetry**

Figure 3.8 Graphical representation of molecules that are probed with TE and TM polarized light and their corresponding charge transfer rates. Molecules that are highlighted show the most probable orientations that contribute to the measured TE and TM charge transfer rates.

3.3.3 Correlation of Orientation Distribution with Charge Transfer Rates

Recently, a combination of polarized TIRF and ATR spectroscopies has been applied for determination of the second and fourth order parameters of molecular orientation in cyt *c* films adsorbed on ITO by Runge et al.[198] From those results, an orientation distribution for the tilt angle of the prosthetic heme group of cyt *c* has been constructed.[179, 198] The experimental and theoretical details can be found elsewhere.[179, 197, 198] Briefly, polarized ATR was used to determine the second order parameter, which was combined with TIRF data to solve for the fourth order parameter.[198] A maximum entropy model was then applied to the order parameters to construct an orientation distribution.[198] The tilt angle distribution of the heme molecular plane in a cyt *c* monolayer adsorbed to ITO is measured and shown in Figure 3.9.[179] The result, shown in Figure 3.9, shows that the orientation distribution is very broad and is centered at around 50 degrees. The very broad orientation distribution should give rise to a broad distribution of heme-electrode separation distances and k_s values. The cyt *c* films studied by Runge et al.[179, 198] were prepared identically to the films used here for PM-ATR measurements. Thus the data in Figure 3.9a provide a framework for interpretation of the rate data listed in Figure 3.8.

Examples of differently oriented cyt *c* heme representation of electric field of differently polarized light are shown in Figure 3.10 a-c. The $k_{s,TM}$ and $k_{s,TE}$ values correspond to subpopulations of the electroactive portion of cyt *c* film. These subpopulations are partially *overlapping* (Figure 3.10), which is due to several factors: (1) TM light is composed of both *z*- and *x*-polarized components, whereas TE light is *y*-polarized.[179, 208] (2) The heme absorption is circularly (or elliptically) polarized in the

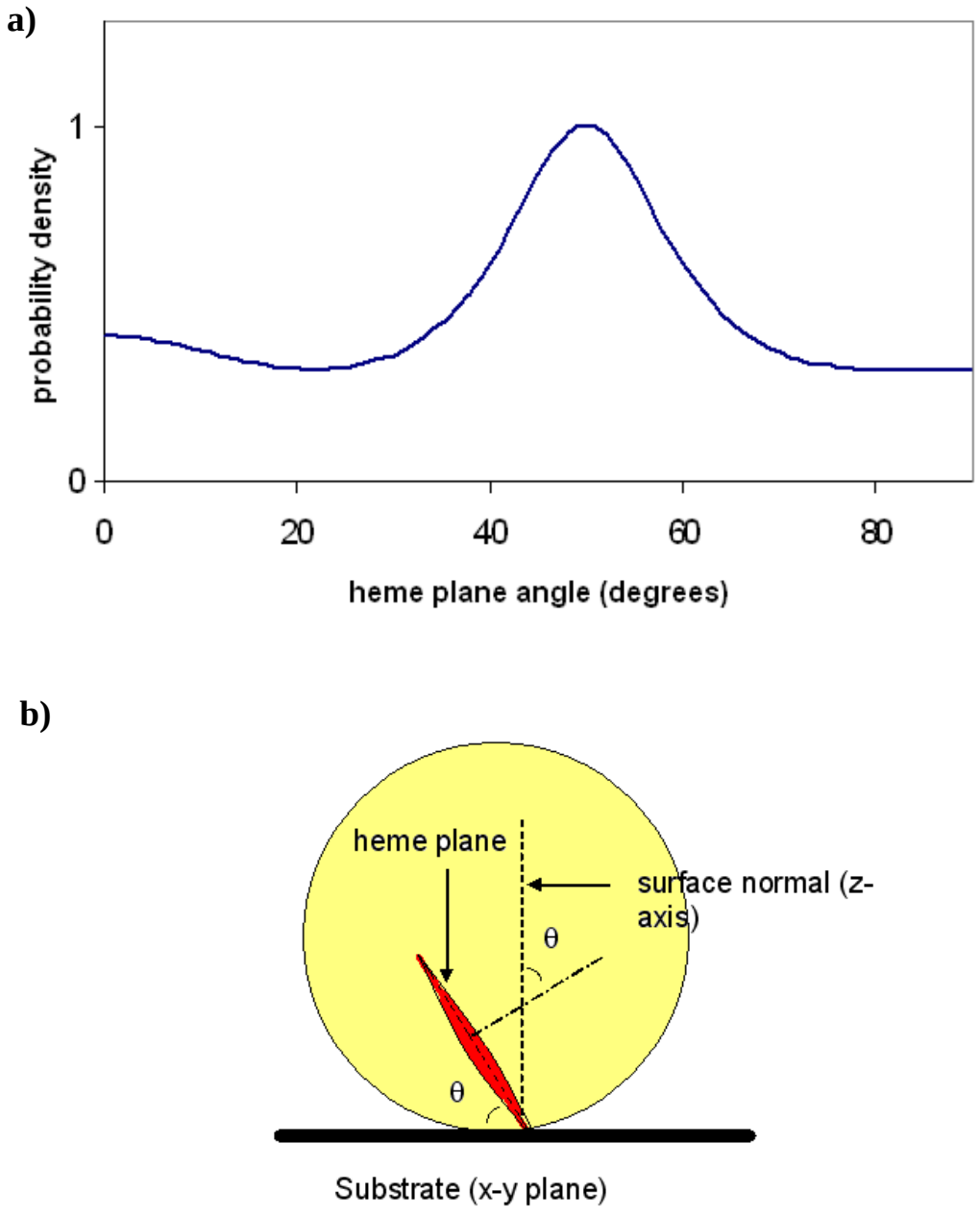

Figure 3.9 a) Orientation distribution of cyt *c* molecules adsorbed on an ITO electrode. It shows a high probability of having molecules tilted at every angle[198] b) A graphic representation of the heme tilt angle, defined as the angle between the heme plane and the surface normal.

molecular plane.[166, 179, 194, 196] (3) The tilt-angle distribution should be uniaxial about the *z*-axis.[166, 179, 194, 196]

Molecules at all tilt angles (from 0° to 90°) therefore contribute to *both* $k_{s,TM}$ and $k_{s,TE}$, but their contributions are weighted by the extent to which their absorption dipoles project onto the electric fields of TE and TM polarized light. Molecules with large tilt angles contribute greater to TM absorption, and if most of these are adsorbed in a "face-down" orientation, that is, with the face of the protein that surrounds the heme crevice in contact with the ITO surface (see Figure 3.11), then their heme-electrode separation distances should be relatively small.[179, 194, 203, 204] TE light is more strongly absorbed by molecules with small tilt angles, for which heme-electrode separation distances should be larger, and this difference is reflected as $k_{s,TM} > k_{s,TE}$.

It is important to note that this analysis assumes that adsorption of cyt *c* to ITO does not induce structural changes that alter the relationship between tilt angle, heme-electrode separation distance, and electrochemical activity.[166, 179, 194, 196]

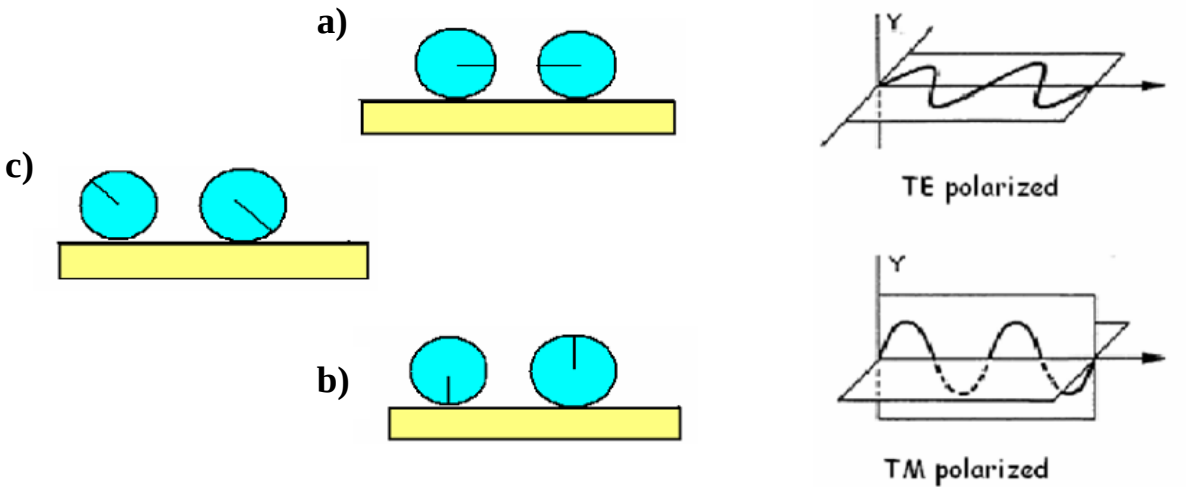

Figure 3.10 Different molecular orientations of the heme plane in cyt *c* molecules adsorbed on ITO (a,b,c) and representation of the electric field in TE and TM polarizations.

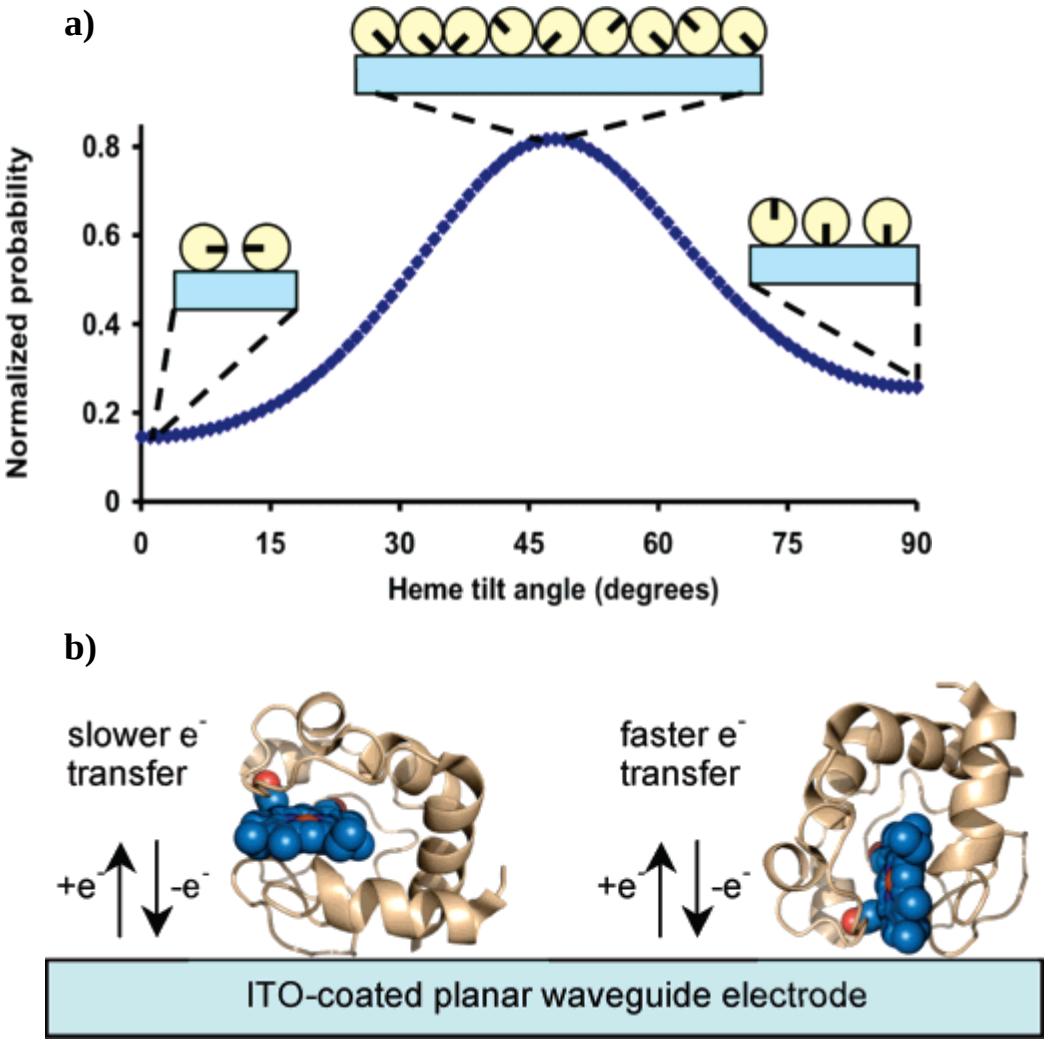

Figure 3.11 a) Distribution of heme plane tilt angles, relative to the electrode surface plane, in a cyt *c* monolayer adsorbed to ITO. Data are re-plotted from the polar coordinate data presented in Figure 3b2 in the literature[179] and normalized to a total probability of unity. The insets show representations of molecules with heme tilt angles near 0°, 50°, and 90°.[208] b) Schematic representation of two different heme plane orientations of cyt *c* on ITO and their relative electron transfer rates.[208]

3.4 Conclusion

Herein it has been demonstrated that PM-ATR is a novel method for studying the orientation dependence of electron transfer rate for immobilized cyt *c* films. With this method, changes in the absorbance as a function of the light polarization, modulation frequency, and amplitude provide information about electron transfer rates and molecular orientation. We have used polarized PM-ATR to obtain two k_S values assigned to differently oriented subpopulations of cyt *c* molecules in an adsorbed film. The $k_{S,TM}$ / $k_{S,TE}$ ratio of 3.3 is consistent with a shorter tunneling distance for proteins adsorbed in a vertical orientation (probed with TM) relative to a horizontal orientation (probed with TE). To our knowledge, these data are the first to correlate a distribution of molecular orientations with a distribution of electron transfer rate constants in a redox-active molecular film.[208]

4. SPECTROELECTROCHEMICAL CHARACTERIZATION OF CHARGE INJECTION PROCESSES IN MOLECULAR MATERIALS FOR ELECTRONIC DEVICE APPLICATION: A CONDUCTIVE POLYMER POLY(3,4-ETHYLENEDIOXYTHIOPHENE/)/POLY(STYRENESULFONATE) (PEDOT/PSS)

The process of interfacial charge injection is of fundamental importance in several types of organic electronic devices, such as in organic photovoltaics (OPVs) and organic light emitting diodes (OLEDs), as it can control the electrical characteristics and/or the efficiency of the device.

In this chapter, we have applied a novel spectroelectrochemical technique, potential modulated attenuated total reflectance (PM-ATR), to study the kinetics of charge transfer processes between poly(3,4-ethylenedioxythiophene/)/poly(styrenesulfonate) (PEDOT/PSS) films and indium tin oxide (ITO) electrodes. Layers of PEDOT/PSS are frequently used to facilitate hole injection between the anode, ITO, and the light emitting layer in an OLED. This measurement cannot be performed electrochemically due to high non-Faradaic background, which is eliminated using the optical method. The charge transfer rate of PEDOT/PSS on ITO is found to be in the range of 200 – 500 s^{-1} which is the first reported measurement of interfacial charge transfer kinetics for PEDOT/PSS on ITO. For the same film, effects of organic modifier on charge transfer efficiency across the ITO/polymer layer interface have also been evaluated.

Before going into the experimental details, a basic introduction to organic electronics and conductive polymers is presented.

4.1 Introduction to Organic Electronics

For the past 20 years several new organic electronic technologies for displays (organic light emitting diodes, OLEDs) and solar energy conversion (organic photovoltaics, OPVs) have been developed. Improved understanding of organic material properties can often be implemented in novel device architectures, and therefore rapid progress in the performance and functionality of devices is expected.[209]

There are several reasons why the use of organic materials is attractive in electronic devices over silicon-based technologies. Clearly, there exists a far greater potential for large-area and low-cost applications for organics as compared to their inorganic counterparts. Organic electronic materials can be deposited at room temperature using simple, industrially applicable and solution-based techniques such as spin-coating, inkjetting, and printing (e.g. microcontact).[210] Using such techniques, it is also possible to print organic electronic materials onto a wide variety of substrates including flexible substrates.[210] Even though the product will be less expensive, to effectively compete with silicon based devices, the electronic properties of the organic materials should be optimized. Furthermore, interfaces between dissimilar materials—organic/organic and organic/inorganic—are inherent in organic electronic devices. [209] These interfaces are critical for device function and efficiency, and detailed investigations of interface science are vital for this research. Thus, the rational design of highly

functional organic electronic devices will be improved by a comprehensive understanding of phenomena at interfaces composed of organic materials. [209]

4.1.1 Organic Light Emitting Diodes (OLEDs)

The earliest report of electroluminescence (EL) from an organic material was made by Pope *et al.* in 1963, using 10-20 mm thick single crystals of anthracene sandwiched between two electrodes at voltages above 400 V (either d.c. or a.c.), however the efficiency of the device was impractical.[211, 212] Two decades later, a relatively efficient device was made by the subsequent research of Tang and VanSlyke in the Kodak Research Laboratories based on electroluminescence from multilayer thin films of small molecules.[213, 214] They sandwiched a p-type, hole-transporting molecular film of an aromatic diamine and an emitting layer of the n-type, electron-transporting metal chelate, tris-hydroxyquinoline aluminum (Alq3), between a transparent hole-injecting anode of ITO anode and a low work-function alloy of magnesium as the electron-injecting cathode.[213] These results were a substantial advance towards a practical OLED technology because it showed that this two-layer structure, purified materials, properly chosen electrodes and simple fabrication methods were adequate and permitted OLEDs to operate at voltages below 10 V for the first time.[212, 215]

EL from polymeric materials, poly(vinylcarbazole), was reported by Partridge in 1983.[216] The first polymer-based light-emitting diode (PLED) was introduced by Burroughes et al.,[217] using conjugated polymers, poly(*p*-phenylenevinylene). This study attracted considerable attention and interest in the investigation of this class of materials

as LED active materials. As a result, LEDs made with soluble conjugated polymers[218], single-layer molecular doped polymers[219] and on flexible plastic substrates with high quantum yield[220] have been demonstrated. After these early reports, tremendous research efforts were directed towards improving the efficiency and functionality of OLEDs, facilitated by a refined understanding of the individual processes leading to light emission in such devices.[209]

To better understand how these devices function and to recognize the importance of interfacial processes and interfaces for device efficiency, a brief introduction to OLED structure and operation is necessary.

A typical OLED is composed of an emissive layer, a conductive layer, a substrate, and anode and cathode terminals (Figure 4.1a). If we consider a simple two-layer design where there are two layers of organic materials, an electrical current flows from the cathode to the anode through the organic layers. Upon application of a voltage across the OLED via external power, the cathode (Al) injects electrons to the emissive layer of organic molecules and the anode (ITO) injects holes to the conductive layer. These charges migrate towards the heterojunction formed between the donor and acceptor (TPD-Alq3 or polymers). They recombine to form bound electron-hole pairs (excitons).[209] When this happens, excited states are produced that relax back to the ground state through radiative processes, and light is emitted from the transparent thin-film device, which is the OLED emission (Figure 4.1b).

a)

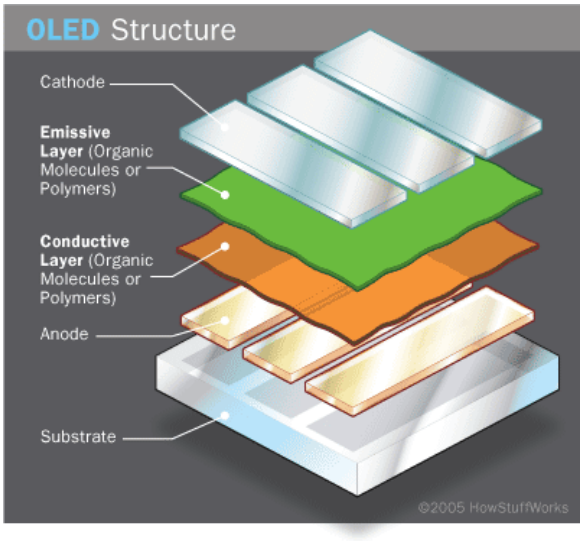

b)

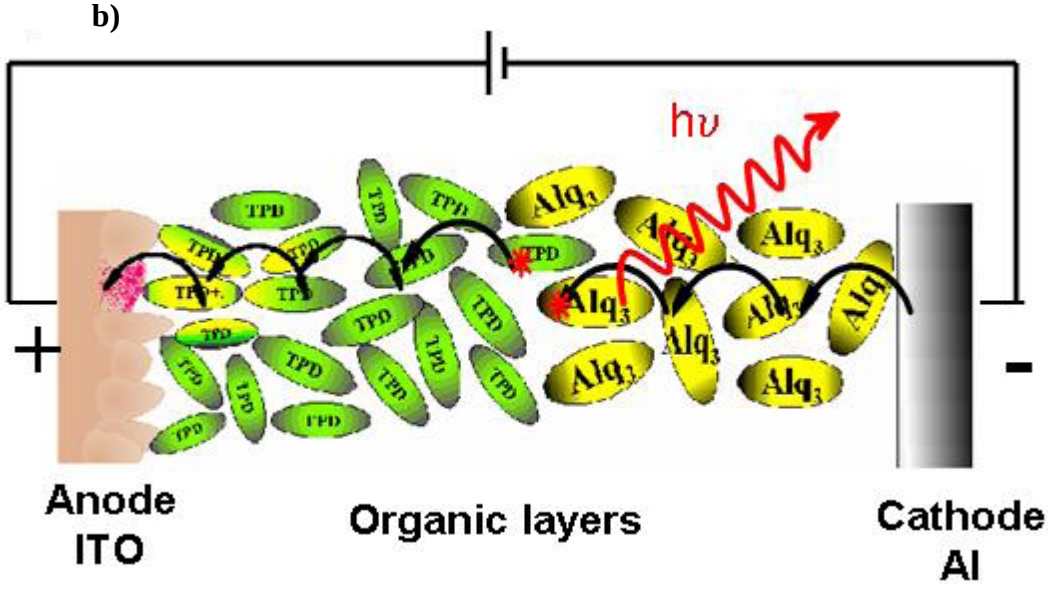

Figure 4.1 a) Side view of the layered structure of an OLED (the figure is from the following website: www.howstuffworks.com). b) A schematic of a typical two-layer OLED. [221, 222]

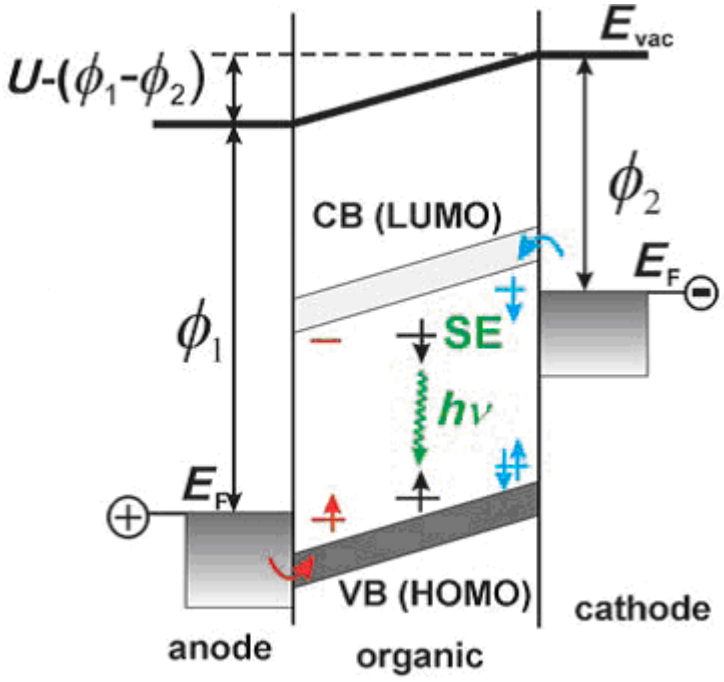

Figure 4.2 Schematic energy level diagram of single layer OLED.[209] Abbreviations are explained in the chapter.

A schematic energy-level diagram of a single-layer OLED is depicted in Figure 4.2. In a single-layer configuration, the active organic layer is sandwiched between a high-work-function ($\varphi 1$) anode and a low-work-function ($\varphi 2$) cathode.[209] Upon application of an external voltage U to the electrodes, electrons and holes are injected into the conduction band (CB) and valence band (VB), respectively, of the active layer, which is a semi-conducting polymer in a PLED. For small molecule materials, the corresponding energy levels are derived from the lowest unoccupied molecular orbital (LUMO) and the highest occupied molecular orbital (HOMO), which are usually confined to one molecule.[209] Upon injection from the electrodes, electrons and holes self-localize to form negative and positive polarons (indicated in blue and red, respectively, in Figure 4.2). When two oppositely charged polarons meet, they can form bound electron–hole pairs (excitons). A high ratio of singlet excitons (SEs)/triplet excitons (TEs) are important for light production since in most conjugated organic systems, the lack of heavy atoms in the molecular structure dictates that only SEs can decay radiatively (i.e. produce light), while phosphorescence from longer lived triplet states is highly improbable.[209] Singlet/triplet formation ratio is still being debated in the literature,[223, 224] and over 50% singlet fractions have been reported.[224, 225]

A relation for the quantum efficiency η_Q for OLEDs (number of emitted photons per injected electron) can be derived accordingly [Eq. (1)]:[209]

$$\eta_Q = \gamma \cdot \eta_{ex} \cdot \eta_{pl} \cdot \eta_{oc} \qquad (1)$$

where γ is the ratio of injected electrons and holes, η_{ex} is the fraction of excitons that can decay radiatively, η_{pl} is the efficiency of radiative decay, and η_{oc} the efficiency of light

out-coupling (the fraction of photons that actually escape the device). Power efficiency η_P (lmW^{-1}) of OLEDs is proportional to η_Q. It is also proportional to the ratio of photon energy and device voltage.[209]

To maximize OLED efficiency and performance, numerous strategies have been developed to address the above contributions such as hole-injection barrier tuning with strong molecular acceptors,[226, 227] energy-level adjustment at interfaces with ITO[228-231] and doping of organic semiconductors[232-235] that are used in these devices, etc. A detailed review on these issues was written by Norbert Koch[209] and can be found in the literature.

Since modern OLEDs and PLEDs are multilayer structures, usually containing a hole-transport layer (HTL), an electron-transport layer (ETL), and an emission layer (EL) in the middle sandwiched between the anode (ITO) and cathode, a comprehensive understanding of charge injection processes occurring at each of these interfaces is crucial as it can control the electrical characteristics and/or the efficiency of the device. This will ultimately improve the rational design of highly functional organic electronic devices.

4.1.2 Organic Photovoltaics (OPVs)

The first practical conversion of solar radiation into electric energy was achieved by Chapin et al., by use of a p–n junction type solar cell in 1954.[236] Ever since and until recently, solid state junction devices mostly made of silicon have dominated the photovoltaics (PV) field, the conversion of sunlight to electrical power. The biggest challenge of using single crystal Si based solar cells, termed as ‘Generation I’, are their

high cost resulting from the requirement for highly pure silicon crystals.[237] To reduce the manufacturing cost, 'Generation II' cells have been developed which utilize thin-film crystalline Si. Later, thin-film inorganic polycrystalline materials with higher absoptivity[238] were utilized on glass or other inexpensive substrates, instead of high quality Si wafers.[239] Even though solar cells with Si as the light absorbing materials can reach efficiencies close to 30%,[240] the biggest challenge remains its high cost.

'Generation III' PV cells, known as Organic-Photovoltaic cells (OPV), were developed after Tang and co-workers demonstrated photovoltaic activity with inexpensive small organic molecules as light absorbing materials.[241] Tang's work inspired fundamental research towards understanding the interplay of individual processes that lead to the overall function of an OPV, identifying new organic materials to efficiently absorb sunlight and new cell fabrication techniques to harness the full spectrum of solar radiation. The maximum power generation efficiency from OPV cells currently is ca. 3-6% and is limited by the presence of various barriers against efficient charge separation and charge collection.[242] Despite the low efficiency of OPVs, the emergence of these new generation cells, based on small organic molecules and conducting polymer films, offer low cost, light weight, ease of processing as well as flexibility. Thus many research groups have been exploring solutions for better device efficiencies and performance.[237, 243-245]

The basic phenomenon for photovoltaics is that photons falling on a semiconductor can create electron–hole pairs, and at a junction between two different materials, this effect can set up an electric potential difference across the interface.[237] The

working principle of an OPV can be explained in 4-step mechanism (Figure 4.3)[209]. Two organic semiconductor materials with electron-acceptor (org1, e.g. C_{60}) and electron-donor (org2, e.g. CuPc) properties are sandwiched between an anode and a cathode (typically exhibiting different work functions, Al as anode, ITO as cathode).[209, 242, 246] In process 1, absorption of photons of energy exceeding that of the band gap generates electron–hole pairs (excitons) within one of the organic layers.[209, 237] Process 2 is the diffusion of excitons towards the organic–organic (donor/acceptor) interface. In process 3, exciton dissociation (charge separation) occurs at this interface, which results in electron transfer to the acceptor material and the hole remaining in the donor. The transport of charge carriers towards respective electrodes (holes to the ITO cathode and electrons to the Al anode) takes place in process 4. As discussed in Section 4.1.1 the opposite phenomenon occurs at OLEDs,[222, 237, 247] where light is generated. (In OLEDs, holes and electrons are ejected from the ITO anode and Al cathode, respectively.)

Some of the requirements for efficient OPVs can be summarized as follows:[209] i) higher absorption coefficients within the organic layers are desirable, ideally covering the entire solar spectrum, ii) the average spacing of organic heterojunctions should be on the length scale of the exciton diffusion lengths, iii) stable exciton dissociation across the organic–organic interface into free charge carriers is necessary, and recombination of carriers should be inhibited, and iv) high charge-carrier mobility is needed, to facilitate fast transport of separated charges away from the organic-organic interface and thus minimize exciton regeneration.

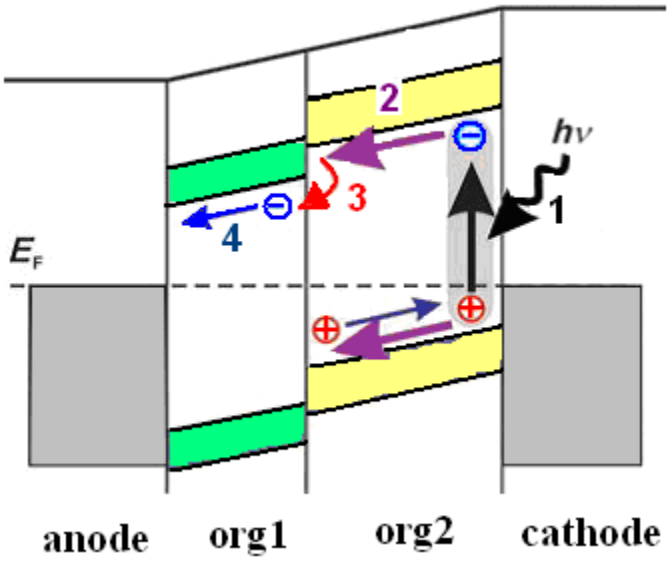

Figure 4.3 Schematic of the four-step operation principle of a bilayer OPV.[209]

The power conversion efficiency, η_P, of OPVs is the ratio of input power (by electromagnetic radiation) and output power (electrical)[209]. For a known irradiance E on an active device area A, η_P can be calculated from the maximum current (short-circuit current I_{SC}), maximum voltage (open-circuit voltage V_{OC}), and the fill factor (FF) [Eq. (2)]:[209]

$$\eta_P = (FF \cdot I_{SC} \cdot V_{OC}) / E \cdot A \quad (2)$$

FF is defined as the maximum power that can be extracted from the actual OPV divided by the product of I_{SC} and V_{OC}.

An OPV cell can be considered as a simple photoactive diode with an equivalent circuit having preferably a small series resistance (R_S less than ca. 5 $\Omega \cdot cm^2$) and a high shunt resistance ($R_P \geq 10$ $K\Omega \cdot cm^2$).[144, 248] The major limit to η_P arises from high R_S, which is a combination of linear additions of ITO sheet resistances ($R_{S,ITO}$), the resistance arising from low charge mobilities in the organic layers ($R_{TRANSPORT}$), and resistances to charge injection at electrode interfaces ($R_{S,ET}$).[144, 221]

For these devices, chemical compatibility between organic layers and electrode surfaces (both anode and cathode) is important since fast and efficient charge transfer at the electrode-thin film interface will lead to better device performance. Understanding and enhancing of charge transfer rates (k_{ET}) at the ITO interface is also predicted to decrease R_S, since $R_{S,ET}$ is proportional to $1/k_{ET}$.[144, 221, 249, 250]

4.2 ITO Surface Modification and Change of Work Function

4.2.1 ITO Surface Treatments and Modifications

Most of the electrode modification started to appear in the literature in 1970's when tin oxide, metal, glassy carbon and graphite electrodes were modified with a variety of different surface modifiers such as silanes, acid chlorides, alkenes, amines[250-256] to produce electrode surfaces with predictable surface compositions and chemistries. Defining and characterizing a predictable and reproducible surface is the first step for surface-based electrochemical studies which then have led to further applications of these surface modifications such as electrochemical sensors.[257]

The modification of transparent conducting oxide thin films, such as indium-tin oxide, continues to be of interest as these materials are increasingly used in electroanalytical sensor platforms,[18, 258] as well as in emerging OLED and OPV technologies.[144, 206, 259-263] As the electrode for the devices, ITO has attracted intensive interest in recent years because of its unique characteristics of good electrical conductivity (maximum at $1 \times 10^4\ \Omega^{-1}\ cm^{-1}$), high optical transmittance over the visible wavelength region (~ 90 %), excellent adhesion to substrates, and easy patterning ability.[221, 263, 264] It can also be deposited as thin films on glass surfaces and flexible substrates.[265, 266] However there are serious drawbacks to the ITO as an electrode in OLEDs and OPVs.[206, 257] For example, there have been reports in the literature of indium migration into the organic layers of OLEDs after device operation.[267, 268] Physical compatibility or wetting of an organic molecule on the oxide is essential for charge transfer, however ITO is chemically incompatible with non-polar organic materials due to

its hydrophilic nature.[221] ITO surface chemistry is also chemically a heterogeneous (not only microscopically, but also on an individual sample level) and varies in chemical composition as-received from the manufacturer and after exposure to cleaning treatments, leading to some problems with reproducible device performance.[257, 269] It has been shown that rate constants for solution probe and/or thin films can differ up to an order of magnitude on ITO samples from different suppliers, samples from the same supplier but different batch numbers, and even between individual sheets of the same batch numbers.[269] At the ITO surface, the indium oxide lattice is truncated, which promotes hydrolysis, forming InOOH and $In(OH)_3$ species.[206] $In(OH)_3$ has low solubility and forms electrically passivating layers[257, 270] therefore ITO may be described as a partially blocked electrode. Some studies indicate that freshly sputtered ITO samples contain low levels of inactive materials such as polymeric In(OH)x and carbonaceous material while certain cleaning agents increase the amount of these materials found on the surface.[206, 269, 271-274]

All of these drawbacks have motivated numerous studies to modify ITO electrodes prior to various organic thin film device applications.

Multiple modification strategies for transparent conducting oxide electrodes have been developed over the years to increase sensitivity and speed of potentiometric response, enhance the wettability of the oxide surface toward non-polar organic materials, improve current density, turn-on voltage, efficiency, lifetime and rates of charge injection to these materials in both OLEDs and OPVs.[221, 275-283] Various surface coating treatments such as: i) the covalent attachment of silane-modifiers, ii) strong chemisorption of molecules such as carboxylic acids, phosphonic acids, thiols, etc., iii)

physisorption and/or electrochemical growth of poly(electroytes), including conducting polymers such as the poly(anilines) and poly(thiophenes), have been proposed. [144, 206, 221, 259, 262, 284, 285]

Chemical treatments with various acids (phosphoric acid, hydrochloric acid) and bases (tetrabutylammonium hydroxide, sodium hydroxide) [276, 281, 286] and different plasma treatments (oxygen, argon, nitrogen, air, SF_6 plasma) [275, 277, 280, 283] have also been investigated. Other methods such as mechanical polishing[281, 287] and annealing[286, 287] have also been reported.[278]

It was shown that oxygen plasma treatment of ITO greatly improves the ITO surface properties, enhances the efficiency, performance and lifetime of electroluminescent devices.[288] Using various surface characterization methods such as atomic force microscopy (AFM), X-ray photoelectron spectroscopy (XPS), contact angle, surface energy measurements and sheet resistance, etc., these improvements are attributed to smoother surfaces, lower sheet resistance, higher work function, and higher surface energy and polarity of the ITO substrate.[263, 278]

4.2.2 Surface Modification Effect on Work Function

In organic electronic devices, in order to achieve efficient charge transfer (hole or electron injection), the barrier height between the work function of the electrode and the highest occupied molecular orbital (HOMO) or the lowest unoccupied molecular orbital (LUMO) of a given organic material, respectively, should be minimized and effective contact areas between the electrodes and the organic layers should be maximized.[289, 290]

Chemical modifications of the oxide bottom contact, typically ITO, have been applied to tune the effective surface work function (the energy required to move an electron from the Fermi level to the vacuum level), and if possible, to control the wettability of such oxides toward non-polar organic layers.[206, 228, 271, 291, 292]

Depending on the commercial source and surface pretreatment, the work function of ITO varies from ca. 4.2–4.9 eV.[228, 272, 291, 292] This low surface work function, however, is often not sufficient and desired for charge injection in contact with many organic hole-transport materials and results in increased series resistance in the organic electronic device through a reduced rate of hole transfer between ITO and the organic film.[291, 293]

Modifying ITO to manipulate the work function has been investigated by various cleaning and etching procedures coupled with adsorption and covalent attachment of small molecules. These approaches to include plasma (air, Ar, oxygen, SF_6) treatment, UV ozone treatment, use of a PEDOT/PSS conducting polymer layer, or use of metal oxide nanoparticles.[271, 272, 277, 289, 294, 295] The surface composition and surface work function, however, rapidly changes and decreases, respectively, under ambient conditions, primarily due to hydrolysis of the ITO surface.[291]

The work function of ITO can also be altered by the chemisorption of a molecule with an interface dipole as a result of the orientation of the molecular dipoles.[269, 289, 293, 296] If we define the work function of an untreated ITO electrode, Φ_0, as the difference between the vacuum level and the Fermi level, E_F, modifying ITO surface with polar molecules with dipole moments, μ, pointing towards the electrode will result in an interfacial electric field directed from the electrode surface. Due to this electric field, the

vacuum level outside the electrode will be increased. Since the Fermi level of the system is not changed, a higher effective work function for the modified electrode will be obtained.[296] The work function of the electrode will be decreased if molecules with the opposite direction of μ are used.[296]

"Work function tuning" is reported in the literature by the application of reactive moieties containing functional groups such as -COOH, -COCl, $-SO_2Cl$ and $-PO_2Cl_2$.[269, 297] Binding groups such as silanes, siloxanes and phosphonic acids have been used to modify ITO surfaces and improve the performance of organic electronic devices.[230, 289]

The aim for surface modification is not only to alter the work function of the electrode but also influence both the polarity and free energy of the oxide surface. Armstrong et al.[144] used carboxylic acid-substituted small molecules to modify ITO before the surface is further modified by electrochemically growing a thin layer of PEDOT/PSS. They obtained higher short-circuit currents in PV devices using these chemically modified interfaces which was attributed to better wettability of the organic layers compared to the unmodified ITO surface, and also enhanced charge transfer between the ITO anode and organic layers using the intermediate PEDOT/ PSS layer.[144]

Phosphonic acids have been developed as oxide surface modifiers.[289, 290, 298-300] Phosphonic acids are thought to produce a more robust modification layer relative to chemisorbed carboxylic acids, especially after the heat annealing to maximize the number of P-O bonds to the metal oxide lattice.[290, 300] They have superior bonding ability with hydroxyl terminated ITO surfaces.[301, 302]

Recently, Sharma et. al[302] used organic phosphonic acid modifiers comprised of a phosphonic acid moiety as the anchoring group covalently bound to various dipolar functional groups to vary both the ITO work function and surface energy. They showed that the use of various surface modifiers or air plasma treatment leads to an increase of the work function of ITO, from values of 4.50 eV up to 5.40 eV, without affecting the values of standard PV device parameters.[302]

Similarly, Paniagua et. al has performed an extensive study of ITO electrodes modified with phosphonic acids.[290] Using XPS/UPS and contact angle measurements, they showed that for ITO surfaces modified with 3,3,4,4,5,5,6,6,7,7,8,8,8-tridecafluorooctyl phosphonic acid (FHOPA), and to a lesser extent with pentafluorobenzyl phosphonic acid (PFBPA), the high work function obtained by oxygen plasma cleaning can be maintained after modification, while decreasing the polar component of surface energy.[290] They concluded that the ability to tune the wetting properties while maintaining high work functions may lead to higher device performances and stability because of the good adhesion between the electrode and the nonpolar layers and decrease in the interactions of these interface with atmospheric water after surface modifications.[290]

4.2.3 Surface Modification Effect on Charge Injection

It is known that significant barriers to charge injection may exist at interfaces between dissimilar materials such as between organic and inorganic materials.[230] Such junctions are found at the anode and cathode of OLEDs and OPVs that comprising

conjugated organic materials.[230] It is proposed that charge transport across interfaces can be enhanced by attaching a functional organic molecule onto ITO anode therefore significant amount of research has been reported in the literature on this subject.[303-309]

As explained in Section 4.2.2, surface dipole manipulation can be used to tune the work function of the electrode. It can also change the efficiency of hole injection from ITO into an organic layer.[310] The hole injection efficiency has been shown to decrease or increase by ITO surface modification of phosphonic acids substituted with electron donating or withdrawing groups, respectively.[303, 306, 311]

Using another modifier, silane-derivatized hole transport layer, on ITO, it was found[312] that the light output of the OLEDs increased proportionally with the thickness of the film, and device current density was enhanced (less than an order of magnitude) versus unmodified ITO.

Charge injection properties have also been modified by introducing strong electron acceptor, tetrafluorotetracyanoquinodimethane (F4-TCNQ) between anode and hole transport layer.[313, 314] In this case, hole injection density was improved in simple devices by several orders of magnitude versus the untreated anode (Au[314] or ITO[313]).

Hanson et. al[230] showed that barrier to hole injection into the hole transport layer can be reduced by the phosphonate monolayer covalently bound to ITO and subsequently doped with an electron acceptor. It was reported that this method has decreased the operating voltage of the device and increased the charge carrier density at the interface between the doped phosphonate-modified ITO and hole transport layer (about 10 000-fold compared to unmodified ITO).[230]

One of the major losses of PV power through the short circuit photocurrent, J_{SC}, originates from high values of series resistance, R_S.[144] The reasons for arising R_S are contact resistances, charge flow resistance within the conductive oxide film, resistances arising from low charge mobilities within the thin organic layers, and resistances arising from low rates of charge transfer at both the anode and cathode interfaces.[144] The portion of R_S contributed by slow heterogeneous charge transfer, $R_{S,ET}$ is proportional to $1/k_{ET}$, where k_{ET} is the heterogeneous charge transfer rate coefficient (e.g. for oxidation/hole injection at the ITO/organic interface) [315, 316] Armstrong et. al compared power conversion efficiencies and R_S of PV cells with a chemisorbed monolayer of the small molecule modifier, e.g. 3-thiophene acetic acid (3-TAA) or Ferrocene dicarboxylic acid ($Fc(COOH)_2$), prior to addition of the poly(3,4-diethoxy-thiophene:poly(styrene-sulfonate), PEDOT/PSS, layer vs. PV cells made on unmodified ITO.[144] They found that the power conversion efficiency increased by ca. 40%, up to 1.14% for 3-TAA-modified ITO cells. R_S is found to be decreased by half by the prior 3-TAA modification of the ITO substrate. ITO modified with chemisorbed monolayers of $Fc(COOH)_2$ showed comparable results. They conclude that the modification of the ITO surface with electroactive small molecules such as $Fc(COOH)_2$ and 3-TAA provides for better wettability of organic layers to the polar ITO surface and enhanced electrical contact (lower series resistance, R_S) between the ITO anode and organic layers.[144] It is stated that the ITO surface modifiers that they have used[144] can increase electron transfer rate constant (since $R_{S,ET}$ is proportional to $1/k_{ET}$) , by increasing the number of active sites for

ET on the ITO surface, and possibly by lowering the reorganization energy for ET at the organic layer/ITO interface.[316]

Similarly Carter et. al[284] showed that whether a conductive polymer modifier layer such as PEDOT/PSS is used or not, ITO modification through chemisorption of small molecule carboxylates such as $Fc(COOH)_2$ and 3-TAA (i) creates a less polar oxide surface, (ii) slowly etches hydrolyzed indium oxide species from the near-surface region to enhance electroactive area, (iii) enhances the rate of electron transfer to a solution probe molecule, and (iv) significantly lowers the leakage currents (several orders of magnitude) and raises the overall efficiency in conventional vacuum deposited OLEDs. They attributed some of the enhancement in solution-probe electron-transfer rates to the slow removal of hydrolyzed indium oxides from the near-surface region due to etching of the surface by surface modification.[284]

4.3 Conductive Polymers: PEDOT/PSS

4.3.1 Introduction to Conductive Polymers

The field of conductive polymers has grown enormously[317-319]since the discovery in the late 1970s that the oxidized polyacetylene could attain a high conductivity by Heeger et al.[320, 321] In 1979, the electrochemical doping of conducting polymers was also demonstrated by the same group.[322] As a proof of the maturity of this field, the Nobel Prize in Chemistry in 2000 was awarded to its pioneers, Alan Heeger, Hideki Shirakawa, and Alan MacDiarmid.[323]

After the first demonstration that poly(aniline) has extensive charge delocalization and its conductivity lies in the metallic regime,[324] research based on the electrochemistry of conducting polymers has impacted the development of OPVs and OLEDs.[144, 259, 262, 325, 326]

The insertion of an intrinsically conducting polymer layer between ITO and the luminescent layer has been shown to be very favorable for OLED performance.[209]

Conducting polymers possess electrochromic properties[327] that are affected by changes in the external medium such as pH, counterion and oxidation state.[328] Also conducting polymers decrease the surface roughness of electrode-organic contacts, stabilize electrode/organic interfaces and allow tuning of the work function.[329] They are also highly used as electrode modifiers since i) simple methods are used for their synthesis ii) various thin film deposition methods are available iii) the monomers can be modified to alter some of their functions [250, 317, 323, 330] All of the mentioned characteristics of these materials have lead to further increase in the efficiency of molecular electronic devices.

Of the many interesting conducting polymers that have been developed over the past 30 years, those based on polyanilines, polypyrroles, polythiophenes, polyphenylenes, and poly(p-phenylene vinylene)s have attracted the most attention.[317, 319, 330] Figure 4.4 shows a few examples of common conducting polymers.[221, 330] Among these polymers, the polyaniline-based materials stand out for their ability to form processable conductive forms at relatively low cost and in bulk amounts.[331, 332] However, possibility of benzidine moieties present in the polymer backbone, which might yield carcinogenic products upon

degradation, is a big drawback in polyaniline research.[332] Even though aromatic polypyrrole, polythiophene, and poly(p-phenylene vinylene) do not yield in toxic by-products, their disadvantage is insolubility and non-processibility.[332] To overcome these problems and still maintain both the physical and electronic properties, many derivatives of these polymers have been developed that carry alkyl, alkoxy, and other substituents along their backbones.[333-336] Although some of the properties of the parent systems are frequently retained in the modified polymers, often the electronic properties are degraded relative to the parent.[332]

In addition to doped polyaniline,[337, 338] the prototypical conducting polymer that is used in many applications today is poly(3,4 ethylenedioxythiophene)/poly(styrenesulfonate)[271, 339] abbreviated as PEDOT/PSS. This conducting polymer will be the focus of the work presented in this Chapter.

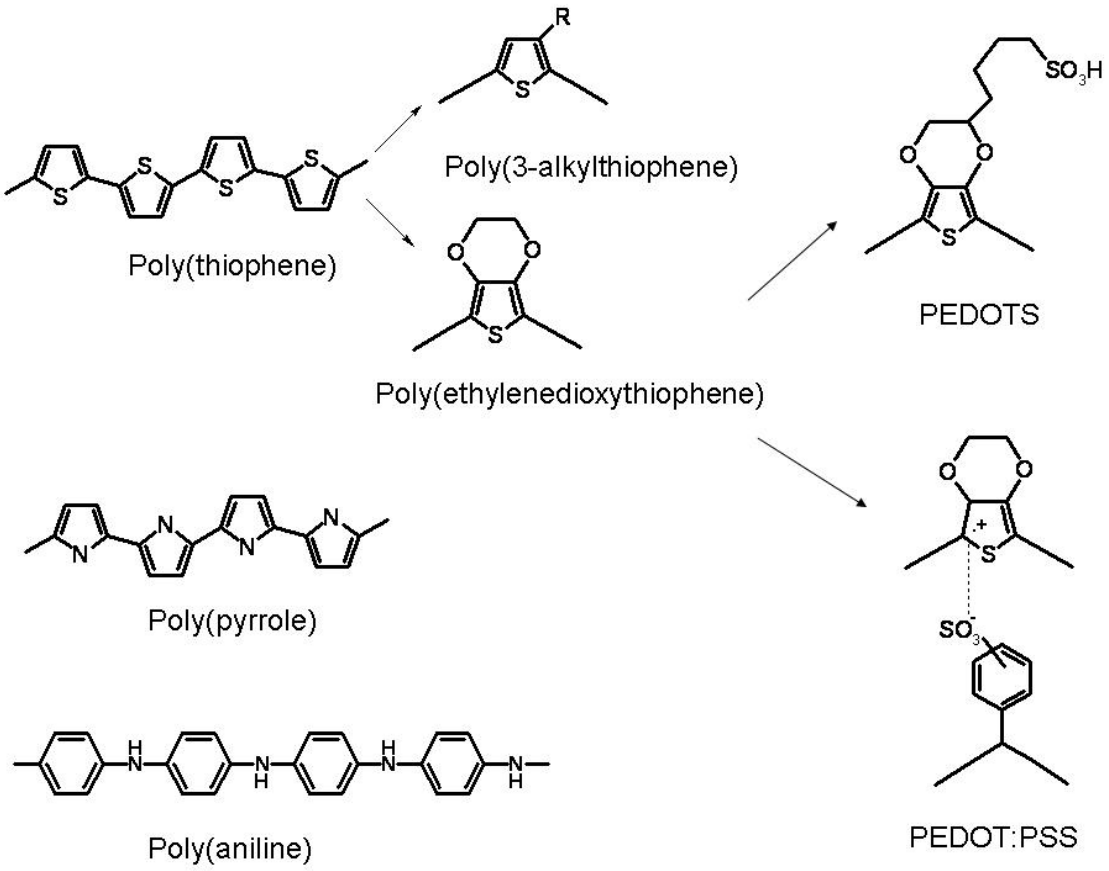

Figure 4.4 Structures of common conducting polymers used in organic electronic devices such as OPVs, OLEDs and electrochromic displays.[330]

4.3.2 Properties and Applications of PEDOT/PSS in Organic Electronics

In late 1980s, scientists at the Bayer AG research laboratories in Germany developed a new polythiophene derivative, poly(3,4-ethylenedioxythiophene), often abbreviated as PEDT or PEDOT.[332, 340] Even though PEDOT was initially found to be an insoluble polymer, it exhibited some very interesting properties such as having high conductivity (ca. 300 S/cm), highly transparent as a thin, oxidized film, and highly stable in the oxidized state.[341, 342] This material has found numerous applications such as anti-static coatings[332], transparent polymer electrodes for capacitors and photodiodes [343, 344]and biosensors.[345] An extensive review of PEDOT and derivatives, their synthesis, chemical, optical and electrical properties can be found in the liteature.[332]

By using poly(4-styrenesulfonic acid) (PSS) as a charge-balancing dopant during polymerization of PEDOT, the solubility problem is circumvented and a water-soluble polyelectrolyte blend (PEDOT/PSS) that preserves many properties of PEDOT can be made (Figure 4.5a).[332, 346] In this polymer mixture, positive charges on the PEDOT are stabilized by negative charges on PSS.[209] PEDOT/PSS, known under its commercial name BAYTRON P (P stands for polymer), has good film-forming properties, high conductivity (ca. 10 S/cm), high visible light transmission, and excellent stability.[347, 348] Detailed research related to synthesis, mechanical, electrochemical and spectroelectrochemical characterization of PEDOT/PSS can be found in the literature.[349-353] In this Section, a brief explanation of the properties of PEDOT/PSS and its applications will be given.

At present, ITO (after various surface treatments) and PEDOT/PSS are the most frequently used anode materials in OLEDs.[209] PEDOT/PSS is used as a hole injection layer, or anode buffer layer, in an OLED and increases efficiency by reducing the energy barrier across the ITO/hole transporting layer interface. As a hydrated gel, it has been shown to smooth the micro roughness of the ITO surface, reducing the occurrence of electrical short circuits.[354]

PEDOT/PSS forms small (a few nanometers) core–shell agglomerates in aqueous dispersions, where PSS forms the shell due to the hydrophobicity of PEDOT, whereas PSS is hydrophilic.[209] While forming a thin film, highly conductive PEDOT-rich domains are separated by insulating PSS-rich domains. Thus, by varying the ratio of PEDOT/PSS it is possible to adjust the overall conductivity of thin films.[355-357] For PEDOT/PSS thin films, a range of work functions has been reported from 4.7 to 5.4 eV.[271, 294, 358-360] Comparable to literature for electropolymerized PEDOT[361, 362] band gap energy of PEDOT/PSS is ~ 1.6 eV.[326, 352, 363]

As recently discussed in several papers, the insulating PSS-rich surface of PEDOT/PSS films has electron blocking properties.[364-366] In most OLEDs based on polymers, upon application of an increasing driving bias, electrons are injected first because the electron injection barrier (EIB) is lower than the hole injection barrier (HIB).[366] The initially injected electrons are hindered from entering the conducting polymer layer due to the surface insulating PSS-rich phase (Figure 4.5b).[209] The accumulation of electrons at the interface facilitates efficient hole injection because of the

increased electric field at that interface. As a result, almost every injected hole can find an electron to form an exciton, which can then recombine.

Figure 4.6 show electrochemical characterization of PEDOT/PSS on ITO using cyclic voltammetry.[352] The large cathodic peak at −0.74 V and the corresponding anodic peak at −0.16 V are due to the change in the oxidation state of the polymer during the first cycle. Since PEDOT/PSS is a cation exchanger under most conditions, the excess of immobile sulfonate groups obtained as a consequence of reduction or partial reduction of the oxidized PEDOT leaves a charge balanced by mobile cations.[351] This could explain the change exhibited in the voltammetric path from the first to second cycle during continued cycling.[352] The non-Faradaic background current needs to be considered since it is hard to distinguish from the Faradaic current by electrochemical methods.

Devices utilizing this polymer film generally show higher current flow under forward bias, and lower leakage currents under reverse bias versus devices built on ITO alone. However, there is still considerable speculation why ITO electrodes utilizing PEDOT/PSS overlayers exhibit favorable charge injection properties.[269]

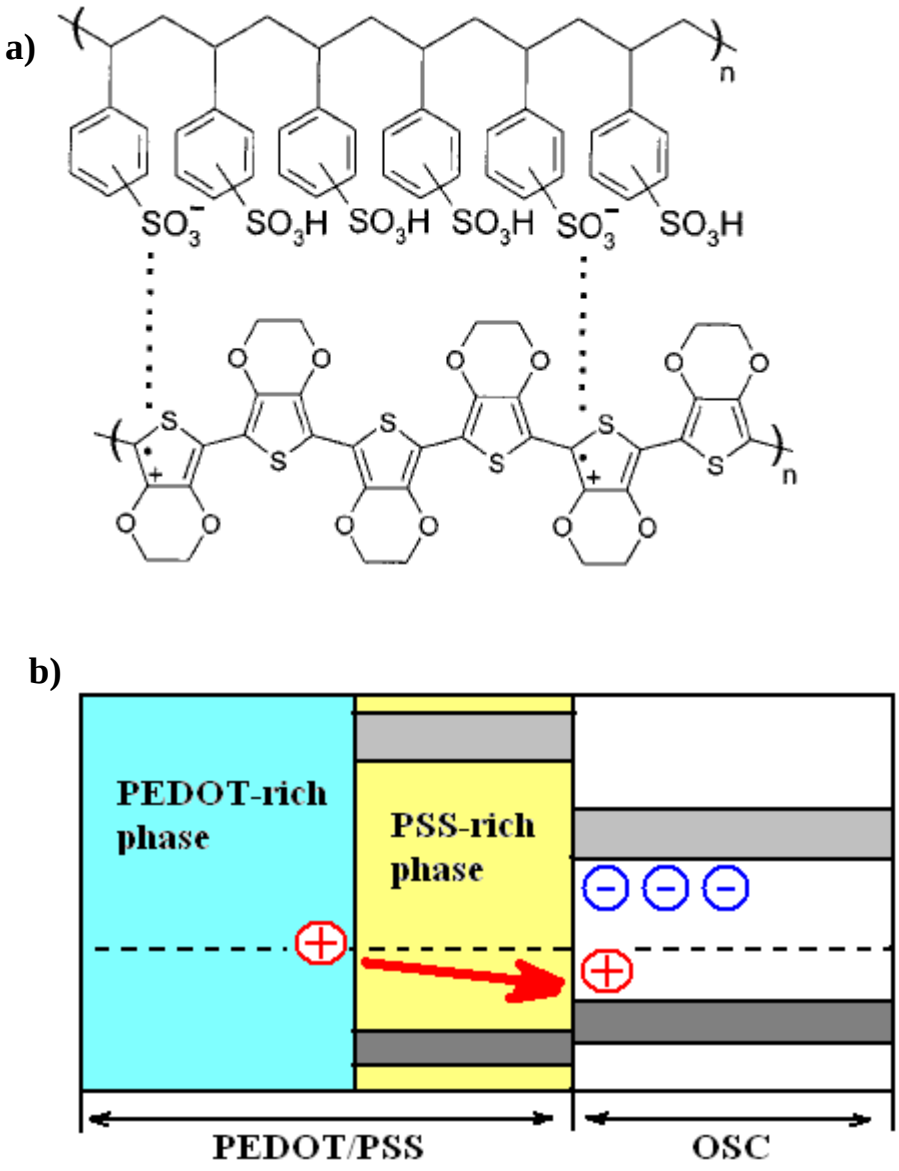

Figure 4.5 a) Chemical structure of conducting polymer mixture (PEDOT/PSS)[332] b) Electron blocking in an organic semiconductor (OSC) at the PSS-rich surface of a PEDOT/PSS electrode.

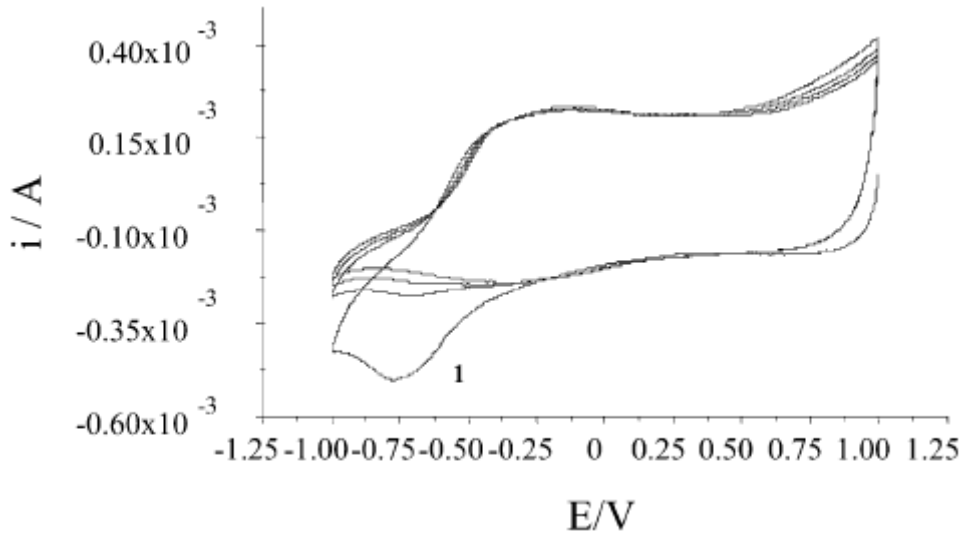

Figure 4.6 Electrochemical characterization of a PEDOT/PSS film on ITO obtained in the potential range from +1 to −1 V at a scan rate of 0.1 V/s. The curves marked with 1 correspond to the first voltammetric cycle.[352]

4.4 Motivation

Improving our understanding of interfacial charge injection processes is one of the key factors needed for development of highly efficient OLEDs and OPVs as these processes control the electrical characteristics of the device.

Currently, studies to characterize interfacial charge injection processes in OLEDs and OPVs typically measure the efficiency of completed thin-layer devices, and usually neglect other factors which may contribute to the measurements.[269] Interface chemistries are complex and assigning observed differences in performance to a particular characteristic of a complete device is very difficult.[269] Therefore, in order to accurately describe the effects of each component in a device, isolation of processes at each interface such as electron transfer kinetics, stability, material impurities, complementary electrode effects, etc. is necessary and independent measurements are important.

In this study, we have focused on charge transfer kinetics between PEDOT/PSS polymer films and ITO electrodes using PM-ATR spectroscopy. The optical method eliminates the high non-Faradaic background and allows measurement of charge transfer kinetics. In this research, charge transfer rate constants have been measured for PEDOT/PSS films for the first time. The effect of a surface modifier, ferrocene methyl phosphonic acid (FMPA), and different surface treatment methods on PEDOT/PSS charge transfer rates have also been evaluated. Characterization of charge transfer kinetics with respect to surface modifiers and/or surface treatments is expected to lead to more effective strategies for designing high performance devices.

4.5 Experimental

4.5.1 Substrate Cleaning and Different Surface Treatments

The ITO-coated planar electrodes used in these studies were obtained from Colorado Concept Coatings Limited, with a sheet resistance of ca. 18 Ω / cm.[2] They were cleaned by scrubbing with a 1% Alconox solution for 1 min and then sonicating for 15 min each in water, 1% TritonX-100, water, and ethanol. After these steps, clean ITO slides were further cleaned before the PEDOT/PSS film deposition, by either i) low temperature air plasma cleaning (Harrick model PDC-3XG) for 5 min[144] at 30 W, ii) or O_2 plasma cleaning (Harrick model PDC-3XG) for 5 min[144] at 30 W, iii) or etching with 5.5 M HI for 10 seconds.

4.5.2 Preparation of Spin Coated PEDOT/PSS

An aqueous dispersion of PEDOT/PSS conductive polymer (OLED grade), BAYTRON P VP AI 4083 from H. C. Starck, was used for this study. Barnstead Nanopure (18 MΩ-cm) water was used for any required dilutions.

Bulk PEDOT/PSS (as it is purchased from the company) is diluted with an equal volume nanopure water and sonicated for 5 minutes in a water bath prior to spin coating. It is filtered through 0.45 μm Millex-HV PVDF-Membrane filters onto cleaned ITO slides. The film is made by applying 3000 rpm for 1 min with the spin coater (Integrated Technologies Inc.). The film is either i) directly used after this step or ii) it is annealed for 1 hour at 100 ^{0}C in a vacuum oven. The ATR cell is assembled with the slide and filled with 0.1 M $LiClO_4$ in AcCN for ATR experiments.

4.5.3 Ferrocene Methyl Phosphonic Acid (FMPA) Modification of ITO

FMPA (Figure 4.7a) has been used as a modifying monolayer to assess if charge transfer rates for PEDOT/PSS are altered with respect to the unmodified ITO surface.

Prior to preparing spincoated PEDOT/PSS films, 1 mM FMPA is adsorbed onto cleaned ITO slides from ethanolic solution for 20 minutes. For all the different ITO cleaning treatments, the electroactive surface coverage close to a monolayer coverage (~ 2×10^{-10} mol/cm^2) is measured by integrating the cathodic peak of a cyclic voltammogram of adsorbed FMPA on ITO (Figure 4.7b). Prior to the PEDOT/PSS deposition, the slides were rinsed with ethanol and dried with nitrogen. After PEDOT/PSS deposition the obtained film is either i) directly used or ii) it is annealed for 1 hour at 100 ^{0}C under vacuum oven. After that, the ATR cell is assembled for the spectroelectrochemical measurements.

4.5.4 Atomic Force Microscopy (AFM)

The morphology and root-mean-square (rms) roughness of PEDOT/PSS films were obtained from phase and height images collected using an atomic force microscope (Model-Nanoscope, Dimension 3100, Digital Instruments Santa Barbara CA). The images were collected in tapping mode with ultrasharp silicon cantilevers (Model TESP-7). Images were obtained in ambient air at scan rate of 1 Hz. The AFM images reported here are either 1 μm x 1 μm scans or 5 μm x 5 μm scans. The thickness of PEDOT/PSS films was obtained from height images by scratching the surface of the film with a sharp, clean razor blade, creating a narrow PEDOT/PSS-free surface. The border between the

film and film-free regions was included in the AFM scan. The edge of a razor blade was used to completely remove the film in this area without scraping the ITO substrate. The step height was obtained by making a line scan using the section analysis tool and measuring the vertical distance by locating the arrows in the center of the “scratch” on the substrate and a flat region on the film (away from the ridges), respectively. The values reported here are averages of several different regions. The minimum thickness measured was at least 3x greater than the rms roughness of the film and substrate.

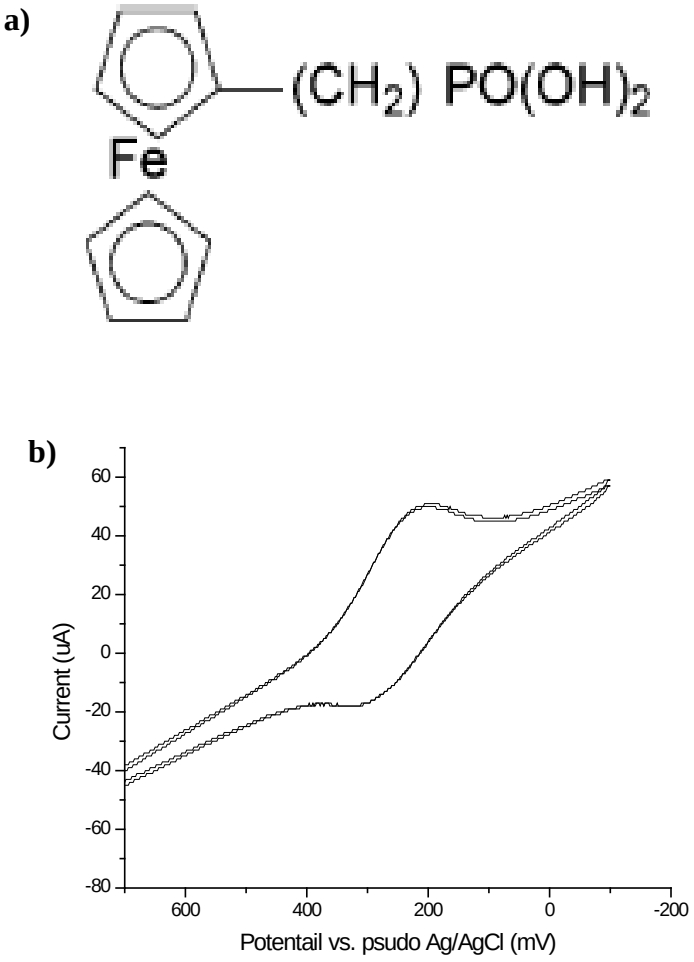

Figure 4.7 a) The chemical structure of FMPA. b) Cyclic voltammogram of FMPA adsorbed to O_2 plasma cleaned ITO without heat annealing. The electroactive surface coverage based on integrated cathodic peak is ~ 3 x 10^{-10} mol/cm^2.

4.6 Results and Conclusion

4.6.1 Estimated Film Thickness of PEDOT/PSS Films and AFM Images

Figure 4.8 shows AFM images of spincoated PEDOT/PSS films that were obtained from tapping mode AFM on HI etched ITO. Prior to AFM imaging, PEDOT/PSS films were annealed at 100 ^{0}C under vacuum. Figure 4.8a and b are examples of height (for roughness analysis) and linescan (for thickness analysis), respectively, for this film.

From images obtained on different samples and analysis of various regions on scratched films, the estimated thickness of spincoated PEDOT/PSS films is ca. 50 nm which is relatively close to the literature value of 60 nm.[144, 221] The rms surface roughness of these films is ~ 2 nm.

4.6.2 Spectroelectrochemical Results

Potential controlled ATR spectra of PEDOT/PSS films were acquired by stepping the potential from -400 mV to + 1300 mV (100 mV intervals) to determine the wavelength region and estimate the optical switching potential (E_{dc}) for PM-ATR experiments. Representative spectra of spincoated and heat annealed films on HI etched ITO are shown in Figure 4.9. Large changes in absorbance occur between 550 and 750 nm at potential between 0 and -400 mV. This is due to molar absorptivity differences between oxidized and reduced forms of PEDOT/PSS. Therefore, HeNe laser (632.8 nm) was selected as a light source for PM-ATR measurements.

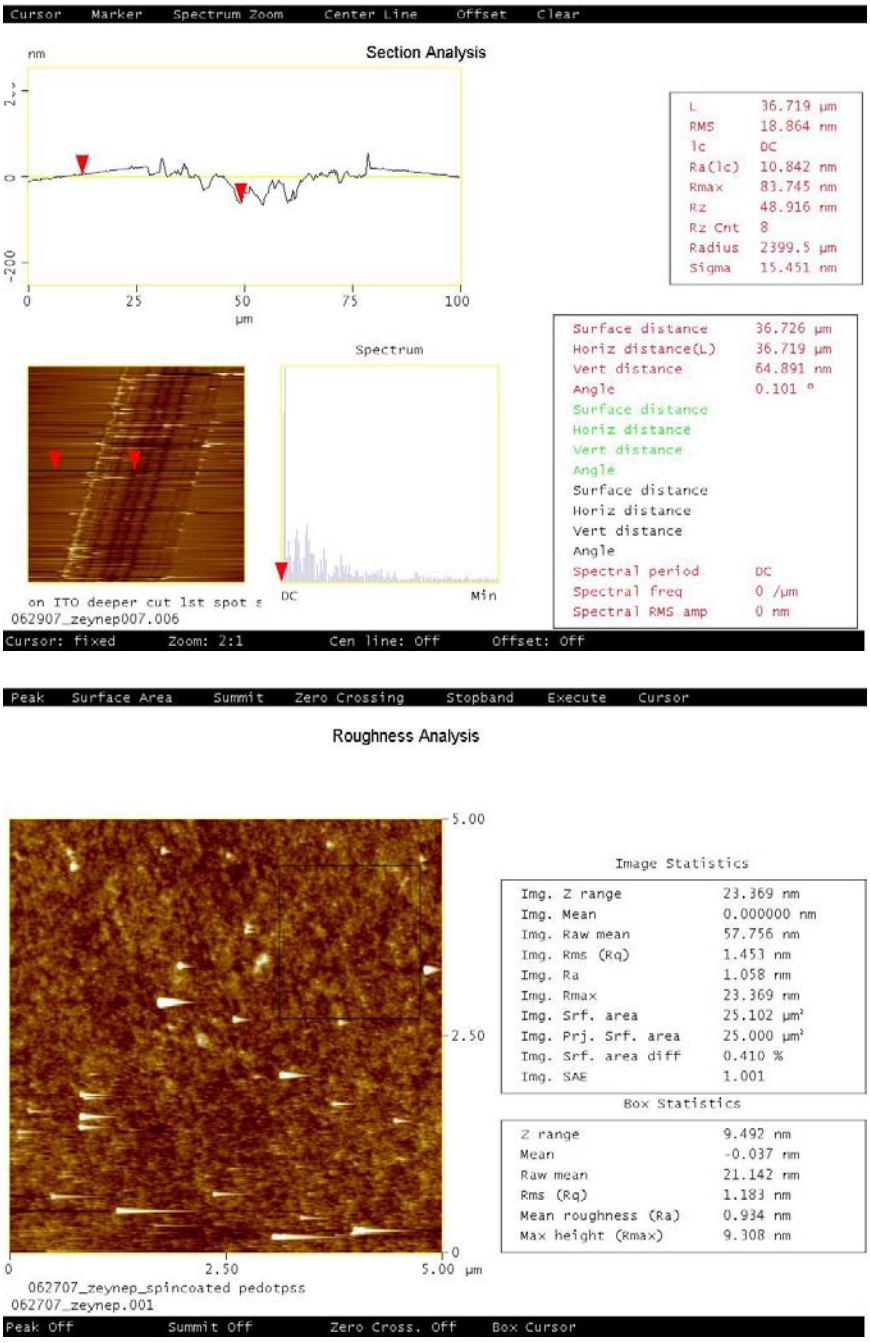

Figure 4.8 AFM images of spincoated PEDOT/PSS films on ITO obtained from tapping mode AFM. a) An image from section analysis of PEDOT/PSS that was scratched with a razor blade. b) An image from roughness analysis of PEDOT/PSS.

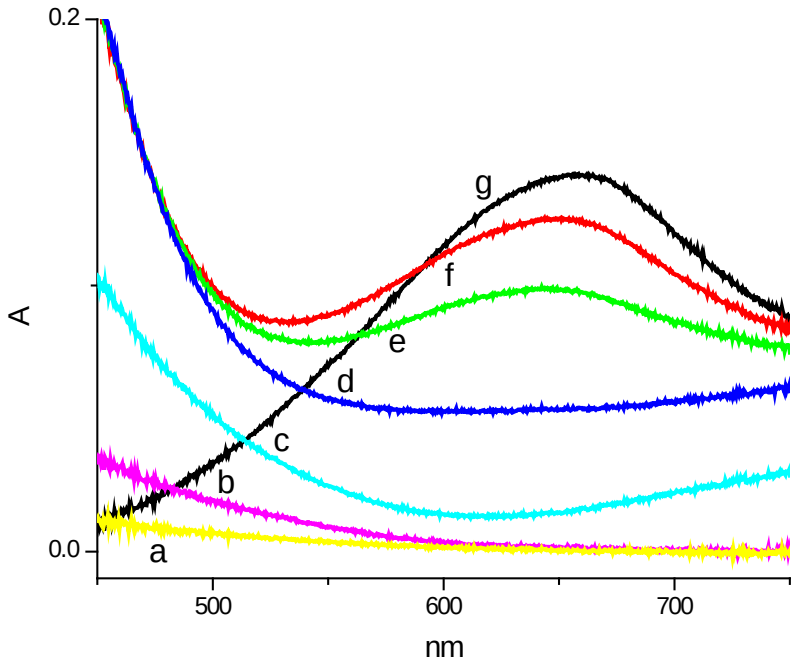

Figure 4.9 ATR spectra of a PEDOT/PSS film at different applied dc potentials: +1200 mV (a), +1000 mV (b), +400 mV (c), 0 mV (d), -200 mV (e), -300 mV (f) and -400 mV (g). Spectrum obtained at +1300 mV applied potential was used as the blank.

Figure 4.10 shows a representative optically detected voltammogram of the same type of PEDOT/PSS film (spin coated, heat annealed and on HI etched ITO). It was acquired by scanning the potential between -300 mV and +1300 mV at 5 mV/s while applying an ac potential modulation of ±12 mV at a frequency of 1 Hz. Oxidation and reduction of PEDOT/PSS on ITO alters the molar absorptivity of the film and therefore R_{ac} varies. The highest change in molar absorptivity results in the maximum change in R_{ac} and this occurs at an E_{dc} value of approximately -213 mV (most E_{dc} values were found in the range of -150 to -230 mV for independently prepared films). The E_{dc} value of -213 mV was selected for PM-ATR experiments based on these data.

The modulation amplitude (E_{ac}) used in PM-ATR experiments was ±30 mV, and was selected based on an experiment in which R_{ac} was measured over a range of modulation amplitudes (4 mV to 50 mV) centered around E_{dc} at a fixed frequency of 1 Hz (data not shown).

PM-ATR experiments were performed on independently prepared PEDOT/PSS films on differently cleaned ITO surfaces with and without a surface modifier. The modulation frequency was gradually increased from 0.1 Hz to 1000 Hz, with E_{dc} = -213 mV and E_{ac} = 30 mV. The in- (X) and out-of-phase (Y) portions of R_{ac} were measured at each frequency, then the values of R_{ac} and θ were normalized. X_{norm} and Y_{norm} values were then calculated and plotted.

For these films, C_{dl} and R_s were also determined separately using impedance spectroscopy and charge transfer rates were calculated.

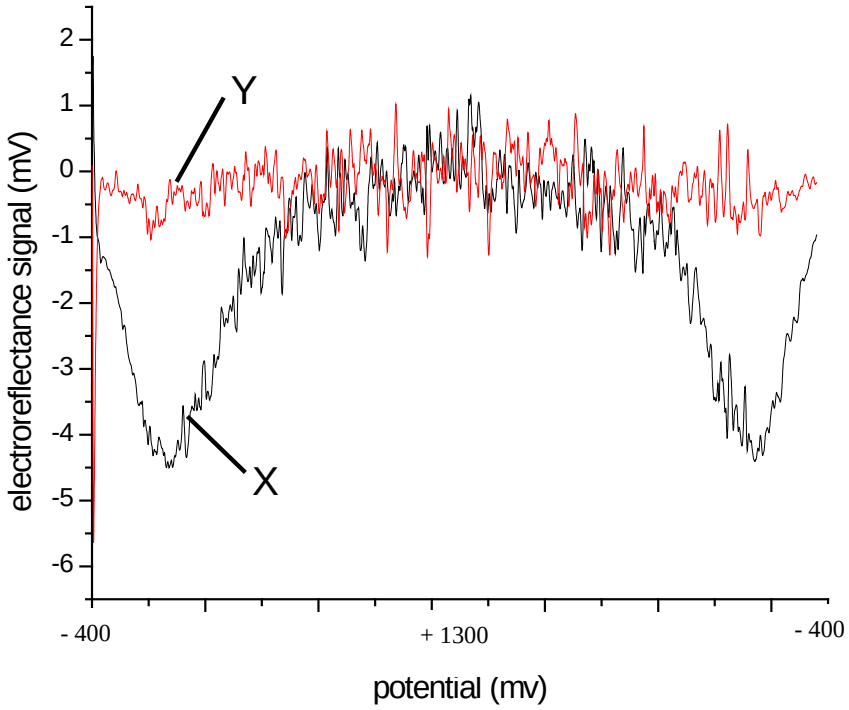

Figure 4.10 Optically detected cyclic voltammogram of a PEDOT/PSS film on ITO. The dc potential of the ITO electrode was scanned from -400 mV to +1300 mV and back to -400 mV at a rate of 5 mV/sec. A modulation amplitude of 12 mV was applied to the dc potential at a frequency of 1 Hz. The intensities of the in-phase (X, black line) and out-of-phase (Y, red line) signals are plotted.

4.6.3 Surface Treatment Effects on Charge Transfer Kinetics

Various independently prepared PEDOT/PSS films on differently treated ITO surface were evaluated using PM-ATR. Different PEDOT/PSS films that were prepared and analyzed: (1) PEDOT/PSS is spuncast onto air plasma cleaned ITO without further heat treatment, (2) PEDOT/PSS is spuncast on O_2 plasma cleaned ITO without heat treatment, (3) PEDOT/PSS is spuncast onto O_2 plasma cleaned ITO followed by heat annealing at 100^0C for 1 hour, (4) PEDOT/PSS is spuncast onto HI etched ITO followed by heat annealing at 100^0C for 1 hour.

Each film resulted in relatively different optical switching frequencies where the real portion of electroreflectance signal (X_{norm}) becomes "zero". These estimated charge transfer rate constants along with R_s and C_{dl} values are summarized in Table 4.1.

It is important to state here that the reproducibility of the data obtained for these four films (1, 2, 3 and 4) were low. Also for all the films, most of the R_s values varied significantly (sometimes an order of magnitude) which affected the calculated rate constants. In order to understand the possible reasons for the irreproducibility, effects of post deposition treatments on PEDOT/PSS morphology and conductivity as well as heterogeneity of ITO surfaces (from batch to batch and even within the same batch) should be considered. Film morphology, and the chemical and physical structure of conducting polymers are affected by the annealing temperature, annealing times, atmosphere and solvent washing; therefore electrical properties (e.g. conductivity) can strongly be influenced by any of these variables.[367, 368] PEDOT/PSS is hygroscopic and

after exposure in air, atmospheric moisture is rapidly uptaken which causes decreases in the conductivity of the film.[369]

First we compare air plasma (1) vs. O_2 plasma (2) cleaned ITO, prior to PEDOT/PSS film deposition without heat treatment. Air plasma cleaning results in lower R_s values and higher charge transfer rate constants relative to O_2 plasma cleaned ITO (Table 4.1).These results are unexpected since O_2 plasma cleaned ITO substrates are expected to give higher device efficiencies and performance because of their higher work functions compared to air-plasma cleaned ITO substrates.[288] As mentioned in Section 4.2, modifying the ITO anode for organic electronic devices to raise the work function has been investigated in the past by various approaches such as plasma (air, argon, oxygen, etc.) treatment.[271, 272, 294, 302] Zhong et.al[263] reported that oxygen plasma treatment decreases the surface roughness, enhances the work function, surface energy, and therefore improves the surface properties of ITO. O_2 plasma cleaning results in higher work function compared to other ITO treatment methods including air plasma cleaning.[277, 288, 295, 302, 370] Therefore charge injection processes are expected to be more favorable with PEDOT/PSS film on O_2 plasma treated ITO. However, it should be noted that for air plasma treated films (1) and O_2 plasma treated films (2), the lowest and the highest obtained rate constants, respectively, were omitted in order to avoid very large standard deviations in the results. Therefore, O_2 plasma cleaned ITO can still potentially lead to faster charge transfer rates. The experiments should be carefully repeated before drawing a conclusion for these types of films.

Table 4.1 PEDOT/PSS series resistance (R_S), double layer capacitance (C_{dl}), and effective charge transfer (optical switching) rate constant (k_S) for various PEDOT/PSS films on ITO.

	Spin coated PEDOT/PSS on ITO electrode			
	no heat		heat annealing	
	air plasma	O_2 plasma	O_2 plasma	HI-etching
R_S (ohm.cm^2)	120 (n = 2)	318 ± 5 (n = 3)	73 (n = 1)	143 (n = 1)
C_{dl} (F/cm^2)	3 x 10^{-5} (n = 2)	4 ± 0.4 x 10^{-5} (n = 3)	4.6 x 10^{-5} (n = 1)	4.7 x 10^{-5} (n = 1)
k_S (s^{-1})	541 (n = 2)	312 (n = 2)	462 (n = 2)	390 (n = 2)
stdev	n/a	n/a	n/a	n/a
Film #	1	2	3	4

Similarly, consistent with the literature, comparing rate constants for films on O_2 plasma cleaned ITO without heat treatment (2) vs. heat annealed films (3) suggests that (3) exhibits relatively faster charge transfer kinetics. (Table 4.1) This result can be attributed to an increase in conductivity within the film after the heat treatment is applied. It is reported in the literature that the chain alignment in thin polymer films (such as PEDOT) often changes with temperature, leading to modified morphologies adopting a more crystalline structure;[371] therefore electrical properties for conducting polymers are affected since they are strongly dependent on their film morphology and structure.[367, 369] The colloidal particle interactions in the PEDOT/PSS composite may also be affected by heat treatment.[369] At a suitable temperature, the number and/or height of the barriers to charge transfer may be reduced by coalescence of PEDOT/PSS particles, e.g. by softening/melting of insulating PSS boundaries which should increase the conductivity (if we assume the conductivity occurs via hopping transport).[369] However it is also reported that above treatment temperatures of 150 ^{0}C, PEDOT films undergo continuous degradation,[342, 372] and increases in treatment times results decreased conductivity.[367] Even though the annealing temperatures and times used in this study were aimed to be below 150 ^{0}C and for 1 hour, the temperatures may sometimes be close to this value since the oven used here was not digitally controlled. This may be one of the reasons for difficulty in reproducibility of the results. It is also important to note that for the heat treated films (3), even though the experimentally obtained optical switching frequencies (ω) were high (~ 400 to 600 Hz) compared to untreated (2) films (~ 150 – 300 Hz), the

relatively low R_s value for (3) somewhat compensated the overall rate constant calculated here.

Next we compare the effects of HI-etching (4) vs. O_2 plasma cleaning (3) on charge transfer kinetics. For both cases (3) and (4), the prepared films are annealed at 100^0C for 1 hour. A somewhat higher rate constant is obtained for film (3) even though a relatively higher R_s value is obtained for film (4) (see Table 4.1). The reason for obtaining similar rate constants for these two types of films can be the effect of heat annealing step. Both of the film structures possibly become more ordered upon evaporation of the solvent molecules within the films. Both the impedance and PM-ATR experiments should be repeated to get more reproducible results. As a future goal, another set of experiments for PEDOT/PSS film on HI etched ITO without the heat treatment should be useful for comparison with the heat treated films (4) and films on O_2 plasma treated ITO (2).

4.6.4 FMPA-modified ITO Surface and Effect on Charge Transfer

The effects of a surface modifier, FMPA, on the charge transfer rate of PEDOT/PSS films on ITO were also evaluated with PM-ATR spectroscopy. Unless otherwise stated, for this study, FMPA is always adsorbed to cleaned ITO prior to PEDOT/PSS film deposition. Different films of PEDOT/PSS on FMPA modified ITO were prepared as follows: (A) PEDOT/PSS is spin coated onto O_2 plasma cleaned and FMPA modified ITO without heat treatment, (B) PEDOT/PSS is spin coated onto O_2 plasma cleaned and FMPA modified ITO, then the film is heat annealed at 100^0C under

vacuum for 1 hour, (C) PEDOT/PSS is spin coated onto HI etched and FMPA-modified ITO and then the film is heat annealed.

PM-ATR was used to extract kinetic information from these films. Representative Cole-Cole plots, where X_{norm} vs Y_{norm} of the electroreflectance signal is plotted for different types of films, are shown in Figure 4.11 and Figure 4.12. Estimated charge transfer rate constants along with R_s and C_{dl} values for these films are summarized in Table 4.2 and Table 4.3. It is relevant here to compare these FMPA-modified films with films that are prepared similarly on unmodified ITO surfaces. Therefore, the plots and tables presented here will include films (2), (3) and (4).

The effect of the surface modifier, FMPA, on the charge transfer rate of PEDOT/PSS can be interpreted as follows:

If we compare unmodified (2) vs. FMPA-modified (A) films on O_2 plasma cleaned ITO without heat treatment, the FMPA-modified ITO shows lower R_s values with a slight increase in rate constant (Table 4.2). For films that lack FMPA, the slower rate constant are obtained which may be attributed to possibility of charge injection is somewhat facilitated by FMPA-modification.

If we compare heat annealed films without FMPA (3) and with (B) on O_2 plasma cleaned ITO, the rate constant on (B) is smaller than on (3) (Table 4.2). This result is opposite to the comparison of (A) vs (2). This may be due to the FMPA film degradation caused by heat treatment which may result in hindered charge transfer. Cyclic voltammograms obtained for FMPA-modified films showed quite stable responses even after heat treatment (except for couple of times). However, the effects of the spuncast

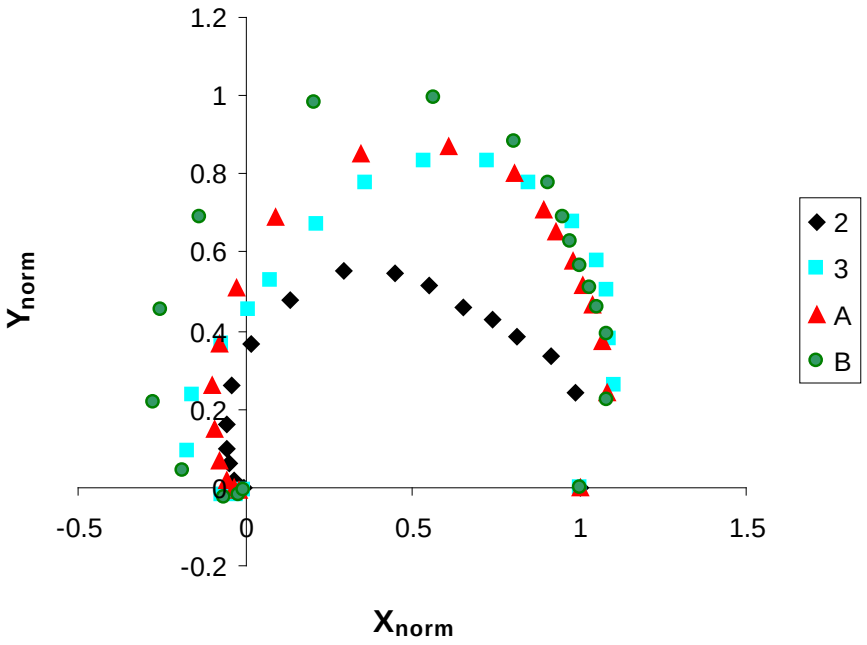

Figure 4.11 Complex plane plot (Cole-Cole) of the electroreflectance signal, composed of pairs of X_{norm},Y_{norm} values at different modulation frequencies, for four types of PEDOT/PSS films: (2) spuncast onto O_2 plasma cleaned ITO, (3) spuncast onto O_2 plasma cleaned ITO and then heat annealed for 1 hour, (A) spuncast onto O_2 plasma cleaned and FMPA-modified ITO without heat annealing, (B) spuncast onto O_2 plasma cleaned and FMPA-modified ITO followed by heat annealing The frequency range is 0.1 Hz - 2500 Hz (the arrow indicates the direction of increasing frequency), E_{dc} = -213 mV and E_{ac} = 30 mV.

Table 4.2 Series resistance (R_S), double layer capacitance (C_{dl}), and effective charge transfer (optical switching) rate constant (k_S) for PEDOT/PSS films on O_2 plasma cleaned, FMPA-modified and unmodified ITO with or without heat annealing.

Spin coated PEDOT/PSS on O_2 plasma cleaned ITO				
	no FMPA		w/ FMPA	
	no heat	heat annealing	no heat	heat annealing
R_S (ohm.cm^2)	318 ± 5 (n = 3)	73 (n = 1)	176 ± 98 (n = 3)	147 ± 46.1 (n = 3)
C_{dl} (F/cm^2)	4 ± 0.4 x 10^{-5} (n = 3)	4.6 x 10^{-5} (n = 1)	3 ± 0.5 x 10^{-5} (n = 3)	4 ± 0.1 x 10^{-5} (n = 3)
ks (s^{-1})	312 (n = 2)	462 (n = 2)	418 (n =3)	332 (n = 3)
stdev	n/a	n/a	107.5	95.8
Film #	2	3	A	B

polymer on FMPA during the heat annealing and subsequent characterization are not known.

Next we compare films (A) and (B) where heat annealing effects can be investigated for PEDOT/PSS films on FMPA-modified ITO. From the rate constants obtained for these two films, heat annealing causes decrease in charge transfer kinetics. Even though heat annealing increases crystalline order and conductivity in PEDOT/PSS films, it doesn't appear to affect the FMPA-modified films. In order to decrease the standard deviations and obtain more accurate rates, repeating these experiments will be required.

Lastly, comparison of unmodified (4) and FMPA-modified (C) heat annealed PEDOT/PSS films on HI etched ITO showed similar results (Table 4.3). No significant difference in rate constants as well as electrochemical parameters such as R_s and C_{dl} were obtained upon ITO surface modification with FMPA .

One of the conclusions that can be drawn here is that for all the films that are on FMPA-modified ITO (A), (B) and (C), more reproducible results were obtained. However, all rates constants including the rate constants on unmodified ITO (films (1), (2), (3) and (4)) are not significantly different. Thus FMPA modification does not appear to have a significant effect on charge transfer. In order to reach a definitive conclusion, some of the experiments needed to be repeated with careful consideration of experimental conditions, including humidity, annealing times and temperatures.

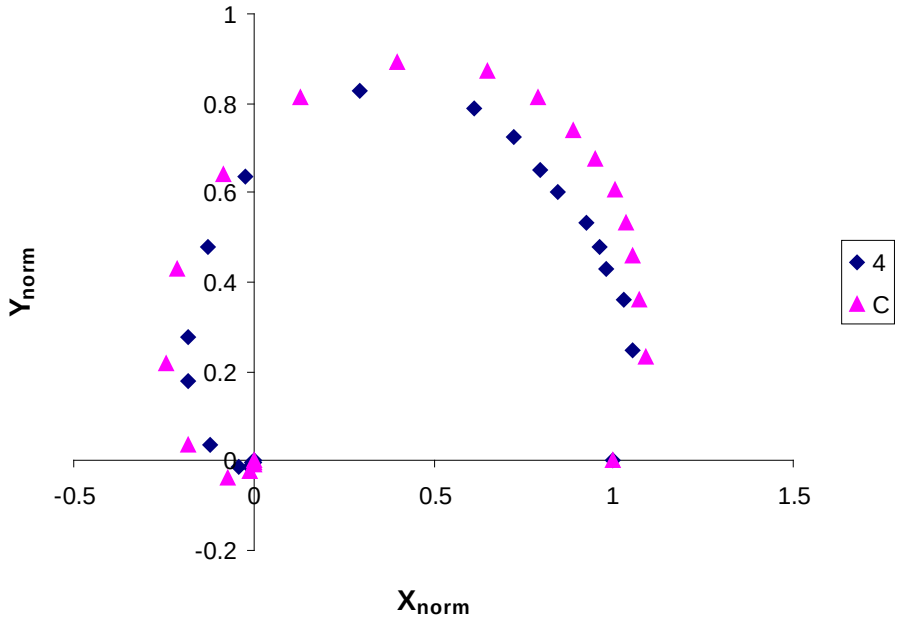

Figure 4.12 Complex plane plot of the electroreflectance signal, composed of pairs of X_{norm},Y_{norm} values at different modulation frequencies for two types of PEDOT/PSS films: (4) spuncast onto unmodified HI etched ITO and then heat annealed for 1 hour , (C) spuncast onto HI etched and FMPA-modified ITO followed by heat annealing. The frequency range is 0.1 Hz - 2500 Hz (the arrow indicates the direction of increasing frequency), E_{dc} = -213 mV and E_{ac} = 30 mV.

Table 4.3 Series resistance (R_S), double layer capacitance (C_{dl}), and effective charge transfer (optical switching) rate constant (k_S) for spin coated and heat annealed PEDOT/PSS films on HI-etched, FMPA-modified and unmodified ITO.

Spin coated and heat-annealed PEDOT/PSS on HI-etched ITO		
	no FMPA	**w/ FMPA**
R_S (ohm.cm^2)	143 (n = 1)	187 (n = 1)
C_{dl} (F/cm^2)	4.7 x 10^{-5} (n = 1)	3.8 x 10^{-5} (n = 1)
k_S (s^{-1})	390 (n = 2)	386 (n = 3)
stdev	n/a	40.3
Film #	**4**	**C**

The study has investigated possible effects of various surface treatments and a surface modifier on the charge transfer kinetics of PEDOT/PSS films. XPS and UPS analysis of these surfaces should be performed to measure surface parameters such as work function. This type of study can lead to a better understanding of effects of surface treatments and organic modifiers which are hypothesized to improve charge transfer efficiency across ITO /organic layer interfaces in PVs and OLEDs.

5. POTENTIAL-MODULATED ATTENUATED TOTAL REFLECTANCE CHARACTERIZATION OF CHARGE INJECTION PROCESSES IN MONOLAYER-TETHERED CdSe NANOCRYSTALS

5.1 Introduction

5.1.1 Introduction to Semiconductor Nanoparticles (SC-NPs)

Nanometer size semiconductor crystallites or nanoparticles (SC-NPs), also known as quantum dots (QDs), have unique optical and electrical properties and are of interest as photocatalysts for the formation of solar fuels,[373-378] as sensitizers for dye-sensitized solar cells based on nanoporous metal oxides,[377, 379-381] as luminescent dopants in organic light emitting diodes,[382, 383] and as light-absorbing, electron transporting materials in polymer-based organic solar cells.[384-386]

SC-NPs are clusters of atoms whose electronic structure is strongly size dependent when its diameter is comparable to or smaller than the bulk exciton diameter.[387-389] Charge carriers and excitons are confined within the boundaries of the NP in all three spatial dimensions; as a result of this confinement, the continuous density of states of the bulk semiconductor collapses into discrete electronic states and the bulk oscillator strength becomes concentrated into discrete transitions (This phenomenon is called quantum confinement).[390, 391] Consequently, the distribution of states of a SC-NP begins to resemble that of a molecule[388, 390-392] such that smaller SC-NPs have: i) increased separation between energy levels[392, 393], ii) higher energy band-edge absorptions[392, 393] and iii) more negative reduction potentials.[390, 394]

Due to quantum confinement, the energy gap between the valence band (VB) and the conduction band (CB) is inversely proportional to the photon emission wavelength upon electron relaxation. Therefore changing the size (radius) of the SC-NP alters the energy gap distance and wavelength of light that the SC-NP emits after excitation (Figure 5.1a and Figure 5.1b)

Not only does the size of the SC-NP correlate with the emission wavelength, the core composition also dictates emission properties (Figure 5.2). SC-NP cores are primarily made of periodic group II-VI, III-V, or IV-VI elements; the most common ones that are studied in the literature include silicon,[395] PbS,[396] CdS,[397] PbSe[398] and CdSe.[399]

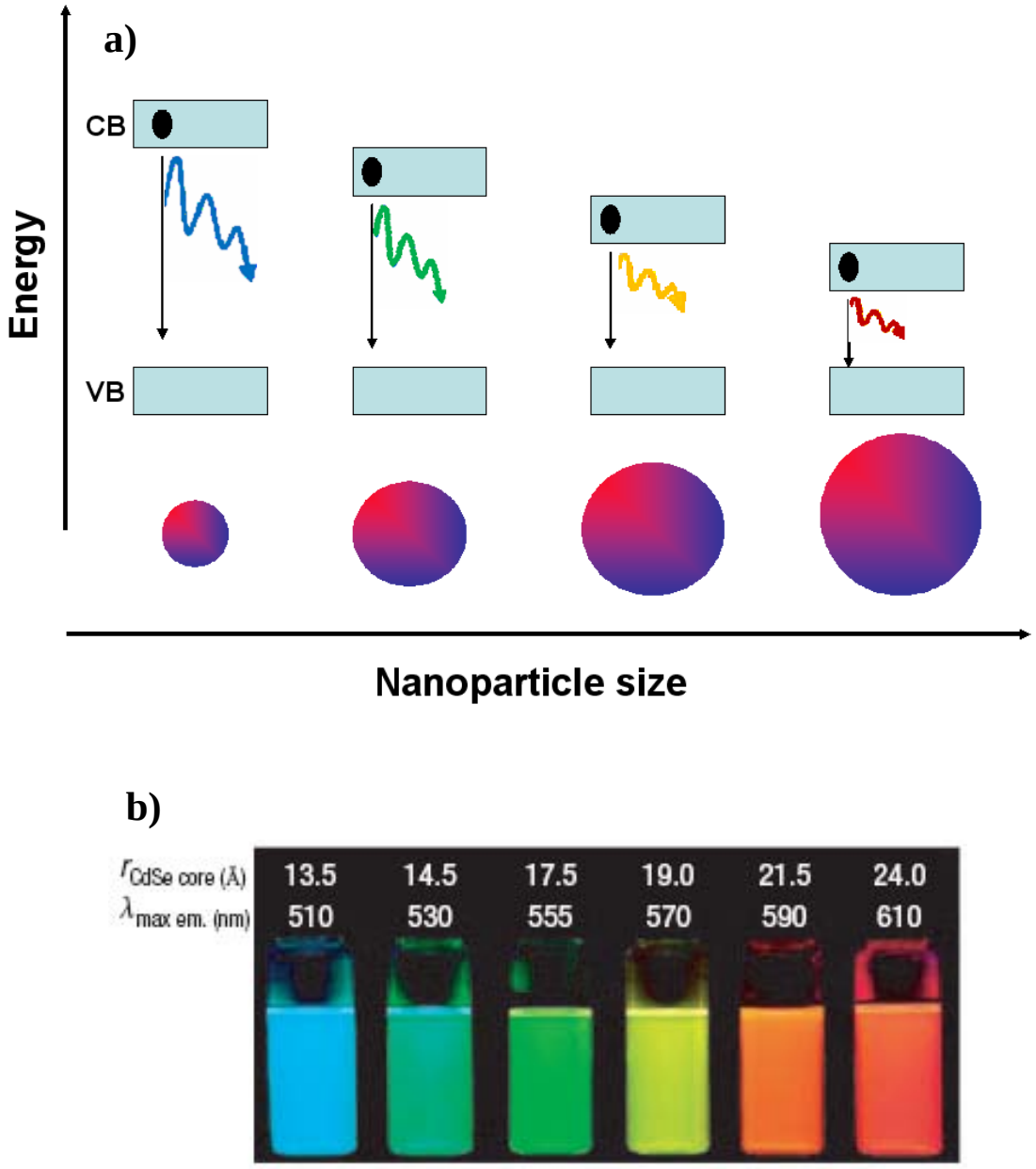

Figure 5.1 a) Representative diagram of energy vs. nanoparticle size. b) Photo demonstrating the size-tunable fluorescence properties and spectral range of six CdSe SC-NPs versus its core size.[400] The larger the SC-NP, the longer the emission wavelength, the smaller the energy band gap.

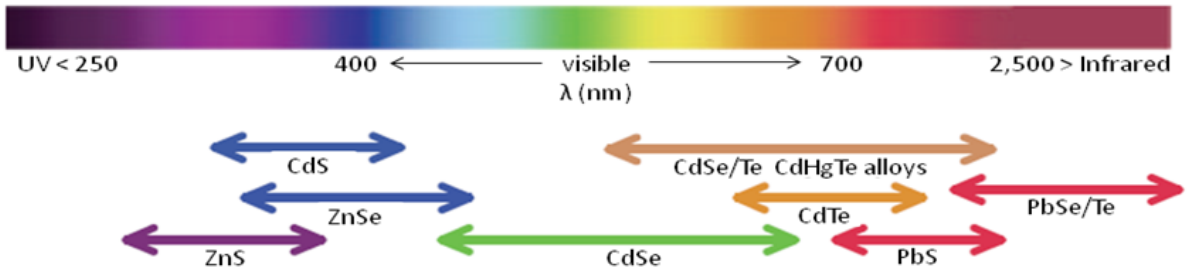

Figure 5.2 Representative NP core materials scaled as a function of their emission wavelength superimposed over the spectrum.[400]

SC-NPs have shown promises for applications in biological imaging[401, 402], light emitting devices[403], photodetectors[404] and solar cells.[384, 405] Besides their size-tunable emission there are several advantages[406, 407] to use these materials in device technologies such as; i) their high effective molar absorptivities means that ultra-thin films will be good light absorbers over a broad spectral range; ii) their frontier orbital energies are positioned so that they may be used to photocatalyze both solution reduction (e.g. H_2 formation) and oxidation; iii) their frontier orbital energies are tunable over a broad spectral range simply by changing the nanoparticle diameter, iv) they are possible candidates for multiple-exciton generation for energy conversion events which will lead to have better efficiencies for device technologies, etc.

Gaining a complete understanding of the frontier orbital energies and electron transfer kinetics for the SC-NPs is crucial and challenging for sensitization of new PV materials. The key steps in solar energy conversion and photovoltaic systems, using hybrid small molecule, polymer, and SC-NP composites, are considered to be:[244, 406-408] *i)* light absorption; *ii)* excited state or exciton dissociation; *iii)* charge separation; *iv)* charge transport; and *v)* charge (electric) collection. Limitations in any one of these steps results in poor energy conversion efficiency for the entire system.[244, 406-408]

5.1.2 Motivation and Overview of the Experiment

Rates of photoactivated electron and hole transfer for nanocrystals (NCs) depend on frontier orbital energies (conduction and valence band edges, E_{CB} and E_{VB}, respectively), which are strongly dependent on NC size and composition, capping ligand,

and the dielectric properties of the surrounding environment (vacuum vs electrolyte solutions vs polymer hosts).[373, 374, 377, 378, 397, 399, 409-414]

Conventional voltammetric techniques, sometimes coupled with characterization of electrogenerated chemiluminescence (ECL) in solutions of ligand-capped CdSe, CdSe and CdTe NCs, have been used to estimate onset potentials for oxidation/ reduction, from which E_{VB}, E_{CB}, and "quasi-particle energy gaps" can be estimated.[399, 410, 413] These oxidation and reduction events can be difficult to resolve from background currents and are chemically irreversible on normal voltammetric time scales. The ECL response of CdSe NCs, however, suggests that the charged states of these ligand-capped NCs are sufficiently stable for direct charge recombination and generation of their lowest energy exciton (emissive) states.[399, 410] Spectroelectrochemical techniques have also been used to study electron injection and bleaching of the lowest energy exciton absorption bands in multilayer films of II-VI nanocrystalline materials, yielding estimates for first-reduction potentials and E_{CB}.[397, 398, 411, 412, 414, 415] Guyot-Sionnest[412, 414, 415] and coworkers have observed that CdS, CdSe, and related NPs can undergo a reversible reduction in aprotic solvents to induce a "charged" state, accompanied by significant changes in optical properties (via the appearance of new IR absorption bands in the one-electron "charged" state (1S $\rightarrow$1P transition), and a bleaching of the visible wavelength excitonic absorbance features). Using relatively thin films of tightly packed (in some cases cross-linked) NPs, estimates of first-reduction potentials have been obtained for a few nanoparticle sizes, and capping ligands.[412, 414, 415] In these studies the film is made by a drop of SC-NP solution that is placed onto the electrode (ITO, Au or Pt) until it is dried which results in

film thicknesses of 100 to 500 nm depending on whether or not cross-linker is used. There were also no apparent attempts to characterize rates of electron injection to monolayer films of the NP, although in some cases voltammetric reversibility was observed.[412, 414, 415]

As explained in the previous Chapters (2, 3 and 4) and in the literature,[109, 205, 208] PM-ATR spectroelectrochemistry on an electroactive waveguide platform provides the sensitivity to characterize redox potentials and rates of electron transfer (ET) for thin films of biomolecules, conducting polymers and charge-transfer salts at submonolayer surface coverages. Monitoring electrochemically generated optical changes in the redox-active monolayer allows clear differentiation of Faradaic versus non-Faradaic events. We show here that PM-ATR enables, for the first time, characterization of reversible electron injection into submonolayer coverages of surface-tethered, pyridine-capped CdSe nanocrystals (pyr-CdSe NCs) (Figure 5.3).[416] Low surface coverages of pyr-CdSe NCs may reduce NC-NC interactions, but the redox processes of such thin and weakly absorbing films can only be characterized by a technique with the sensitivity of waveguide-based spectroelectrochemistry.[146, 417-419] We anticipate that waveguide spectroelectrochemistry will allow systematic examination of the effects of capping ligand, electrolyte environment, and interparticle interactions on frontier orbital energies and rates of ET of semiconductor NCs films, which are critical parameters in designing new energy conversion materials.[373, 374, 376-379, 382, 383, 386, 398, 409, 411, 412, 415, 420, 421]

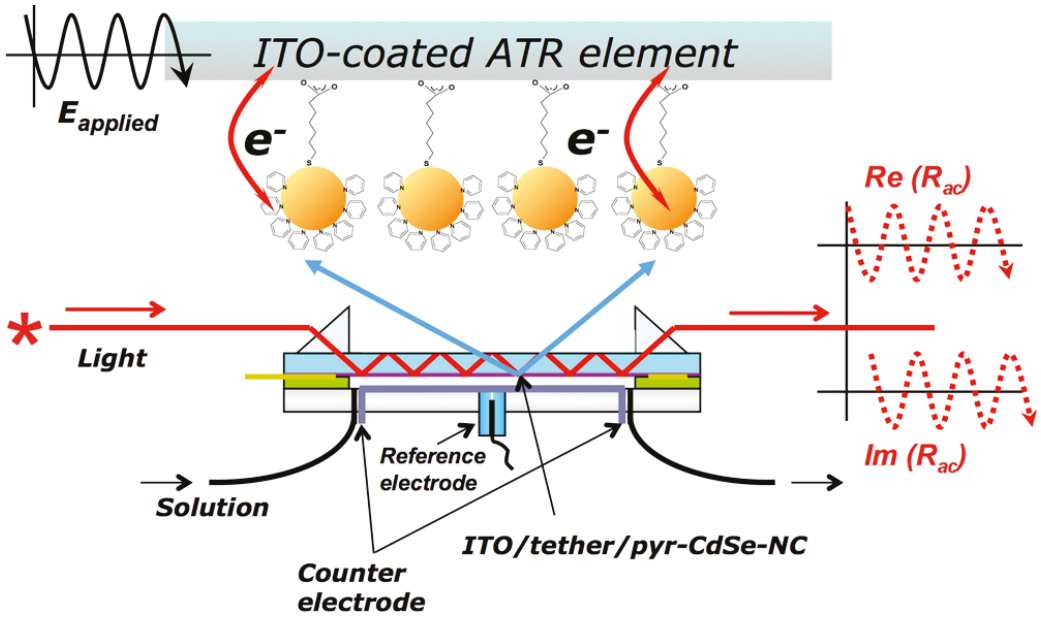

Figure 5.3 Schematic view of PM-ATR spectroelectrochemistry for monolayer-tethered NCs.[416] Light is prism-coupled into and out of an ITO-coated waveguide, with pyr-CdSe NCs chemisorbed at the electrode/solution interface. The ITO electrode potential is modulated ±50 mV about -1.47 V vs Fc/Fc^{+}, which is the midpoint potential ($E_{applied}$) for reversible electron injection into the tethered NCs. The real (*Re*) and imaginary (*Im*) components of the ac portion of the electroreflectance response (R_{ac}) are monitored as a function of the modulation frequency, which is varied from 0.1 Hz to 1 kHz.

5.2 Experimental

5.2.1 Preparation of Pyridine-capped CdSe NPs

CdSe NCs (ca. 5 nm diameter), capped with mixed trioctylphosphine oxide/hexadecylamine (TOPO)/HDA) ligands, were prepared using the synthetic protocols detailed in the literature.[378, 416, 422, 423] After precipitation (3X) to remove excess ligand, capping ligands were displaced from the NCs in neat pyridine solutions. The resultant pyr-CdSe NCs were precipitated using hexanes, washed, and dried.

UV-VIS analysis of NPs in 1:10 pyr-MeOH solution is used to estimate bulk concentration and NP diameter (assuming spherical geometry and 10^{-10} mol/cm^2 ligand coverage on surface) according to literature.[423] Required dilutions were made using dry 1:10 pyr:MeOH.

5.2.2 Adsorption of Mercaptoalkylcarboxylic Acids on ITO Electrodes and Formation of NP Films on Modified ITO Surface

Planar ITO electrodes, consisting of a 100 nm thick ITO layer coated on 1 mm thick soda lime glass (Colorado Concept Coatings, LLC), were used in this study as planar waveguides.[146, 179] ITO electrodes were cleaned similarly as explained in the previous Sections (2.2.1 and 3.2.1) excluding plasma cleaning step. Briefly, they were cleaned by lightly scrubbing with a 1% Alconox solution for 1 min and then sonicating for 15 min each in water, 1% Triton X-100, water, and ethanol. The water used in all cleaning steps was obtained from a Barnstead Nanopure system with a measured resistivity of 18.0 MΩ•cm or greater. Prior to surface modification with a

mercaptoalkylcarboxylic acid, the ITO surface was acid activated with 5.5 M HI for 10 sec.[245, 270, 424] After etching, the ITO electrode was rinsed with water, dried with nitrogen and immediately transferred to an ethanol or acetonitrile solution containing 10 mM mercaptoalkylcarboxylic acid, either 3-mercaptopropionic acid (3-MPA), 6-mercaptohexanoic acid (6-MHA), or 11-mercaptoundecanoic acid (11-MUA), and kept in the solution at room temperature overnight.[425, 426] The electrode was then rinsed with ethanol or acetonitrile and dried with nitrogen prior to adsorption of pyr-CdSe NCs.

NCs were deposited by immersing electrodes in 1 μM pyr-CdSe NC solutions (1:10 v/v pyridine/methanol) for periods up to 1 h (along with unmodified ITO as a control).

5.2.3 PM-ATR

For frequency modulation, the lock-in amplifier, potentiostat and Labview software were used as described in Chapter 2. In this study, sinusoidally modulating the electrode potential over a small range near the charge injection potential (midpoint between the oxidation and reduction potentials of the NC film) produces a modulated change in the electroreflectance (*R*, which is proportional to the intensity of light outcoupled from the waveguide) at the same frequency, due to the difference in molar absorptivities of oxidized and reduced forms.

5.3 Results and Discussion

5.3.1 Surface Analysis of 11-MUA-modified ITO

Figure 5.4 shows the angle-resolved X-ray photoelectron spectroscopy result of an ITO surface modified with 11-MUA. The normal and tilted angle results show that In/S atomic concentration % 94 / 5.4 and 88 / 11.3, respectively. Consistent with the literature,[426, 427] these findings support our assumption of carboxythiols in this study bind to ITO via the carboxylic acids, forming a thiol-terminated SAMs. Previous studies of adsorption of mercaptoalkylcarboxylic acids to ITO have also shown that the carboxy groups are bound to the oxide surface,[426] leaving the terminal thiols available for subsequent capture of the pyr-CdSe NCs.[427]

5.3.2 ATR Spectra and Adsorption Isotherm of NP

ATR spectroscopy was used to monitor the adsorption of pyr-CdSe NCs to modified ITO electrodes using instrumentation similar to that described previously[146] (except that, in these experiments, a tungsten lamp was used as the source). Spectra were acquired every 2-3 min for 45 min after introduction of the pyr-CdSe NC solution to the ATR flow cell (see Figure 5.5a).[416] The expected increase in absorbance for the lowest energy exciton band of 5 nm CdSe NCs was observed, with $\lambda max \approx 609$ nm. A representative uptake curve on 3-MPA-modified ITO is shown in Figure 5.5b.[416] Limiting coverages at this NC solution concentration are reached in ca. 20 minutes. Similar results were obtained for NCs adsorbed to 6-MHA- and 11-MUA-modified ITO. On the basis of these results, in subsequent experiments ITO

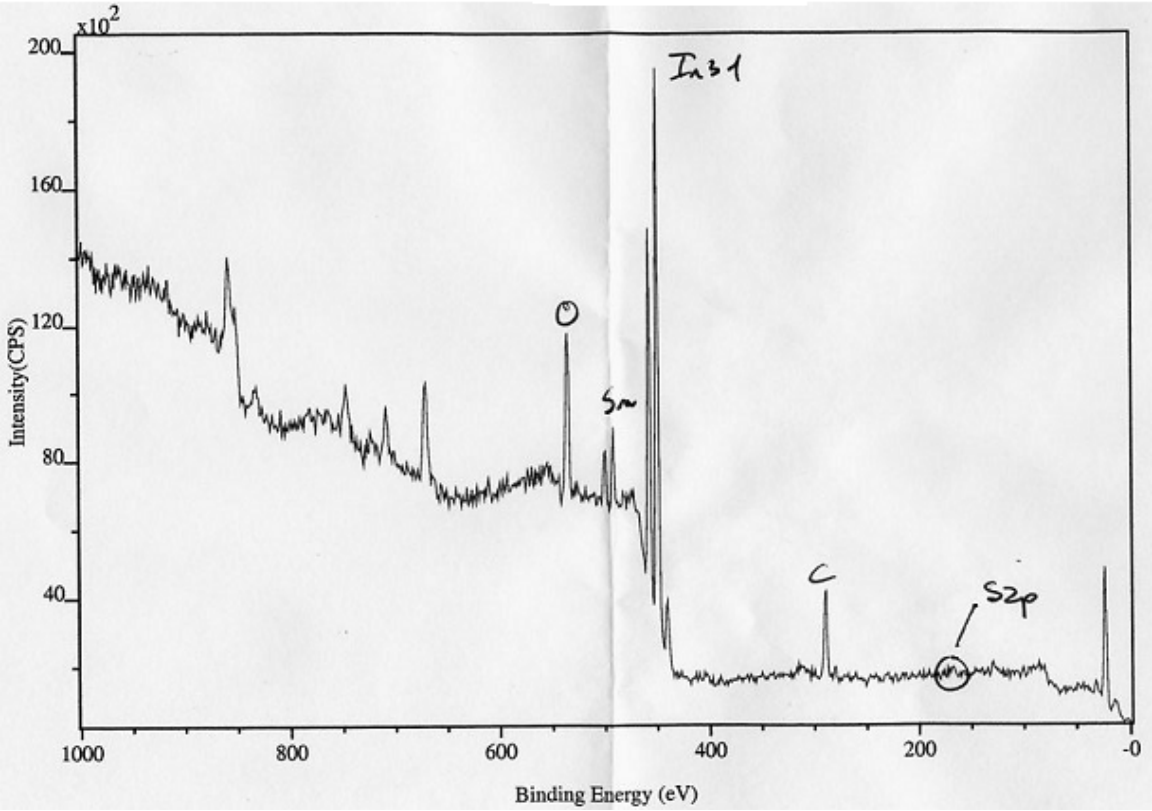

Figure 5.4 Plot of intensity vs. binding energy from angle-resolved X-ray photoelectron spectroscopy of an ITO surface modified with 11-MUA. The peaks corresponding to Oxygen (O), Tin (Sn), Indium (In), Carbon (C) and Sulphur (S) are labeled.

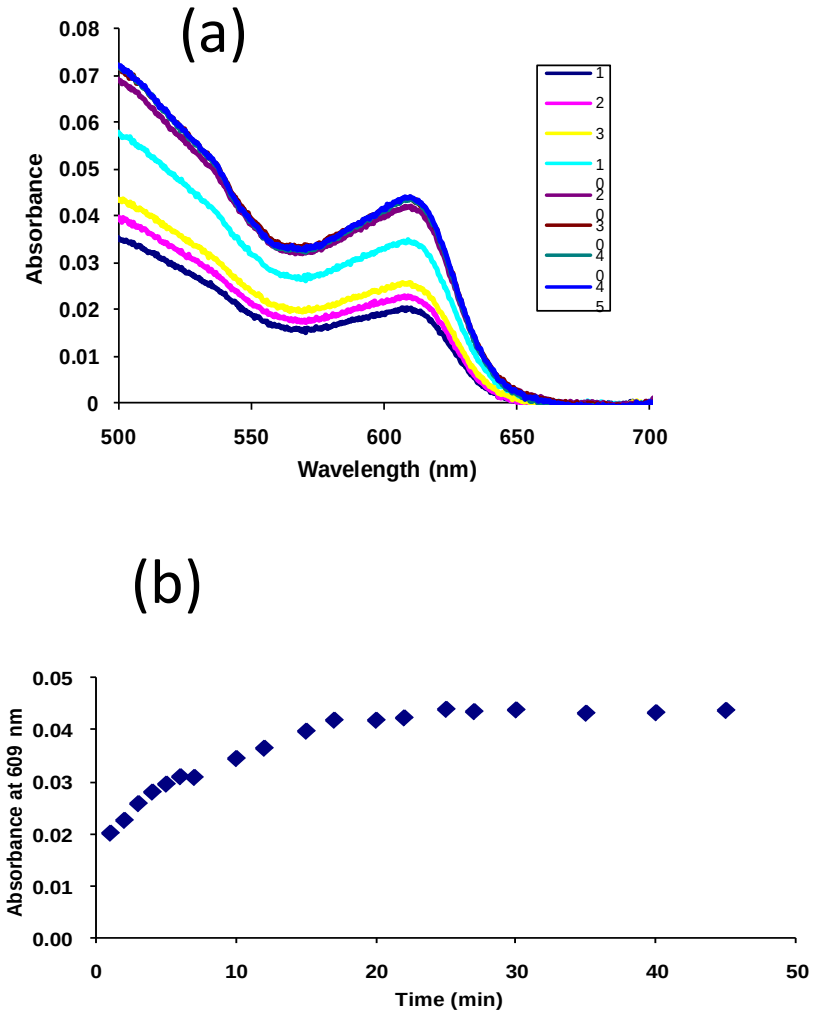

Figure 5.5 (a) Representative ATR spectra acquired during adsorption of pyr-CdSe NCs from a 1 μM solution to 3-MPA-modified ITO.[416] The legend indicates the time (in minutes) at which the spectra were acquired. The spectra are normalized to absorbance values at 700 nm where there is no spectral response from CdSe NCs. (b) Absorbance (λ = 609 nm) versus exposure time to the pyr-CdSe NC solution; limiting coverages, corresponding to 10-20% of a monolayer (see text), were reached in under 30 min.[416]

electrodes were incubated for ca. 30 min for each NC deposition, to form the thin films that were the subject of the spectroelectrochemical studies described below.

5.3.3 Surface Coverage Calculation of NP

Surface coverages of adsorbed pyr-CdSe NCs were estimated from the ATR spectra. After NC adsorption reached saturation on each type of electrode, the ATR flow cell was flushed with the electrolyte (0.1 M tetrabutyl ammonium perchlorate in acetonitrile (ACN)) that was used for the spectroelectrochemical measurements. An ATR spectrum was then acquired. The measured absorbance, Af, is related to the surface coverage, Γ, by

$$\Gamma = A_f \cdot [1000N \cdot \varepsilon_f \cdot (I_e/I_i)]^{-1} \qquad (1)$$

where N is the number of internal reflections at the interface between the ATR element and the sample (N = 10 in these experiments), and ε_f is the estimated molar absorptivity.[428] A value of 430 000 cm^{-1} M^{-1} for ε_f was estimated from the absorbance spectrum of dissolved 5 nm CdSe NCs using the empirical approach of Yu et al.[423] The term (I_e/I_i) is the evanescent transmitted interfacial intensity per unit incident intensity; it was calculated using a two-phase (glass/ACN) approximation as previously described.[419, 428] In these experiments, the angle of internal reflection (θ) was ~65^0 and the refractive indices used for glass and ACN were 1.51 and 1.34, respectively. Estimated Γ values for pyr-CdSe NCs adsorbed on 3-MPA-, 6-MHA-, and 11-MUA-modified ITO were near 10^{-12} mol/cm^2 (Table 5.1),[416] which is approximately 10-20 % of a close-packed monolayer, with an average NC-NC separation distance of ca. three NC diameters (10-15 nm).

Absorbance values at $\lambda_{max} \approx 609$ nm are ca. 0.1 A.U. at these coverages, which suggests that the limit of detection (LOD) with the conventional ATR platform used here is ca. 1% of a monolayer. The LOD would be substantially lower using a much thinner, single-mode waveguide platform, where the equivalent number of internal reflections exceeds 1000 per cm along the beam propagation axis in the waveguide.[418, 429] On unmodified ITO surfaces, pyr-CdSe NCs adsorbed weakly relative to modified ITO, with saturation coverages of ca. 10^{-13} mol/cm^2.

Table 5.1 Surface Coverage (Γ), Cell Series Resistance (R_S), Double Layer Capacitance (C_{dl}), and Electron Injection Rate Constants (k_S) for pyr-CdSe Films Adsorbed to Modified ITO Electrodes[416]

	3-MPA/ITO	6-MHA/ITO	11-MUA/ITO
Γ (mol/cm^2)	**1.3 x 10^{-12}**	**1.8 x 10^{-12}**	**0.8 x 10^{-12}**
R_S (Ω•cm^2)	**75 ± 3 (n = 3)**	**55 (n = 2)**	**72 ± 9 (n = 4)**
C_{dl} (μF/cm^2)	**22 ± 1 (n = 3)**	**21 (n = 2)**	**15.0 ± 0.4 (n = 4)**
k_S (s^{-1})	**650 ± 230 (n = 6)**	**530 ± 32 (n = 3)**	**530 ± 38 (n = 3)**

5.3.4 Field Emission Scanning Electron Microscopy (FE-SEM) on Pyridine-capped CdSe Nanocrystals Adsorbed to Bare and Modified ITO

SEM images of CdSe NCs on bare ITO (i), 3-MPA modified ITO (ii) and 6-MHA modified ITO (iii) were acquired in the FE-SEM facility in Material Sciences at the University of Arizona. SEM images were taken on a Hitachi 4800 FE-SEM (15 kV accelerating voltage) on as-prepared samples (i.e. no metallic over coating). The same surface cleaning and film preparation procedures were used as in the spectroelectrochemical experiments (except for the electrolyte rinse in the last step), before the images are taken.

Figure 5.6 shows field-emission scanning electron microscopy (FE-SEM) images of an unmodified ITO electrode and 3-MPA- and 6-MHA-modified ITO to which pyr-CdSe NCs have been adsorbed.[416] Just a few NCs can be imaged on the unmodified ITO electrode. Relatively larger numbers of apparently isolated NCs and small clusters of NCs are visible on the 3-MPA- and 6-MHA-modified electrodes. The NCs appear to be mainly concentrated along grain boundaries in the ITO surface. They are spaced farther apart on average relative to the spacing expected based on the Γ values in Table 5.1,[416] but this difference is not unexpected. Counting adsorbed NCs in these SEM images will likely lead to an underestimate of the actual surface coverage because (a) it is difficult to determine the number of NCs in clusters and (b) the rough ITO surface morphology and the tendency of NCs to localize in/along grain boundaries makes it probable that less than 100% of the adsorbed NCs are imaged. Higher resolution FE-SEM images of pyr-CdSe NCs adsorbed to bare and modified ITO are shown in Figure 5.7.[416]

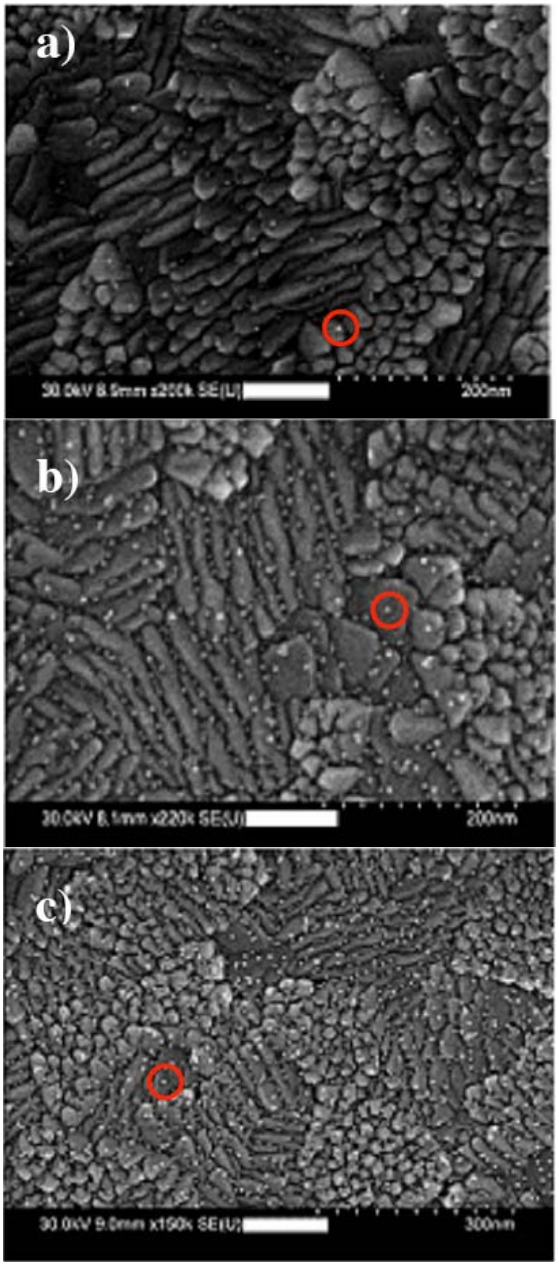

Figure 5.6 Representative FE-SEM images of pyr-CdSe NCs adsorbed to different ITO surfaces: (a) on bare ITO; (b) on 3-MPA-modified ITO; (c) on 6-MHA-modified ITO. In panels a and b, the scale bar = 200 nm; in panel c, the scale bar = 300 nm. Isolated NCs and small clusters of NCs are observable (examples are circled in red).[416]

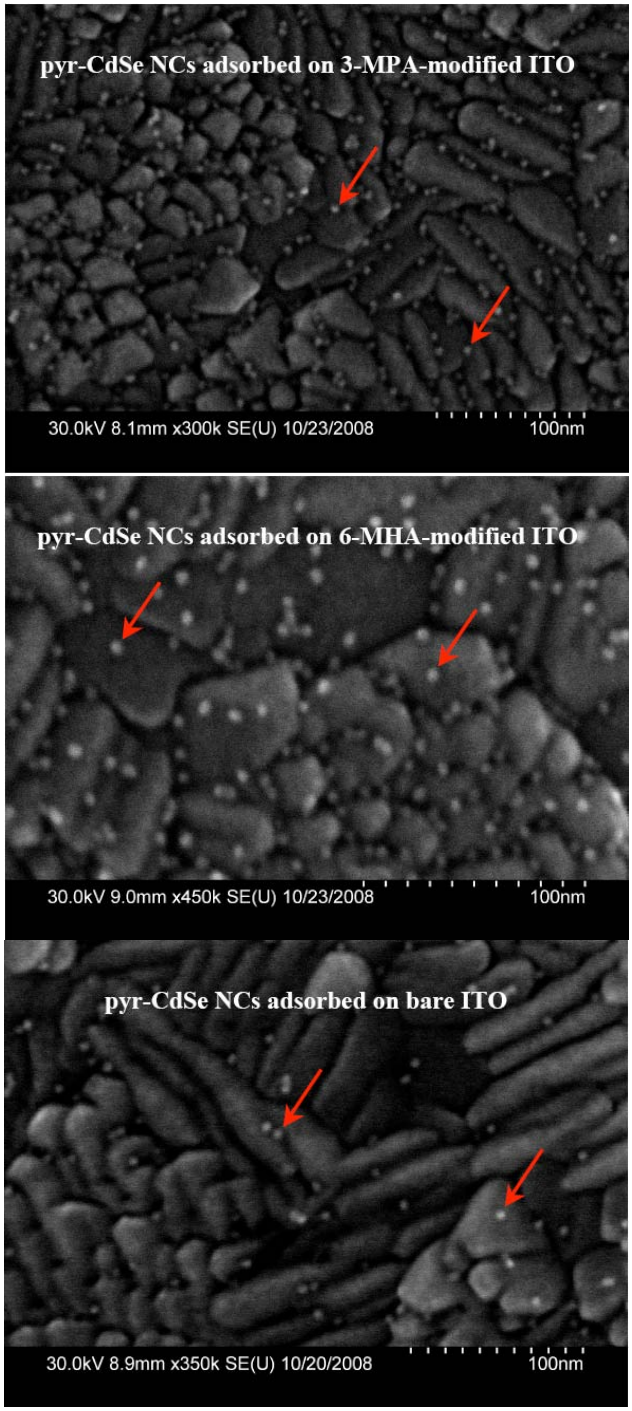

Figure 5.7 Higher resolution FE-SEM images of pyr-CdSe NCs. The red arrows highlight some individual or small clusters of NCs. In all panels, the scale is set to 100 nm.[416]

5.3.5 Potential-controlled ATR on NPs

Potential controlled ATR spectra of NC films were acquired to determine the wavelength region and midpoint potential (E_{dc}) for PM-ATR experiments. The electrode potential is stepped from + 0 V to – 1.5 V vs. psudo Ag/AgCl and the spectra were take every 100 mV difference.

On unmodified (bare) ITO surfaces, the spectroelectrochemical responses of adsorbed pyr-CdSe NCs were difficult to detect. In contrast, for NCs tethered to 3-MPA-, 6-MHA-, and 11-MUA-modified electrodes, complete and reversible bleaching of the lowest energy exciton absorption band (1S → 1P transition) was observed at potentials estimated to be sufficient to inject electrons into the NC conduction band (Figure 5.8A).[412-414] The midpoint potential for the bleaching process was observed at -1.47 V versus ferrocene/ferrocenium (Fc/Fc^+) with complete bleaching at -1.75 V, and these values were invariant with tether length (Figure 5.8B). The optical gap of 5 nm CdSe NCs, ~ 2.04 eV, was calculated[423] from the λ_{max} of 609 nm. From the onset potentials for reduction and correction of the reference electrode to the vacuum scale,[430] E_{CB} and E_{VB} were estimated to be -3.5 eV and -5.5 eV, respectively. These energy levels are consistent with values estimated from solution and thin film voltammetric and spectroelectrochemical studies of CdSe NCs.[381, 412-414] However, they are smaller (i.e., the energies are closer to the vacuum level) by ca. 0.8-1 eV versus E_{CB} and E_{VB} values estimated from UV photoemission studies of surface-confined CdSe NCs (and corrected for shifts in local vacuum level).[380, 387, 427] Differences in the frontier orbital energy levels between vacuum and electrolyte environments have been predicted by Brus and

coworkers, resulting from polarization effects in the NC and differences in the dielectric constants of electrolyte versus vacuum environments.[421, 431] Resolving the apparent differences in these frontier orbital energies will be important in future studies using these NCs as either photocatalysts, or as donors or acceptors in photovoltaic platforms, since these energies determine the driving force for ET reactions to host polymers, host oxides, and/or to solution electron acceptors or donors.[373, 374, 377, 380, 409]

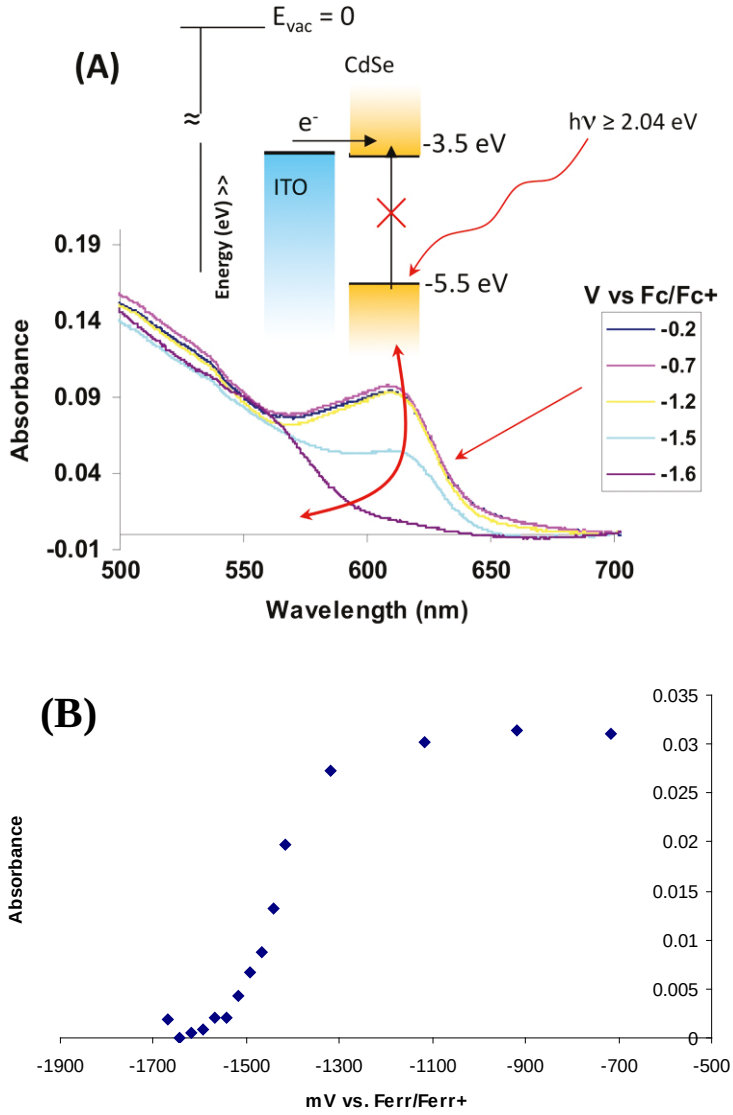

Figure 5.8 (A) Representative ATR spectra obtained for a submonolayer film of 5 nm pyr-CdSe NCs adsorbed on 3-MPA-modified ITO, immersed in electrolyte, as a function of applied potential.[416] The 1S → 1P absorption band is reversibly bleached at a midpoint potential of -1.47 V vs Fc/Fc^+ (-1.1 V vs normal hydrogen electrode (NHE)). Above the spectra is a schematic view of estimated frontier orbital energies of these 5.0 nm NCs with respect to vacuum (assumed value for NHE = -4.6 eV[430]). (B) Absorbance vs. potential plot for NCs adsorbed to 3-MPA modified ITO surface.

5.3.6 PM-ATR Results and Discussion

In the PM-ATR experiments, a 610 nm bandpass filter (~17 nm fwhm) was placed between the ATR cell and photomultiplier tube detector to control the spectral bandwidth. The potential applied to the pyr-CdSe NC/tether/ITO electrode was modulated (±50 mV) about a midpoint potential ($E_{applied}$) of -1.47 V versus Fc/Fc^+. The real and imaginary reflectance components were measured over a modulation frequency range of 0.1 Hz to 1 kHz (Figure 5.9).[416] The frequency, ω, at which the real component of the reflectance signal is zero, coupled with measurements of the series (uncompensated) resistance, R_S, and double layer capacitance, C_{dl}, leads to an estimate for the apparent rate constant (k_S) for the reversible electron injection/bleaching in the NC film.[109, 208] R_S, C_{dl}, and k_S values are listed in Table 5.1 for pyr-CdSe NCs tethered on 3-MPA-, 6-MHA-, and 11-MUA-modified electrodes. The apparent rate constants are ca. 500 s^{-1} and show no dependence on tether length.

These rate constants are greater than previous measurements on films of small molecules and metalloproteins linked or absorbed to ITO, but less than that of thiophene-based conducting polymers grown electrochemically from ITO.[109, 205, 208] We have recently shown that ITO electrodes such as those used here, modified or unmodified, are electrochemically active only at small fractions of their geometric area, and this results in relatively low rates of ET for a variety of dissolved and adsorbed molecules and conducting polymers.[206, 208, 270, 284, 432, 433] Here we observe nearly quantitative and fully reversible bleaching of the lowest energy excitonic absorbance band of adsorbed NCs, which shows that the fraction of the NC film that is

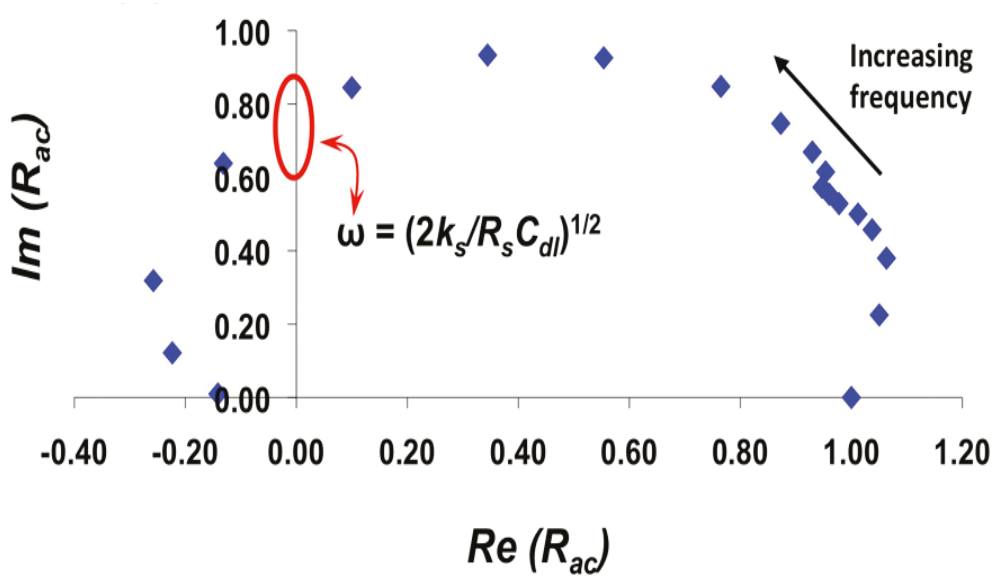

Figure 5.9 Plot of normalized values of imaginary (*Im* (R_{ac})) vs real (*Re* (R_{ac})) reflectance components measured in a PM-ATR experiment for pyr-CdSe NCs adsorbed to 3-MPA-modified ITO.[416] The curve was fit to a polynomial function to determine the frequency (ω) at which *Re* (R_{ac}) is zero (indicated by the red ellipse). In conjunction with the cell series resistance (R_S) and the double-layer capacitance (C_{dl}), determined from impedance experiments, ω was used to calculate the rate constant (k_S) for reversible electron injection into the tethered NCs (data listed in Table 5.1).

electroactive is near unity. It is unlikely, however, that NCs adsorb only to electrochemically active regions of the ITO surface. Given that k_S does not depend on tether length, we hypothesize that electron injection into a subpopulation of the adsorbed NCs occurs at high rates at a limited number of electroactive sites (i.e., "hot spots") on the heterogeneous ITO surface, and at much reduced rates elsewhere, owing to the barriers that exist at the electrode surface toward charge injection.[432] Self-exchange between adjacent NCs is also possible, but given the low NC surface coverages used in this study, these self-exchange rates are likely to be quite low.

Waveguide ATR spectroelectrochemistry is a relatively easily implemented technology that enables two important types of future experiments: (i) For CdSe and related semiconductor NCs that can be reduced in solution environments, we will be able to easily estimate first-reduction potentials and ECB, for both low and high coverage NC films and as a function of NC diameter. Different solvents and dipolar capping ligands may change frontier orbital energies and/or local vacuum levels, and we anticipate good sensitivity for quantification of these changes, down to ca. ± 50 meV. Waveguide spectroelectrochemistry allows the characterization of these electron injection processes under conditions that ensure that they are chemically reversible, something that has not been observed in previous solution or voltammetric studies.15-22 (ii) Switching rates for these electron injection processes can be measured using potential-modulated waveguide ATR. We anticipate that PM-ATR will enable characterization of the dynamics of electrochemical processes for a wide range of nanocrystalline materials, as bare NCs, or

surrounded by ultrathin polymer, oxide, or electrolyte hosts, or electrolyte environments of variable dielectric strength.

6. CONCLUSIONS AND FUTURE DIRECTIONS

6.1 Summary of Results

The overall goal of this project is to improve our understanding of charge transfer processes occurring at the interface between electroactive thin films and an indium tin oxide surface. More specifically, this research project has addressed: i) the orientation dependence of charge transfer rates of thin films of biomolecules, ii) surface treatment and modification effects on charge transfer kinetics of conducting polymers and, iii) estimation of rates of electron injection and conduction band edge of semiconductor nanocrystalline materials. These topics can be important for many applications of redox-active thin films such as biosensors and/or energy conversion systems.

A novel spectroelectrochemical technique, PM-ATR, has been used to evaluate four different redox-active films for these aims. First, a Prussian blue film was used to examine the PM-ATR technique for determination of charge transfer rates between an electrode and a molecular film. Second, an anisotropic cytochrome *c* protein film was used to probe charge transfer rates with respect to molecular orientation. Third, the effects of ITO surface treatment and modification on charge transfer kinetics on a conducting polymer, PEDOT/PSS, were studied. Fourth, PM-ATR was used for characterization of redox processes between submonolayer coverages of surface-tethered, pyr-CdSe NCs and ITO electrodes, and estimation of onset potentials for oxidation/reduction of this film was enabled by spectroelectrochemistry.

Four major results have been obtained during the course of this research project:

First, the rate of electron transfer of Prussian blue galvanostatically deposited on an ITO electrode has been successfully obtained by PM-ATR. The attenuated reflectivity was monitored in response to the applied potential waveform to extract the rate of electro-optical switching in PB films. The apparent electron transfer rate of PB on ITO obtained using PM-ATR was calculated to be $13.1 \pm 5.4\ s^{-1}$ ($n = 3$) which is about an order of magnitude higher than the results obtained by conventional cyclic voltammetry. This discrepancy may arise from differences in the rate constant calculation methodology between the optical and electrochemical technique, the assumptions made in Laviron's model used to obtain rate constants from CV, the effect of charging current on CV measurements, and/or the (slower) rate of counter ion movement within the film.

The second major result is that the structure of the adsorbed cytochrome *c* / ITO interface has been characterized in terms of the charge transfer rate with respect to the orientation of the protein using polarized PM-ATR. Consistent with a shorter tunneling distance, the protein adsorbed to ITO with the heme in a vertical orientation, which is probed with TM polarized light, was found to give a higher charge transfer rate with respect to the heme in a horizontal orientation. Using PM-ATR, this work has shown that one could determine the orientation-dependent electron transfer rate at particular wavelengths and/or potentials in order to individually probe specific redox events or subpopulations within the film. Correlation of molecular orientations with electron transfer rates in a redox-active molecular film has been achieved for the first time.

Third, charge transfer kinetics of PEDOT/PSS films (which are frequently used to facilitate hole injection between the transparent conductive oxide and an organic layer in

an OLED) on ITO have been studied with respect to various ITO surface treatments and modification. The apparent interfacial charge transfer rate constant for PEDOT/PSS on ITO has been reported for the first time. This measurement cannot be performed electrochemically due to high non-Faradaic background, which is eliminated using the optical method. Charge transfer kinetics of PEDOT/PSS were found to be almost independent of the surface modifier, FMPA, used in this study. The PEDOT/PSS films treated with heat indicate that the charge injection rates can be enhanced with respect to untreated films. However, in order to reach conclusive and reproducible results, the effects of surface treatments as well as surface modifier need to be further studied.

Fourth, PM-ATR enables, for the first time, characterization of reversible electron injection into submonolayer coverages of surface-tethered (via mercaptoalkylcarboxylic acids) pyr-CdSe NCs. The conduction band edge (E_{CB}) was estimated from optically determined onset potentials for electron injection, measured as bleaching/recovery of the exciton absorption band. Apparent rate constants for electron injection have been estimated (~500 s^{-1}) by PM-ATR and were found to be independent of tether chain length. We hypothesize communication between tethered NCs and electrochemically less active (i.e., less conductive) regions on the ITO surface is rate-limiting.

6.2 Future Directions

Electron transfer is a fundamental reaction in biological systems, especially in bioenergetic processes.[201] Binding of a protein to an electrode gives rise to a major simplification in kinetic analysis as a result of the absence of diffusional contributions to

the rate.[434] Understanding the orientation and conformation of proteins adsorbed on solid surfaces is important in design of biomaterials, biosensors, and bioanalytical systems.[170] The rates of electron transfer reactions of proteins in electrochemical systems appear to depend on the orientation of the immobilized protein molecules.[159, 189]

The process of interfacial charge injection is also of fundamental importance in several types of organic electronic devices, such as in solar cells, organic photovoltaics (OPVs) and organic light emitting diodes (OLEDs), as it can control the electrical characteristics and/or the efficiency of the device.[435, 436] Thus, control and improvement of the charge injection for the processing, storage and display of information is a major research focus. Molecular materials with optical properties are currently used in organic electronic devices and a great deal of contemporary research addresses various aspects of metal/organic interfaces, such as morphology, energetics and charge transport.[436]

Waveguide ATR spectroelectrochemistry, more specifically PM-ATR, is a relatively easily implemented technology should enable several important types of future experiments, some of which are summarized as follows:

i) As explained in Chapter 3, optimization of the orientation is required not only to achieve a fast electron transfer process between the protein active center and the electrode but also to facilitate the access of a binding partner protein or substrate from the solution phase to the immobilized protein.[166] Establishing structure-function relationships is crucial to the development of molecular devices based on immobilized proteins (e.g. biosensors). Application of PM-ATR to determine charge transfer kinetics and correlate rates with orientation distributions in other systems, such as redox active molecular films

with suitable intrinsic spectroscopic probes (that contain orientation information) in the visible region of the spectrum (for example cytochrome *c* oxidase) could be useful in the field of biosensors. A difficulty and limitation that the orientation distribution of various types of these films may be very broad, as observed for cyt *c* adsorbed to ITO. On the other hand, fixing an electroactive and anisotropic protein, e.g. cyt *c*, on a transparent electrode, e.g. ITO, may possibly narrow the molecular orientation distribution of the heme and can reduce the overlapping orientations which contribute to the measured TM and TE rate constants. In the literature, different chemical methods have been used to fix cyt *c* molecules on electrode surfaces, including electrostatic adsorption on ω-carboxylalkanethiols,[169] coordinative binding to pyridine-terminated alkanethiols[169] on Au/Ag surfaces, and covalent attachment using a carbodiimide under an applied potential[159] on a glassy carbon electrode. By fixing the protein to the electrode to achieve a defined and narrow orientation distribution, the contributions from small tilt angles (where TE light is more strongly absorbed) and large tilt angles (where the TM light is more strongly adsorbed) to the measured rate can easily be differentiated, and more accurate TE and TM rate constants with respect to the molecular orientation can be achieved.

ii) It is well recognized that interfaces between dissimilar materials (organic/organic and organic/inorganic) are a key factor for device function and efficiency.[209] The molecular dynamics of materials that are used at these interfaces in energy conversion devices often differ from the bulk behavior of these materials. Characterizing already-available and newly synthesized materials in terms of their

kinetics of charge transfer is needed to provide rational approaches towards device design. Improved understanding of the charge injection/collection kinetics at these interfaces should enable the design of more efficient and high performance power conversion technologies.

Organic modifiers such as perylene, phthalocyanine (Pc), and 4,4'-bis(*m*-tolylphenylamino) biphenyl (TPD) derivatives have been studied as transparent conducting oxide modifiers and are hypothesized to improve charge transfer efficiency across ITO/organic layer interfaces in organic electronic devices. Using waveguide-based spectroelectrochemistry (e.g. PM-ATR) systematic characterization of charge injection kinetics of these modifiers is possible which can help to design appropriate modifiers to be used in organic electronics to achieve high performance. In Figure 6.1a-c, molecular structures of organic modifiers, TPD-phosphonic acid (synthesized in the Marder group at Georgia Tech), N,N'-dialkyl-3,4,9,10- perylenetetracarboxyldiimides (PTCDI) and copper Pc (CuPc) are shown. Possible TPD-phosphonic acid orientations on ITO are also shown in Figure 6.1d. By using polarized PM-ATR, the effect of molecular orientation on the rate of electron transfer between organic modifiers and the ITO surface should also be possible. Preliminary results show that TPD-phosphonic acid monolayer are not stable and desorb from ITO surface. However, stability might be maintained by attachment of another phosphonic acid group and this may also be useful to achieve a defined orientation on the surface.

Another important area for future study is the effects of various surface treatments (ozone, acid etching, O_2 plasma treatments, etc.) and film deposition conditions (spin

coating, electrochemical deposition, adsorption, etc.) on charge transfer at transparent conducting oxide/organic interfaces. Surface energy measurements (contact angle measurements), XPS and UPS analysis of these differently treated and modified surfaces coupled with PM-ATR measurements will be useful to provide deeper understanding of the interface between organic layer and ITO to construct more efficient molecular devices.

Using different organic modifiers and surface treatments, the following questions can be addressed:

- Can the rate of electron transfer for modifier films be related to their molecular orientation distribution and does this affect the performance of OLED and photovoltaic devices?
- Can the electron transfer rate be tuned by changing the interactions (and thus the orientation) between the ITO surface and the organic modifier?
- How much (if any) are charge transfer rates to an overlying conducting layer (such as PEDOT/PSS) altered with a modifying layer with respect to the unmodified surface? Or can the rate be altered simply by changing the surface treatment of ITO or the film treatment?
- How do differences in surface treatments and film deposition affect charge injection rates, surface energy, and work function?

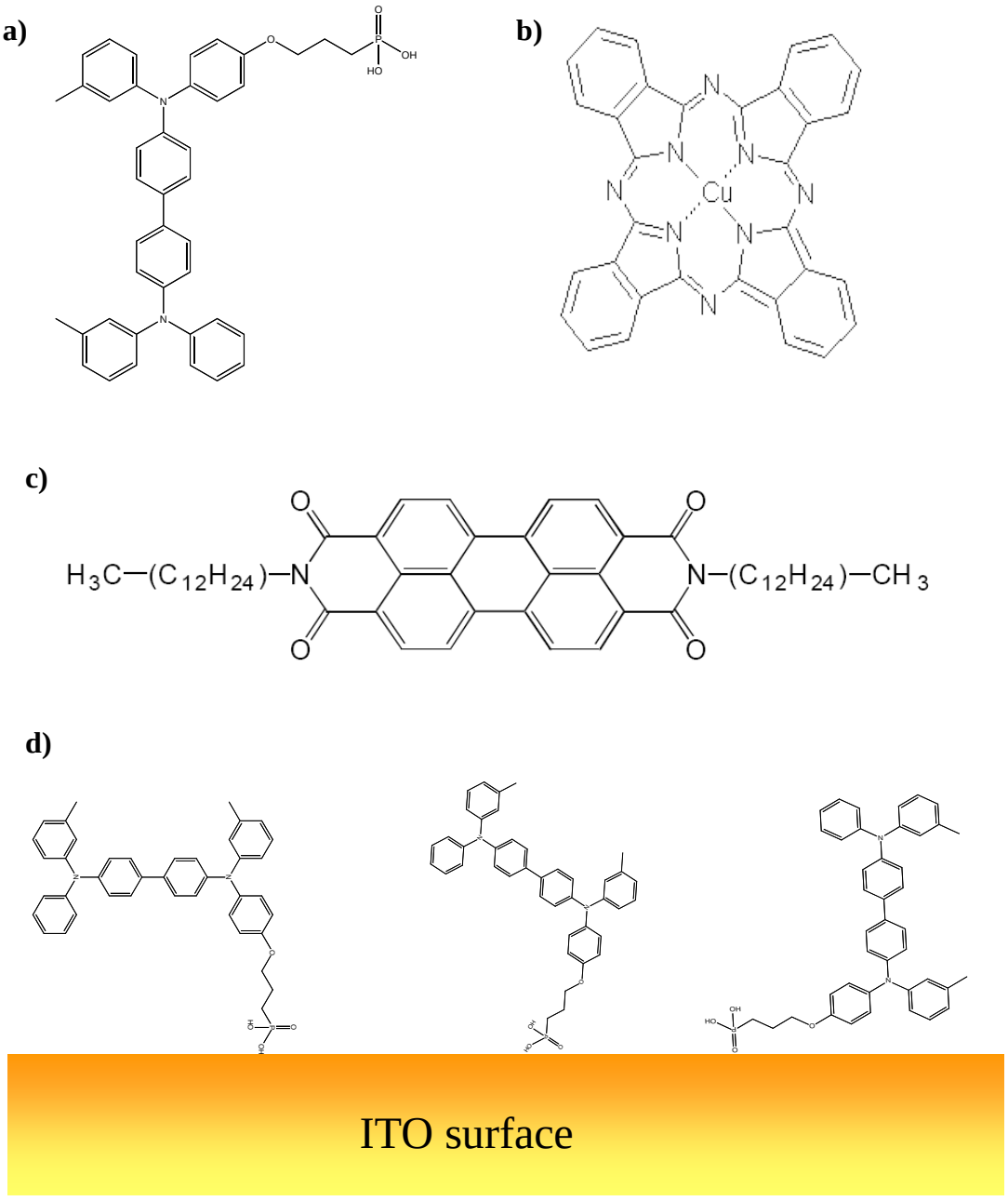

Figure 6.1 Molecular structures of organic modifiers and a diagram representing possible orientations of a surface modifier on ITO. Molecular structures of a) TPD-phosphonic acid, b) CuPc, and c) PTCDI. d) Possible molecular orientations of TPD phosphonic acid on an ITO (phosphonic acid groups anchor the molecules to ITO).

(iii) As explained in Chapter 5, gaining a complete understanding of the frontier orbital energies for both the polymer host and the SC-NP, in environments which closely approximate those found in photovoltaic devices, is required to engineer efficient charge injection in these devices. Two physical parameters can influence the ratio of injected electrons and holes, which are directly related to the quantum efficiency of the device:[209] 1) the injection barrier height and 2) the charge-carrier mobility. There are energy barriers for the injection/collection of charges from/to the electrodes into the charge conduction levels within the organic materials, and they need to be minimized. The energy barriers for charge injection at organic/electrode interfaces have usually been estimated by "vacuum-level alignment" using separately determined values for electrode work function, organic material ionization energy (IE or valence band energy), and electron affinity (EA or conduction band energy).[209] Experimentally determined hole and electron injection barriers (HIBs, EIBs) were found to be significantly different (sometimes more than 1 eV) from those estimated using vacuum-level alignment.[209, 310, 437, 438] Therefore developing an understanding of organic/electrode interface energetics in device-like environments and developing rational methods for controlling the charge injection barriers is needed.

From our spectroelectrochemical waveguide experiments on tethered submonolayer pyr-CdSe NCs, it has been shown that the energy band edges (conduction and valence band edges) and the rates of charge injection can be obtained quantitatively and sensitively. This approach can be extended to various NP films (CdS, InAs, PbSe, etc.) tethered to textured polymer hosts (e.g, poly(ethylenedioxythiophenes) such as

PEDOT/PSS or poly(alkylthiophenes) such as P3HT). Knowledge and subsequent optimization of frontier orbital energy levels and rates of charge injection at each electrode/NP and NP/host interface within these devices and ultimately can lead to more efficient energy conversion systems.

It is also important to investigate changes in valence band and conduction band energy levels due to the interaction between NCs and their local environment, especially the nature of capping ligands, host polymers, or small molecules. Changing the organic capping ligands can affect charge transport between NCs[427, 439-441] and it is hypothesized that frontier orbital energies of colloidal NCs can be altered using different ligands.[427, 442, 443] Differences in molecular dipole moment due to differences in capping ligand structure can shift the valence band edge of the NP. Examination of these energy levels of a select group of NPs such as CdSe, with different ligand environments to examine interface dipole effects, is possible by waveguide spectroelectrochemistry and corresponding charge transfer kinetics can be probe by PM-ATR spectroscopy. A schematic of possible capping ligands on NCs that are tethered to an ITO surface via a SAM is shown in Figure 6.2. Here, different ligands that surround a NC form a dielectric layer that may electronically and energetically isolate a NC from the local environment and create an interface dipole on NC surface which may affect surface work function and energy band edges.

Characterization of changes in charge transfer rates and shifts in band edge energies of these tethered NCs due to capping ligands of varying structure may be crucial to achieve efficient charge injection in a solid-state device. Spectroelectrochemical

waveguide techniques, e.g. PM-ATR along with UV- and X-ray photoelectron spectroscopies, should give a deeper understanding of the molecular processes at these interfaces. Correlation of these rates and band edge energies measured in electrolyte to measurements of device efficiency should enable design of these interfaces so that the resistance to charge collection can be minimized.

Overall, we anticipate that PM-ATR will enable characterization of the chemically reversible dynamics of electrochemical processes for a wide range of nanocrystalline materials, as bare NCs, or surrounded by ultrathin polymer, oxide, or electrolyte hosts, or electrolyte environments of variable dielectric strength (something that has not been observed in previous solution or voltammetric studies[397-399, 410-413, 415]). Waveguide spectroelectrochemistry will allow sensitive and systematic examination of frontier orbital energies and rates of ET of these various semiconductor NCs films. Working with high surface coverages of SC-NCs, e.g. pyr-CdSe NCs, can increase the NC-NC interactions and effects of these interactions on charge transfer rates and frontier orbital energies can also be evaluated.

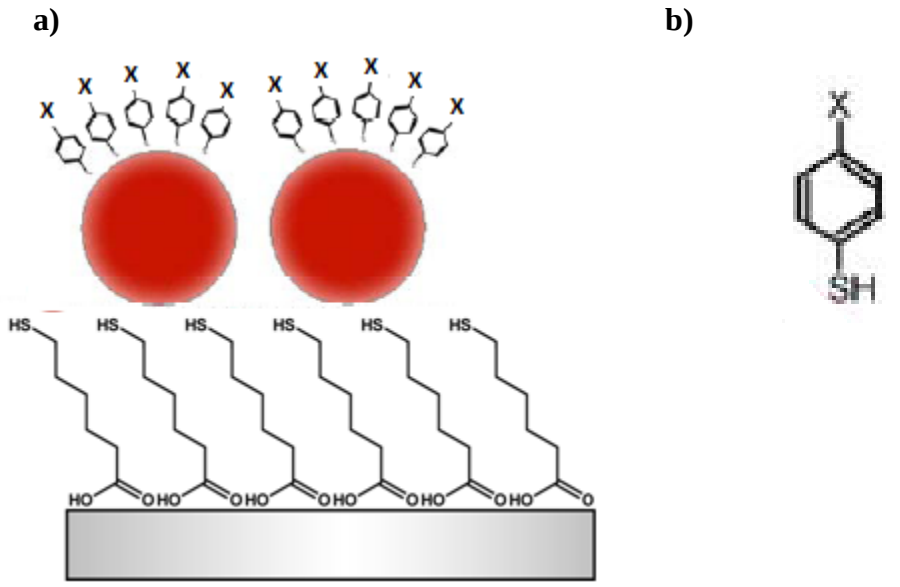

Figure 6.2 a) Schematic of NCs (CdSe, CdS, etc.) tethered to ITO with SAMs (e.g., mercaptoalkyl carboxylic acids). The capping ligands, benzenethiol (BT) derivatives, can be varied for each sample, with X substituents such as: -OCH_3, -CH_3, -F, -Cl, -NO_2. b) The structure of BT derivatives showing the X substituent.

.

REFERENCES

1. Gale, R. J., *Spectroelectrochemistry theory and practice*. Plenum Press: NewYork, 1988.

2. Heineman, W. R.; Hawkridge, F. M.; Blount, H. N., Spectroelectrochemistry At Optically Transparent Electrodes .2. Electrodes Under Thin-Layer And Semi-Infinite Diffusion Conditions And Indirect Coulometric Titrations. *Electroanalytical Chemistry* **1984,** 13, 1-113.

3. Kuwana, T.; Heineman, W. R., Study Of Electrogenerated Reactants Using Optically Transparent Electrodes. *Accounts Of Chemical Research* **1976,** 9, (7), 241-248.

4. Kuwana, T.; Winograd, N., Spectroelectrochemistry at optically transparent electrodes. I. Electrodes under semi-infinite diffusion conditions. In *Electroanalytical Chemistry*, Bard, A. J., Ed. Dekker: NewYork, 1974; Vol. 7, p 1.

5. Yamaguchi, T.; Valli, M.; Miyata, S.; Wakita, H., In-situ X-ray absorption spectroelectrochemistry for determination of the oxidation states and the local structure of metalloprotein model compounds. *Analytical Sciences* **1997,** 13, 37-40.

6. Hamnett, A.; Christensen, P. A.; Higgins, S. J., Analysis Of Electrogenerated Films By Ellipsometry And Infrared Spectrometry. *Analyst* **1994,** 119, (5), 735-747.

7. Clark, R. J. H.; Dyson, P. J.; Humphrey, D. G.; Johnson, B. F. G., In situ infrared spectroelectrochemical studies of [Ru6C(CO)(17)] and [Ru6C(CO)(16)](2-): the redox induced conversion of carbon monoxide to carbon dioxide. *Polyhedron* **1998,** 17, (17), 2985-2991.

8. Ito, T.; Hamaguchi, T.; Nagino, H.; Yamaguchi, T.; Washington, J.; Kubiak, C. P., Effects of rapid intramolecular electron transfer on vibrational spectra. *Science* **1997,** 277, (5326), 660-663.

9. Wang, X. M.; Yan, M. D.; Zhu, J. J.; Chen, H. Y., The surface-enhanced Raman spectroelectrochemical study on the interaction between beta-cyclodextrin and the electrochemically generated radical intermediate of flavin. *Journal Of Electroanalytical Chemistry* **1998,** 451, (1-2), 187-192.

10. Bancroft, E. E.; Sidwell, J. S.; Blount, H. N., Derivative Linear Sweep And Derivative Cyclic Voltabsorptometry. *Analytical Chemistry* **1981,** 53, (9), 1390-1394.

11. Dunphy, D. R. Ultrasensitive spectroelectrochemistry of monolayer and submonolayer thin films using an electroactive integrated optical waveguide. Dissertation, University of Arizona, Tucson, 1998.

12. Harrick, N. J., *Internal Reflection Spectroscopy*. Harrick Scientific Corporation: Ossining, NewYork, 1987.

13. Fahrenfort, J., Attenuated Total Reflection - A New Principle For The Production Of Useful Infra-Red Reflection Spectra Of Organic Compounds. *Spectrochimica Acta* **1961,** 17, (7), 698-&.

14. Hansen, W. N., A New Spectrophotometric Technique Using Multiple Attenuated Total Reflection. *Analytical Chemistry* **1963,** 35, (6), 765-&.

15. Hansen, W. N.; Kuwana, T.; Osteryou.Ra, Observation Of Electrode-Solution Interface By Means Of Internal Reflection Spectrometry. *Analytical Chemistry* **1966,** 38, (13), 1810-&.

16. Kuwana, T.; Darlington, R. K.; Leedy, D. W., Electrochemical Studies Using Conducting Glass Indicator Electrodes. *Analytical Chemistry* **1964,** 36, (10), 2023-&.

17. Itoh, K.; Fujishima, A., An Application Of Optical Wave-Guides To Electrochemistry - Construction Of Optical Wave-Guide Electrodes. *Journal Of Physical Chemistry* **1988,** 92, (25), 7043-7045.

18. Dunphy, D. R.; Mendes, S. B.; Saavedra, S. S.; Armstrong, N. R., The electroactive integrated optical waveguide: Ultrasensitive spectroelectrochemistry of submonolayer adsorbates. *Anal. Chem.* **1997,** 69, (15), 3086-3094.

19. Piraud, C.; Mwarania, E.; Wylangowski, G.; Wilkinson, J.; Odwyer, K.; Schiffrin, D. J., Optoelectrochemical Thin-Film Chlorine Sensor Employing Evanescent Fields On Planar Optical Wave-Guides. *Analytical Chemistry* **1992,** 64, (6), 651-655.

20. DiVirgilio-Thomas, J. M.; Heineman, W. R.; Seliskar, C. J., Spectroelectrochemical sensing based on multimode selectivity simultaneously achievable in a single device. 6. Sensing with a mediator. *Analytical Chemistry* **2000,** 72, (15), 3461-3467.

21. Maizels, M.; Seliskar, C. J.; Heineman, W. R., Spectroelectrochemical sensing based on multimode selectivity simultaneously achievable in a single device. 7. Sensing of Fe(CN)(6)(4-). *Electroanalysis* **2000,** 12, (17), 1356-1362.

22. Maizels, M.; Seliskar, C. J.; Heineman, W. R.; Bryan, S. A., Spectroelectrochemical sensing based on multimode selectivity simultaneously

achievable in a single device. 10. Sensing of ferrocyanide in Hanford tank waste simulant solution. *Electroanalysis* **2002,** 14, (19-20), 1345-1352.

23. Shi, Y. N.; Seliskar, C. J.; Heineman, W. R., Spectroelectrochemical sensing based on multimode selectivity simultaneously achievable in a single device .2. Demonstration of selectivity in the presence of direct interferences. *Analytical Chemistry* **1997,** 69, (23), 4819-4827.

24. Shi, Y. N.; Slaterbeck, A. F.; Seliskar, C. J.; Heineman, W. R., Spectroelectrochemical sensing based on multimode selectivity simultaneously achievable in a single device .1. Demonstration of concept with ferricyanide. *Analytical Chemistry* **1997,** 69, (18), 3679-3686.

25. Slaterbeck, A. F.; Ridgway, T. H.; Seliskar, C. J.; Heineman, W. R., Spectroelectrochemical sensing based on multimode selectivity simultaneously achievable in a single device. 3. Effect of signal averaging on limit of detection. *Analytical Chemistry* **1999,** 71, (6), 1196-1203.

26. Gao, L. T.; Seliskar, C. J.; Heineman, W. R., Spectroelectrochemical sensing based on multimode selectivity simultaneously achievable in a single device. 8. Selectivity at poly(vinyl alcohol)-polyelectrolyte blend modified optically transparent electrodes. *Electroanalysis* **2001,** 13, (8-9), 613-620.

27. Richardson, J. N.; Dyer, A. L.; Stegemiller, M. L.; Zudans, I.; Seliskar, C. J.; Heineman, W. R., Spectroelectrochemical sensing based on multimode selectivity simultaneously achievable in a single device. 13. Detection of aqueous iron by in situ complexation with 2,2 '-bipyridine. *Analytical Chemistry* **2002,** 74, (14), 3330-3335.

28. Slaterbeck, A. F.; Stegemiller, M. L.; Seliskar, C. J.; Ridgway, T. H.; Heineman, W. R., Spectroelectrochemical sensing based on multimode selectivity simultaneously achievable in a single device. 5. Simulation of sensor response for different excitation potential waveforms. *Analytical Chemistry* **2000,** 72, (22), 5567-5575.

29. Ross, S. E.; Seliskar, C. J.; Heineman, W. R., Spectroelectrochemical sensing based on multimode selectivity simultaneously achievable in a single device. 9. Incorporation of planar waveguide technology. *Analytical Chemistry* **2000,** 72, (22), 5549-5555.

30. Bumm, L. A.; Arnold, J. J.; Dunbar, T. D.; Allara, D. L.; Weiss, P. S., Electron transfer through organic molecules. *J. Phys. Chem. B* **1999,** 103, (38), 8122-8127.
31. Joachim, C., The Conductance Of A Single Molecule. *New J. Chem.* **1991,** 15, (2-3), 223-229.

32. Miller, J. S., Molecular Materials .2a. Molecular Electronics. *Adv. Mater.* **1990,** 2, (8), 378-379.

33. Miller, J. S., Molecular Electronics .2. *Adv. Mater.* **1990,** 2, (10), 495-497.

34. Marcus, R. A., Chemical + Electrochemical Electron-Transfer Theory. *Annual Review Of Physical Chemistry* **1964,** 15, 155-&.

35. Marcus, R. A., Theory Of Oxidation-Reduction Reactions Involving Electron Transfer .3. Applications To Data On The Rates Of Organic Redox Reactions. *Journal Of Chemical Physics* **1957,** 26, (4), 872-877.

36. Marcus, R. A., Theory Of Oxidation-Reduction Reactions Involving Electron Transfer .2. Applications To Data On The Rates Of Isotopic Exchange Reactions. *Journal Of Chemical Physics* **1957,** 26, (4), 867-871.

37. Marcus, R. A., On The Theory Of Oxidation-Reduction Reactions Involving Electron Transfer .1. *Journal Of Chemical Physics* **1956,** 24, (5), 966-978.

38. Marcus, R. A., Theory Of Electron-Transfer Reaction Rates Of Solvated Electrons. *Journal Of Chemical Physics* **1965,** 43, (10P1), 3477-&.

39. Marcus, R. A., On Theory Of Electron-Transfer Reactions .6. Unified Treatment For Homogeneous And Electrode Reactions. *Journal Of Chemical Physics* **1965,** 43, (2), 679-&.

40. Chandra, A., A theoretical study of outersphere electron transfer reactions in electrolyte solutions. *Journal Of Chemical Physics* **1999,** 110, (3), 1569-1580.

41. Hynes, J. T., Outer-Sphere Electron-Transfer Reactions And Frequency-Dependent Friction. *Journal Of Physical Chemistry* **1986,** 90, (16), 3701-3706.

42. Fawcett, W. R., The role of the metal and the solvent in simple heterogeneous electron transfer reactions. *Electrochimica Acta* **1997,** 42, (5), 833-839.

43. Smith, B. B.; Hynes, J. T., Electronic Friction And Electron-Transfer Rates At Metallic Electrodes. *Journal Of Chemical Physics* **1993,** 99, (9), 6517-6530.

44. Hartnig, C.; Koper, M. T. M., Molecular dynamics simulations of solvent reorganization in electron-transfer reactions. *Journal Of Chemical Physics* **2001,** 115, (18), 8540-8546.

45. Leite, V. B. P., Smooth landscape solvent dynamics in electron transfer reactions. *Journal Of Chemical Physics* **1999,** 110, (20), 10067-10075.

46. Kim, H. J.; Hynes, J. T., Role Of Solvent Electronic Polarization In Electron-Transfer Processes. *Journal Of Physical Chemistry* **1990,** 94, (7), 2736-2740.

47. Calef, D. F.; Wolynes, P. G., Classical Solvent Dynamics And Electron-Transfer .1. Continuum Theory. *Journal Of Physical Chemistry* **1983,** 87, (18), 3387-3400.

48. Calef, D. F.; Wolynes, P. G., Classical Solvent Dynamics And Electron-Transfer .2. Molecular Aspects. *Journal Of Chemical Physics* **1983,** 78, (1), 470-482.

49. Leopold, M. C. Interfacial investigation of a biological electron transfer model: cytochrome c adsorbed on gold electrodes modified with self-assembled monolayers. Dissertation, North Carolina State University, 2000.

50. Taube, H., *Electron transfer reactions of Complex ions in Solution.* Academic: NewYork, 1970.

51. Bard, A. J.; Faulkner, L. R., *Electrochemical Methods, Fundamentals and Applications.* John Wiley & Sons, Inc.: NewYork, 2001; p 87-132.

52. Clegg, A. D.; Rees, N. V.; Klymenko, O. V.; Coles, B. A.; Compton, R. G., Marcus theory of outer-sphere heterogeneous electron transfer reactions: Dependence of the standard electrochemical rate constant on the hydrodynamic radius from high precision measurements of the oxidation of anthracene and its derivatives in nonaqueous solvents using the high-speed channel electrode. *Journal Of The American Chemical Society* **2004,** 126, (19), 6185-6192.

53. Zhang, X.; Leddy, J.; Bard, A. J., Dependence Of Rate Constants Of Heterogeneous Electron-Transfer Reactions On Viscosity. *Journal Of The American Chemical Society* **1985,** 107, (12), 3719-3721.

54. Amatore, C.; Saveant, J. M.; Tessier, D., Charge-Transfer At Partially Blocked Surfaces - A Model For The Case Of Microscopic Active And Inactive Sites. *Journal Of Electroanalytical Chemistry* **1983,** 147, (1-2), 39-51.

55. Amatore, C.; Saveant, J. M.; Tessier, D., Kinetics Of Electron-Transfer To Organic-Molecules At Solid Electrodes In Organic Media. *Journal Of Electroanalytical Chemistry* **1983,** 146, (1), 37-45.

56. Chidsey, C. E. D., Free-Energy And Temperature-Dependence Of Electron-Transfer At The Metal-Electrolyte Interface. *Science* **1991,** 251, (4996), 919-922.

57. Murray, R. W.; Ewing, A. G.; Durst, R. A., Chemically Modified Electrodes - Molecular Design For Electroanalysis. *Analytical Chemistry* **1987,** 59, (5), A379-&.

58. Faulkner, L. R., Chemical Microstructures On Electrodes. *Chemical & Engineering News* **1984,** 62, (9), 28-&.

59. Bard, A. J., Chemical Modification Of Electrodes. *Journal Of Chemical Education* **1983,** 60, (4), 302-304.

60. Murray, R. W., Chemically Modified Electrodes. *Accounts Of Chemical Research* **1980,** 13, (5), 135-141.

61. Hong, H. G.; Mallouk, T. E., Electrochemical Measurements Of Electron-Transfer Rates Through Zirconium 1,2-Ethanediylbis(Phosphonate) Multilayer Films On Gold Electrodes. *Langmuir* **1991,** 7, (10), 2362-2369.

62. Hush, N. S., Electron transfer in retrospect and prospect 1: Adiabatic electrode processes (vol 460, p 5, 1999). *Journal Of Electroanalytical Chemistry* **1999,** 470, (2), 170-195.

63. Marcus, R. A.; Sutin, N., Electron Transfers In Chemistry And Biology. *Biochimica Et Biophysica Acta* **1985,** 811, (3), 265-322.

64. Newton, M. D.; Sutin, N., Electron-Transfer Reactions In Condensed Phases. *Annual Review Of Physical Chemistry* **1984,** 35, 437-480.

65. Hush, N. S., Adiabatic Rate Processes At Electrodes .1. Energy-Charge Relationships. *Journal Of Chemical Physics* **1958,** 28, (5), 962-972.

66. Marcus, R. A., Electrostatic Free Energy And Other Properties Of States Having Nonequilibrium Polarization .1. *Journal Of Chemical Physics* **1956,** 24, (5), 979-989.

67. Whittle, C. E. Electron transfer within various organometallic species. Dissertation, University of Florida, 2000.

68. http://www.chem.unc.edu/undergrads/2002fall/chem145_murray/classnotes/ETheory.pdf

69. Armstrong, F. A.; Heering, H. A.; Hirst, J., Reactions of complex metalloproteins studied by protein-film voltammetry. *Chemical Society Reviews* **1997,** 26, (3), 169-179.

70. Avila, A.; Gregory, B. W.; Niki, K.; Cotton, T. M., An electrochemical approach to investigate gated electron transfer using a physiological model system: Cytochrome c immobilized on carboxylic acid-terminated alkanethiol self-assembled monolayers on gold electrodes. *Journal Of Physical Chemistry B* **2000,** 104, (12), 2759-2766.

71. Bard, A. J.; Faulkner, L. R., *Electrochemical Methods: Fundamentals and Applications.* 2nd ed.; John Wiley & Sons, Inc.: New York, 2001; p 368-630.

72. Brett, C. M. A.; Brett, A. M. O., *Electrochemistry - Principles, Methods, and Applications.* Oxford University Press: Oxford, 1993.

73. Laviron, E., General Expression Of The Linear Potential Sweep Voltammogram In The Case Of Diffusionless Electrochemical Systems. *J. Electroanal. Chem.* **1979,** 101, (1), 19-28.

74. Runge, A. F. Structure-activity studies of surface immobilized cytochrome c films on indium tin oxide: solution adsorbed and microcontact printed films. Dissertation, University of Arizona, Tucson, 2005.

75. Li, G. Electrochemical investigation of copper deposition onto silicon from hydrofluoric acid and buffered hydrofluoric acid solutions. Dissertation, U of A, Tucson, 1998.

76. Roberge, P. R.; Beaudoin, R., EVALUATION OF CHARGE-TRANSFER RESISTANCE BY GEOMETRICAL EXTRAPOLATION OF THE CENTER OF SEMICIRCULAR IMPEDANCE DIAGRAMS. *Journal of Applied Electrochemistry* **1988,** 18, (1), 38-42.

77. Laviron, E., Ac Polarography And Faradaic Impedance Of Strongly Adsorbed Electroactive Species .1. Theoretical And Experimental-Study Of A Quasi-Reversible Reaction In The Case Of A Langmuir Isotherm. *J. Electroanal. Chem.* **1979,** 97, (2), 135-149.

78. MacDonald, J., *Impedance Spectoscopy, Emphasizing Solid Materials and Systems.* John Wiley & Sons Inc.: 1987.

79. Mansfeld, F., Electrochemical Impedance Spectroscopy (Eis) As A New Tool For Investigating Methods Of Corrosion Protection. *Electrochimica Acta* **1990,** 35, (10), 1533-1544.

80. Nahir, T. M.; Bowden, E. F., The distribution of standard rate constants for electron transfer between thiol-modified gold electrodes and adsorbed cytochrome c. *Journal Of Electroanalytical Chemistry* **1996,** 410, (1), 9-13.

81. Song, S.; Clark, R. A.; Bowden, E. F.; Tarlov, M. J., Characterization Of Cytochrome-C Alkanethiolate Structures Prepared By Self-Assembly On Gold. *Journal Of Physical Chemistry* **1993,** 97, (24), 6564-6572.

82. Creager, S. E.; Wooster, T. T., A new way of using ac voltammetry to study redox kinetics in electroactive monolayers. *Analytical Chemistry* **1998,** 70, (20), 4257-4263.

83. Harrington, D. A., Ac Voltammetry For Measurement Of Surface Kinetics. *Journal Of Electroanalytical Chemistry* **1993,** 355, (1-2), 21-35.

84. Hansen, W. N., Internal Reflection Spectroscopy And Determination Of Optical Constants. *Isa Transactions* **1965,** 4, (3), 263-&.

85. Hansen, W. N., Expanded Formulas For Attenuated Total Reflection And Derivation Of Absorption Rules For Single And Multiple Atr Spectrometer Cells. *Spectrochimica Acta* **1965,** 21, (4), 815-&.

86. Harrick, N. J., *Internal Reflection Spectroscopy*. 2nd ed.; Harrick Scientific Corporation: Ossining, NewYork, 1979.

87. Reichert, W. M., Evanescent Detection Of Adsorbed Films - Assessment Of Optical Considerations For Absorbance And Fluorescence Spectroscopy At The Crystal Solution And Polymer-Solution Interfaces. *Critical Reviews In Biocompatibility* **1989,** 5, (2), 173-205.

88. Bohn, P. W., Optical Wave-Guide Techniques For Structural And Chemical-Analysis In Thin-Film And Interfacial Systems. *Trac-Trends In Analytical Chemistry* **1987,** 6, (9), 223-233.

89. Doherty, W. J. Polymer-mediated electrochemistry in sol-gel thin films and spectroelectrochemical characterization of molecular adlayers on indium-tin oxides electrode surfaces. Dissertation, University of Arizona, Tucson, 2005.

90. Petty, M. C.; Bryce, M. R.; Bloor, D., *An Introduction to Molecular Electronics*. Oxford University Press: NewYork, 1995.

91. Feng, Z. Q.; Imabayashi, S.; Kakiuchi, T.; Niki, K., Determination of the electrode kinetic parameters of a species immobilized on electrodes using the electroreflectance (ER) voltammogram. *J. Electroanal. Chem.* **1996,** 408, (1-2), 15-20.

92. Feng, Z. Q.; Sagara, T.; Niki, K., Application Of Potential-Modulated Uv-Visible Reflectance Spectroscopy To Electron-Transfer Rate Measurements For Adsorbed Species On Electrode Surfaces. *Anal. Chem.* **1995,** 67, (19), 3564-3570.

93. Sagara, T.; Igarashi, S.; Sato, H.; Niki, K., Voltammetric Application Of Electromodulated Electroreflection Absorption-Spectroscopy - Electroreflectance Voltammetry As An Insitu Spectroelectrochemical Technique. *Langmuir* **1991,** 7, (5), 1005-1012.

94. Yamada, T.; Hashimoto, T.; Kikushima, S.; Ohtsuka, T.; Nango, M., Electron transfer of manganese halogenated tetraphenylporphyrin derivatives assembled on gold electrodes. *Langmuir* **2001,** 17, (15), 4634-4640.

95. Yamada, T.; Nango, M.; Ohtsuka, T., Potential modulation reflectance of manganese halogenated tetraphenylporphyrin derivatives assembled on gold electrodes. *Journal Of Electroanalytical Chemistry* **2002,** 528, (1-2), 93-102.

96. Gaigalas, A. K.; Niaura, G., Measurement of electron transfer rates between adsorbed azurin and a gold electrode modified with a hexanethiol layer. *Journal Of Colloid And Interface Science* **1997,** 193, (1), 60-70.

97. Feng, Z. Q.; Imabayashi, S.; Kakiuchi, T.; Niki, K., Long-range electron-transfer reaction rates to cytochrome c across long- and short-chain alkanethiol self-assembled monolayers: Electroreflectance studies. *Journal Of The Chemical Society-Faraday Transactions* **1997,** 93, (7), 1367-1370.

98. Feng, Z. Q.; Imabayashi, S.; Kakiuchi, T.; Niki, K., Electroreflectance Spectroscopic Study Of The Electron-Transfer Rate Of Cytochrome-C Electrostatically Immobilized On The Omega-Carboxyl Alkanethiol Monolayer Modified Gold Electrode. *Journal Of Electroanalytical Chemistry* **1995,** 394, (1-2), 149-154.

99. Ruzgas, T.; Wong, L.; Gaigalas, A. K.; Vilker, V. L., Electron transfer between surface-confined cytochrome c and an N-acetylcysteine-modified gold electrode. *Langmuir* **1998,** 14, (25), 7298-7305.

100. Sagara, T.; Niwa, K.; Sone, A.; Hinnen, C.; Niki, K., Redox Reaction-Mechanism Of Cytochrome-C At Modified Gold Electrodes. *Langmuir* **1990,** 6, (1), 254-262.

101. Sagara, T.; Murase, H.; Komatsu, M.; Nakashima, N., Toward the interpretation of electroreflectance spectral profiles: Hemin adsorbed on an HOPG electrode revisited. *Applied Spectroscopy* **2000,** 54, (2), 316-323.

102. Amemiya, T.; Hashimoto, K.; Fujishima, A., Frequency-Resolved Faradaic Processes In Polypyrrole Films Observed By Electromodulation Techniques - Electrochemical Impedance And Color Impedance Spectroscopies. *J. Phys. Chem.* **1993,** 97, (16), 4187-4191.

103. Amemiya, T.; Hashimoto, K.; Fujishima, A., Faradaic Charge-Transfer With Double-Layer Charging And Or Adsorption-Related Charging At Polymer-Modified Electrodes As Observed By Color Impedance Spectroscopy. *J. Phys. Chem.* **1993,** 97, (38), 9736-9740.

104. Amemiya, T.; Hashimoto, K.; Fujishima, A., Dynamics Of Faradaic Processes In Polypyrrole Polystyrenesulfonate Composite Films In The Presence And Absence Of A Redox Species In Aqueous-Solutions. *J. Phys. Chem.* **1993,** 97, (16), 4192-4195.

105. Amemiya, T.; Hashimoto, K.; Fujishima, A., Color Impedance Spectroscopy Of Polypyrrole Films. *J. Electroanal. Chem.* **1994,** 377, (1-2), 143-148.

106. Garcia-Canadas, J.; Meacham, A. P.; Peter, L. M.; Ward, M. D., Electrochromic switching in the visible and near IR with a Ru-dioxolene complex adsorbed on a nanocrystalline SnO2 electrode. *Electrochemistry Communications* **2003,** 5, (5), 416-420.

107. Riley, D. J.; Tull, E. J., Potential modulated absorbance spectroscopy: an investigation of the potential distribution at a CdS nanoparticle modified electrode. *Journal Of Electroanalytical Chemistry* **2001,** 504, (1), 45-51.

108. Toyota, A.; Nakashima, N.; Sagara, T., UV-visible transmission-absorption spectral study of Au nanoparticles on a modified ITO electrode at constant potentials and under potential modulation. *Journal Of Electroanalytical Chemistry* **2004,** 565, (2), 335-342.

109. Doherty, W. J.; Wysocki, R. J.; Armstrong, N. R.; Saavedra, S. S., Potential-modulated, attenuated total reflectance spectroscopy of poly(3,4-ethylenedioxythiophene) and poly(3,4-ethylenedioxythiophene methanol) copolymer films on indium-tin oxide. *Journal Of Physical Chemistry B* **2006,** 110, (10), 4900-4907.

110. Bard, A. J.; Faulkner, L. R., *Electrochemical Methods*. John Wiley & Sons, Inc.: NewYork, 1980.

111. Lelievre, D.; Plichon, V.; Laviron, E., Ac Polarography And Faradaic Impedance Of Strongly Adsorbed Electroactive Species .4. Experimental-Study Of The Faradaic Impedance Of The Redox System Benzo(C)Cinnoline-Dihydrobenzo(C) Cinnoline. *Journal Of Electroanalytical Chemistry* **1980,** 112, (1), 137-145.

112. Laviron, E.; Roullier, L.; Degrand, C., A Multilayer Model For The Study Of Space Distributed Redox Modified Electrodes .2. Theory And Application Of Linear Potential Sweep Voltammetry For A Simple Reaction. *J. Electroanal. Chem.* **1980,** 112, (1), 11-23.

113. Sagara, T.; Niki, K., Surface Processes And Adsorption States Of Methylene-Blue At Graphite Electrode Surfaces In An Acidic Medium - An Electroreflectance Study. *Langmuir* **1993,** 9, (3), 831-838.

114. Sagara, T.; Iizuka, J.; Niki, K., Electroreflectance Study Of The Redox Reaction Of Methylene-Blue Adsorbed On A Pyrolytic-Graphite Electrode. *Langmuir* **1992,** 8, (3), 1018-1025.

115. Garciajareno, J. J.; Navarro, J. J.; Roig, A. F.; Scholl, H.; Vicente, F., Impedance Analysis Of Prussian-Blue Films Deposited On Ito Electrodes. *Electrochimica Acta* **1995,** 40, (9), 1113-1119.

116. Saliba, R.; Agricole, B.; Mingotaud, C.; Ravaine, S., Voltammetric and impedance analysis of dimethyldioctadecylammoniunl/Prussian Blue Langmuir-Blodgett films on ITO electrodes. *Journal Of Physical Chemistry B* **1999,** 103, (44), 9712-9716.

117. Mortimer, R. J.; Reynolds, J. R., In situ colorimetric and composite coloration efficiency measurements for electrochromic Prussian blue. *Journal Of Materials Chemistry* **2005,** 15, (22), 2226-2233.

118. Buser, H. J.; Schwarzenbach, D.; Petter, W.; Ludi, A., Crystal-Structure Of Prussian Blue - Fe4[Fe(Cn)6]3.Xh2o. *Inorg. Chem.* **1977,** 16, (11), 2704-2710.

119. Abbaspour, A.; Kamyabi, M. A., Electrochemical formation of Prussian blue films with a single ferricyanide solution on gold electrode. *Journal Of Electroanalytical Chemistry* **2005,** 584, (2), 117-123.

120. Aoki, K.; Miyamoto, T.; Ohsawa, Y., The Determination Of The Selectivity Coefficient Of Na+ Versus Li+ On Prussian Blue Thin-Film In Propylene Carbonate By Means Of A Quartz Crystal Microbalance. *Bull. Chem. Soc. Jpn.* **1989,** 62, (5), 1658-1659.

121. Feldman, B. J.; Murray, R. W., Electron-Diffusion In Wet And Dry Prussian Blue Films On Interdigitated Array Electrodes. *Inorg. Chem.* **1987,** 26, (11), 1702-1708.

122. Garcia-Jareno, J. J.; Benito, D.; Navarro-Laboulais, J.; Vicente, F., Electrochemical behavior of electrodeposited Prussian blue films on ITO electrodes - An attractive laboratory experience. *Journal Of Chemical Education* **1998,** 75, (7), 881-884.

123. Garcia-Jareno, J. J.; Navarro-Laboulais, J.; Vicente, F., Charge transport in Prussian Blue Films Deposited on ITO Electrodes. *Electrochim. Acta* **1996,** 41, (6), 835-841.

124. Garcia-Jareno, J. J.; Sanmatias, A.; Navarro-Laboulais, J.; Benito, D.; Vicente, F., Temperature dependence of impedance spectra of Prussian Blue films deposited on ITO electrodes. *Electrochim. Acta* **1998,** 43, (3-4), 235-243.

125. Garcia-Jareno, J. J.; Sanmatias, A.; Navarro-Laboulais, J.; Vicente, F., The role of potassium and hydrogen ions in the Prussian Blue reversible arrow Everitt's salt process. *Electrochim. Acta* **1998,** 44, (2-3), 395-405.

126. Garcia-Jareno, J. J.; Sanmatias, A.; Navarro-Laboulais, J.; Vicente, F., Chronoamperometry of prussian blue films on ITO electrodes: ohmic drop and film thickness effect. *Electrochim. Acta* **1999,** 44, (26), 4753-4762.

127. Itaya, K.; Ataka, T.; Toshima, S., Spectroelectrochemistry And Electrochemical Preparation Method Of Prussian Blue Modified Electrodes. *J. Amer. Chem. Soc.* **1982,** 104, (18), 4767-4772.

128. Karyakin, A. A.; Gitelmacher, O. V.; Karyakina, E. E., Prussian Blue Based First-Generation Biosensor - A Sensitive Amperometric Electrode For Glucose. *Anal. Chem.* **1995,** 67, (14), 2419-2423.

129. Nakayama, M.; Lino, M.; Ogura, K., In situ infrared spectroscopic investigations on the electrochemical properties of Prussian blue-polyaniline-modified electrodes with various anionic Fe(II) complexes working as a mediator for the electroreduction of CO2. *J. Electroanal. Chem.* **1997,** 440, (1-2), 251-257.

130. Neff, V. D., Electrochemical Oxidation And Reduction Of Thin-Films Of Prussian Blue. *J. Electrochem. Soc.* **1978,** 125, (6), 886-887.

131. Ogura, K.; Nakayama, M.; Kusumoto, C., In situ Fourier transform infrared spectroscopic studies on a metal complex-immobilized polyaniline Prussian blue modified electrode and the application to the electroreduction of CO2. *J. Electrochem. Soc.* **1996,** 143, (11), 3606-3615.

132. Pan, K. C.; Chuang, C. S.; Cheng, S. H.; Su, Y. O., Electrocatalytic reactions of nitric oxide on Prussian blue film modified electrodes. *Journal Of Electroanalytical Chemistry* **2001,** 501, (1-2), 160-165.

133. Roig, A.; Navarro, J.; Garcia, J. J.; Vicente, F., Voltammetric Study On The Stability Of Deposited Prussian Blue Films Against Successive Potential Cycling. *Electrochim. Acta* **1994,** 39, (3), 437-442.

134. Itaya, K.; Ataka, T.; Toshima, S.; Shinohara, T., Electrochemistry Of Prussian Blue - An Insitu Mossbauer-Effect Measurement. *J. Phys. Chem.* **1982,** 86, (13), 2415-2418.

135. Garcia-Jareno, J. J.; Navarro-Laboulais, J.; Sanmatias, A.; Vicente, F., The correlation between electrochemical impedance spectra and voltammograms of PB films in aqueous NH4Cl and CsCl. *Electrochim. Acta* **1998,** 43, (9), 1045-1052.

136. Ricci, F.; Palleschi, G., Sensor and biosensor preparation, optimisation and applications of Prussian Blue modified electrodes. *Biosensors & Bioelectronics* **2005,** 21, (3), 389-407.

137. Ziegler, J. P.; Hemminger, J. C., Spectroscopic And Electrochemical Characterization Of The Photochromic Behavior Of Prussian Blue Films On N-Srtio3. *Journal Of The Electrochemical Society* **1987,** 134, (2), 358-363.

138. Itaya, K.; Akahoshi, H.; Toshima, S., Electrochemistry Of Prussian Blue Modified Electrodes - An Electrochemical Preparation Method. *Journal Of The Electrochemical Society* **1982,** 129, (7), 1498-1500.

139. Roig, A.; Navarro, J.; Tamarit, R.; Vicente, F., Stability Of Prussian Blue Films On Ito Electrodes - Effect Of Different Anions. *Journal Of Electroanalytical Chemistry* **1993,** 360, (1-2), 55-69.

140. Brennan, C. B.; Sun, L. F.; Weber, S. G., Investigations of prussian blue films using surface plasmon resonance. *Sensors And Actuators B-Chemical* **2001,** 72, (1), 1-10.

141. Ogura, K.; Nakayama, M.; Nakaoka, K., Electrochemical quartz crystal microbalance and in situ infrared spectroscopic studies on the redox reaction of Prussian blue. *Journal Of Electroanalytical Chemistry* **1999,** 474, (2), 101-106.

142. Garcia-Jareno, J. J. N., J. J. ; Roig, A. F.; Scholl H. and Vicente, F., Impedance Analysis of Prussian Blue Films Deposited on ITO Electrodes. *Electrochim. Acta* **1995,** 40, (9), 1113-1119.

143. Ellis, D.; Eckhoff, M.; Neff, V. D., Electrochromism In The Mixed-Valence Hexacyanides .1. Voltammetric And Spectral Studies Of The Oxidation And Reduction Of Thin-Films Of Prussian Blue. *Journal Of Physical Chemistry* **1981,** 85, (9), 1225-1231.

144. Armstrong, N. R.; Carter, C.; Donley, C.; Simmonds, A.; Lee, P.; Brumbach, M.; Kippelen, B.; Domercq, B.; Yoo, S. Y., Interface modification of ITO thin films: organic photovoltaic cells. *Thin Solid Films* **2003,** 445, (2), 342-352.

145. Mortimer, R. J.; Rosseinsky, D. R., Electrochemical Polychromicity In Iron Hexacyanoferrate Films, And A New Film Form Of Ferric Ferricyanide. *J. Electroanal. Chem.* **1983,** 151, (1-2), 133-147.

146. Doherty, W. J.; Donley, C. L.; Armstrong, N. R.; Saavedra, S. S., Broadband spectroelectrochemical attenuated total reflectance instrument for molecular adlayer studies. *Appl. Spectrosc.* **2002,** 56, (7), 920-927.

147. Ge, C. H.; Doherty, W. J.; Mendes, S. B.; Armstrong, N. R.; Saavedra, S. S., Voltammetric and waveguide spectroelectrochemical characterization of ultrathin poly (aniline)/poly (acrylic acid) films self-assembled on indium-tin oxide. *Talanta* **2005,** 65, (5), 1126-1131.

148. Siperko, L. M.; Kuwana, T., Electrochemical And Spectroscopic Studies Of Metal Hexacyanometalate Films .1. Cupric Hexacyanoferrate. *J. Electrochem. Soc.* **1983,** 130, (2), 396-402.

149. Toyoda, Y.; Katoh, N.; Kuwabara, K., Dependence of redox characteristics in Prussian blue-modified electrode on pH of electrolytic solution. *Materials Science And Engineering B-Solid State Materials For Advanced Technology* **2004,** 108, (3), 271-277.

150. Agrisuelas, J.; Garcia-Jareno, J. J.; Gimenez-Romero, D.; Vicente, F., Innovative Combination of Three Alternating Current Relaxation Techniques: Electrical Charge, Mass, and Color Impedance Spectroscopy. Part II: Prussian Blue <--> Everitt's Salt Process. *Journal Of Physical Chemistry C* **2009,** 113, (19), 8438-8446.

151. Agrisuelas, J.; Garcia-Jareno, J. J.; Gimenez-Romero, D.; Vicente, F., Innovative Combination of Three Alternating Current Relaxation Techniques: Electrical Charge, Mass, and Color Impedance Spectroscopy. Part I: The Tool. *Journal Of Physical Chemistry C* **2009,** 113, (19), 8430-8437.

152. Agrisuelas, J.; Bueno, P. R.; Ferreira, F. F.; Gabrielli, C.; Garcia-Jareno, J. J.; Gimenez-Romero, D.; Perrot, H.; Vicente, F., Electronic Perspective on the Electrochemistry of Prussian Blue Films. *Journal Of The Electrochemical Society* **2009,** 156, (4), P74-P80.

153. Scott, R. A.; Mauk, A. G., *Cytochrome c: A Multidisciplinary Approach*. University Science Books: Sausalito, CA, 1996; p 738.

154. Sivakolundu, S. G.; Mabrouk, P. A., Cytochrome c structure and redox function in mixed solvents are determined by the dielectric constant. *Journal Of The American Chemical Society* **2000,** 122, (7), 1513-1521.

155. Brooks, C. L., Viewing protein folding from many perspectives. *Proceedings Of The National Academy Of Sciences Of The United States Of America* **2002,** 99, (3), 1099-1100.

156. Jain, R. K.; Hamilton, A. D., Designing protein denaturants: Synthetic agents induce cytochrome c unfolding at low concentrations and stoichiometries. *Angewandte Chemie-International Edition* **2002,** 41, (4), 641-+.

157. Wei, J. J.; Liu, H. Y.; Dick, A. R.; Yamamoto, H.; He, Y. F.; Waldeck, D. H., Direct wiring of cytochrome c's heme unit to an electrode: Electrochemical studies. *Journal Of The American Chemical Society* **2002,** 124, (32), 9591-9599.

158. Bowden, E. F.; Hawkridge, F. M.; Blount, H. N., Interfacial Electrochemistry Of Cytochrome-C At Tin Oxide, Indium Oxide, Gold, And Platinum-Electrodes. *Journal Of Electroanalytical Chemistry* **1984,** 161, (2), 355-376.

159. Kuznetsov, B. A.; Byzova, N. A.; Shumakovich, G. P., The Effect Of The Orientation Of Cytochrome-C Molecules Covalently Attached To The Electrode Surface Upon Their Electrochemical Activity. *Journal Of Electroanalytical Chemistry* **1994,** 371, (1-2), 85-92.

160. Reed, D. E.; Hawkridge, F. M., Direct Electron-Transfer Reactions Of Cytochrome-C At Silver Electrodes. *Analytical Chemistry* **1987,** 59, (19), 2334-2339.

161. Taniguchi, I.; Toyosawa, K.; Yamaguchi, H.; Yasukouchi, K., Voltammetric Response Of Horse Heart Cytochrome-C At A Gold Electrode In The Presence Of Sulfur Bridged Bipyridines. *Journal Of Electroanalytical Chemistry* **1982,** 140, (1), 187-193.

162. Yuan, X. L.; Hawkridge, F. M.; Chlebowski, J. F., Thermodynamic And Kinetic-Studies Of Cytochrome-C From Different Species. *Journal Of Electroanalytical Chemistry* **1993,** 350, (1-2), 29-42.

163. Sagara, T.; Murakami, H.; Igarashi, S.; Sato, H.; Niki, K., Spectroelectrochemical Study Of The Redox Reaction-Mechanism Of Cytochrome-C At A Gold Electrode In A Neutral Solution In The Presence Of 4,4'-Bipyridyl As A Surface Modifier. *Langmuir* **1991,** 7, (12), 3190-3196.

164. Armstrong, F. A., Probing Metalloproteins By Voltammetry. *Structure And Bonding* **1990,** 72, 137-230.

165. Hawkridge, F. M.; Taniguchi, I., The Direct Electron-Transfer Reactions Of Cytochrome-C At Electrode Surfaces. *Comments On Inorganic Chemistry* **1995,** 17, (3), 163-187.

166. Sagara, T.; Kubo, Y.; Hiraishi, K., Estimation of the orientation of heme in cytochrome c immobilized on a carboxylate-terminated alkanethiol monolayer on a Au electrode by the use of electroreflectance spectroscopy with polarized light incidence. *Journal Of Physical Chemistry B* **2006,** 110, (33), 16550-16558.

167. Tarlov, M. J.; Bowden, E. F., Electron-Transfer Reaction Of Cytochrome-C Adsorbed On Carboxylic-Acid Terminated Alkanethiol Monolayer Electrodes. *Journal Of The American Chemical Society* **1991,** 113, (5), 1847-1849.

168. Taniguchi, I.; Toyosawa, K.; Yamaguchi, H.; Yasukouchi, K., Reversible Electrochemical Reduction And Oxidation Of Cytochrome-C At A Bis(4-Pyridyl) Disulfide-Modified Gold Electrode. *Journal Of The Chemical Society-Chemical Communications* **1982**, (18), 1032-1033.

169. Yue, H. J.; Khoshtariya, D.; Waldeck, D. H.; Grochol, J.; Hildebrandt, P.; Murgida, D. H., On the electron transfer mechanism between cytochrome c and metal electrodes. Evidence for dynamic control at short distances. *Journal Of Physical Chemistry B* **2006,** 110, (40), 19906-19913.

170. Chen, X. X.; Ferrigno, R.; Yang, J.; Whitesides, G. A., Redox properties of cytochrome c adsorbed on self-assembled monolayers: A probe for protein conformation and orientation. *Langmuir* **2002,** 18, (18), 7009-7015.

171. Murgida, D. H.; Hildebrandt, P., Electron-transfer processes of cytochrome c at interfaces. New insights by surface-enhanced resonance Raman spectroscopy. *Accounts Of Chemical Research* **2004,** 37, (11), 854-861.

172. Khoshtariya, D. E.; Wei, J. J.; Liu, H. Y.; Yue, H. J.; Waldeck, D. H., Charge-transfer mechanism for cytochrome c adsorbed on nanometer thick films. Distinguishing frictional control from conformational gating. *Journal Of The American Chemical Society* **2003,** 125, (25), 7704-7714.

173. Wei, J. J.; Liu, H. Y.; Niki, K.; Margoliash, E.; Waldeck, D. H., Probing electron tunneling pathways: Electrochemical study of rat heart cytochrome c and its mutant on pyridine-terminated SAMs. *Journal Of Physical Chemistry B* **2004,** 108, (43), 16912-16917.

174. Collinson, M.; Bowden, E. F., Chronoabsorptometric Determination Of Adsorption-Isotherms For Cytochrome-C On Tin Oxide Electrodes. *Langmuir* **1992,** 8, (10), 2552-2559.

175. Willit, J. L.; Bowden, E. F., Determination Of Unimolecular Electron-Transfer Rate Constants For Strongly Adsorbed Cytochrome-C On Tin Oxide Electrodes. *Journal Of Electroanalytical Chemistry* **1987,** 221, (1-2), 265-274.

176. Willit, J. L.; Bowden, E. F., Adsorption And Redox Thermodynamics Of Strongly Adsorbed Cytochrome-C On Tin Oxide Electrodes. *Journal Of Physical Chemistry* **1990,** 94, (21), 8241-8246.

177. Bowden, E. F.; Hawkridge, F. M.; Chlebowski, J. F.; Bancroft, E. E.; Thorpe, C.; Blount, H. N., Cyclic Voltammetry And Derivative Cyclic Voltabsorptometry Of Purified Horse Heart Cytochrome-C At Tin-Doped Indium Oxide Optically Transparent Electrodes. *Journal Of The American Chemical Society* **1982,** 104, (26), 7641-7644.

178. Daido, T.; Akaike, T., Electrochemistry Of Cytochrome-C - Influence Of Coulombic Attraction With Indium Tin Oxide Electrode. *Journal Of Electroanalytical Chemistry* **1993,** 344, (1-2), 91-106.

179. Runge, A. F.; Mendes, S. B.; Saavedra, S. S., Order parameters and orientation distributions of solution adsorbed and microcontact printed cytochrome c protein films on glass and ITO. *Journal Of Physical Chemistry B* **2006,** 110, (13), 6732-6739.

180. Koppenol, W. H.; Margoliash, E., The Asymmetric Distribution Of Charges On The Surface Of Horse Cytochrome-C - Functional Implications. *Journal Of Biological Chemistry* **1982,** 257, (8), 4426-4437.

181. Margoliash, E.; Frohwirt, N., Spectrum Of Horse-Heart Cytochrome-C. *Biochemical Journal* **1959,** 71, 570-578.

182. Fukuda, K.; Ohno, H., Electron transfer reaction of cytochrome c at the electrode surface analyzed with noncontact optical waveguide spectroscopy. *Electroanalysis* **2002,** 14, (9), 605-610.

183. Fujita, K.; Suzuki, C.; Ohno, H., Non-contact spectral analysis of cytochrome c on carbon electrodes with optical waveguide spectroscopy. *Electrochemistry Communications* **2003,** 5, (1), 47-50.

184. Hildebrandt, P.; Stockburger, M., Cytochrome-C At Charged Interfaces .1. Conformational And Redox Equilibria At The Electrode Electrolyte Interface Probed By Surface-Enhanced Resonance Raman-Spectroscopy. *Biochemistry* **1989,** 28, (16), 6710-6721.

185. Murgida, D. H.; Hildebrandt, P., Proton-coupled electron transfer of cytochrome c. *Journal Of The American Chemical Society* **2001,** 123, (17), 4062-4068.

186. Murgida, D. H.; Hildebrandt, P., Active-site structure and dynamics of cytochrome c immobilized on self-assembled monolayers - A time-resolved surface enhanced resonance Raman spectroscopic study. *Angewandte Chemie-International Edition* **2001,** 40, (4), 728-731.

187. Cheng, Y. Y.; Lin, S. H.; Chang, H. C.; Su, M. C., Probing adsorption, orientation and conformational changes of cytochrome c on fused silica surfaces with the soret band. *Journal Of Physical Chemistry A* **2003,** 107, (49), 10687-10694.

188. Brusatori, M. A.; Tie, Y.; Van Tassel, P. R., Protein adsorption kinetics under an applied electric field: An optical waveguide lightmode spectroscopy study. *Langmuir* **2003,** 19, (12), 5089-5097.

189. Mayo, S. L.; Ellis, W. R.; Crutchley, R. J.; Gray, H. B., Long-Range Electron-Transfer In Heme-Proteins. *Science* **1986,** 233, (4767), 948-952.

190. Zhou, J.; Zheng, J.; Jiang, S. Y., Molecular simulation studies of the orientation and conformation of cytochrome c adsorbed on self-assembled monolayers. *Journal Of Physical Chemistry B* **2004,** 108, (45), 17418-17424.

191. Niki, K.; Hardy, W. R.; Hill, M. G.; Li, H.; Sprinkle, J. R.; Margoliash, E.; Fujita, K.; Tanimura, R.; Nakamura, N.; Ohno, H.; Richards, J. H.; Gray, H. B., Coupling to lysine-13 promotes electron tunneling through carboxylate-terminated alkanethiol self-assembled monolayers to cytochrome c. *Journal Of Physical Chemistry B* **2003,** 107, (37), 9947-9949.

192. Imabayashi, S.; Mita, T.; Kakiuchi, T., Effect of mono-CDNP substitution of lysine residues on the redox reaction of cytochrome c electrostatically adsorbed on a mercaptoheptanoic acid modified Au(111) surface. *Langmuir* **2005,** 21, (6), 2474-2479.

193. Allen, P. M.; Hill, H. A. O.; Walton, N. J., Surface Modifiers For The Promotion Of Direct Electrochemistry Of Cytochrome-C. *Journal Of Electroanalytical Chemistry* **1984,** 178, (1), 69-86.

194. Edmiston, P. L.; Lee, J. E.; Cheng, S. S.; Saavedra, S. S., Molecular orientation distributions in protein films .1. Cytochrome c adsorbed to substrates of variable surface chemistry. *Journal Of The American Chemical Society* **1997,** 119, (3), 560-570.

195. Ataka, K.; Heberle, J., Functional vibrational spectroscopy of a cytochrome c monolayer: SEIDAS probes the interaction with different surface-modified electrodes. *Journal Of The American Chemical Society* **2004,** 126, (30), 9445-9457.

196. Dick, L. A.; Haes, A. J.; Van Duyne, R. P., Distance and orientation dependence of heterogeneous electron transfer: A surface-enhanced resonance Raman scattering study of cytochrome c bound to carboxylic acid terminated alkanethiols adsorbed on silver electrodes. *Journal Of Physical Chemistry B* **2000,** 104, (49), 11752-11762.

197. Runge, A. F.; Rasmussen, N. C.; Saavedra, S. S.; Mendes, S. B., Determination of anisotropic optical constants and surface coverage of molecular films using polarized visible ATR spectroscopy. Application to adsorbed cytochrome c films. *Journal Of Physical Chemistry B* **2005,** 109, (1), 424-431.

198. Runge, A. F.; Saavedra, S. S.; Mendes, S. B., Combination of polarized TIRF and ATR spectroscopies for determination of the second and fourth order parameters of molecular orientation in thin films and construction of an orientation distribution based on the maximum entropy method. *Journal Of Physical Chemistry B* **2006,** 110, (13), 6721-6731.

199. Brash, J. L.; Horbett, T. A., *Proteins at Interfaces II*. American Chemical Society: Washington DC, 1995.

200. Fedurco, M., Redox reactions of heme-containing metalloproteins: dynamic effects of self-assembled monolayers on thermodynamics and kinetics of cytochrome c electron-transfer reactions. *Coordination Chemistry Reviews* **2000,** 209, 263-331.

201. Yue, H. J.; Waldeck, D. H., Understanding interfacial electron transfer to monolayer protein assemblies. *Current Opinion In Solid State & Materials Science* **2005,** 9, (1-2), 28-36.

202. Yue, H. J.; Waldeck, D. H.; Petrovic, J.; Clark, R. A., The effect of ionic strength on the electron-transfer rate of surface immobilized cytochrome c. *Journal Of Physical Chemistry B* **2006,** 110, (10), 5062-5072.

203. El Kasmi, A.; Leopold, M. C.; Galligan, R.; Robertson, R. T.; Saavedra, S. S.; El Kacemi, K.; Bowden, E. F., Adsorptive immobilization of cytochrome c on indium/tin oxide (ITO): electrochemical evidence for electron transfer-induced conformational changes. *Electrochemistry Communications* **2002,** 4, (2), 177-181.

204. Runge, A. F.; Saavedra, S. S., Comparison of microcontact-printed and solution-adsorbed cytochrome C films on indium tin oxide electrodes. *Langmuir* **2003,** 19, (22), 9418-9424.

205. Araci, Z. O.; Runge, A. F.; Doherty, W. J.; Saavedra, S. S., Potential modulated attenuated total reflectance spectroscopy of Prussian blue films on ITO. *Israel Journal of Chemistry* **2006,** 46, (3), 249-255.

206. Donley, C.; Dunphy, D.; Paine, D.; Carter, C.; Nebesny, K.; Lee, P.; Alloway, D.; Armstrong, N. R., Characterization of indium-tin oxide interfaces using X-ray photoelectron spectroscopy and redox processes of a chemisorbed probe molecule: Effect of surface pretreatment conditions. *Langmuir* **2002,** 18, (2), 450-457.

207. Liau, Y. H.; Scherer, N. F.; Rhodes, K., Nanoscale electrical conductivity and surface spectroscopic studies of indium-tin oxide. *Journal Of Physical Chemistry B* **2001,** 105, (16), 3282-3288.

208. Araci, Z. O.; Runge, A. F.; Do Herty, W. J.; Saavedra, S. S., Correlating molecular orientation distributions and electrochemical kinetics in subpopulations of an immobilized protein film. *Journal Of The American Chemical Society* **2008,** 130, (5), 1572-+.

209. Koch, N., Organic electronic devices and their functional interfaces. *Chemphyschem* **2007,** 8, (10), 1438-1455.

210. Khan, R. U. A.; Hunziker, C.; Gunter, P., Perspectives on organic light-emitting diodes for display applications. *Journal Of Materials Science-Materials In Electronics* **2006,** 17, (6), 467-474.

211. Pope, M.; Magnante, P.; Kallmann, H. P., Electroluminescence In Organic Crystals. *Journal Of Chemical Physics* **1963,** 38, (8), 2042-&.

212. Dodabalapur, A., Organic light emitting diodes. *Solid State Communications* **1997,** 102, (2-3), 259-267.

213. Tang, C. W.; Vanslyke, S. A., Organic Electroluminescent Diodes. *Applied Physics Letters* **1987,** 51, (12), 913-915.

214. Tang, C. W.; Vanslyke, S. A.; Chen, C. H., Electroluminescence Of Doped Organic Thin-Films. *Journal Of Applied Physics* **1989,** 65, (9), 3610-3616.

215. Bernius, M. T.; Inbasekaran, M.; O'Brien, J.; Wu, W. S., Progress with light-emitting polymers. *Advanced Materials* **2000,** 12, (23), 1737-1750.

216. Partridge, R. H., Electro-Luminescence From Polyvinylcarbazole Films .1. Carbazole Cations. *Polymer* **1983,** 24, (6), 733-738.

217. Burroughes, J. H.; Bradley, D. D. C.; Brown, A. R.; Marks, R. N.; Mackay, K.; Friend, R. H.; Burns, P. L.; Holmes, A. B., Light-Emitting-Diodes Based On Conjugated Polymers. *Nature* **1990,** 347, (6293), 539-541.

218. Braun, D.; Heeger, A. J., Visible-Light Emission From Semiconducting Polymer Diodes. *Applied Physics Letters* **1991,** 58, (18), 1982-1984.

219. Kido, J.; Kohda, M.; Okuyama, K.; Nagai, K., Organic Electroluminescent Devices Based On Molecularly Doped Polymers. *Applied Physics Letters* **1992,** 61, (7), 761-763.

220. Gustafsson, G.; Cao, Y.; Treacy, G. M.; Klavetter, F.; Colaneri, N.; Heeger, A. J., Flexible Light-Emitting-Diodes Made From Soluble Conducting Polymers. *Nature* **1992,** 357, (6378), 477-479.

221. Marikkar, F. S. Molecular Design of Electrode Surfaces and Interfaces: for Optimized Charge Transfer at Transparent Conducting Oxide Electrodes and Spectroelectrochemical Sensing. Dissertation, University of Arizona, Tucson, 2006.

222. Kato, K.; Takahashi, K.; Suzuki, K.; Sato, T.; Shinbo, K.; Kaneko, F.; Shimizu, H.; Tsuboi, N.; Tadokoro, T.; Ohta, S., Organic light emitting diodes with nanostructured

ultrathin layers at the interface between electron- and hole-transport layers. *Current Applied Physics* **2005,** 5, (4), 321-326.

223. Reufer, M.; Walter, M. J.; Lagoudakis, P. G.; Hummel, B.; Kolb, J. S.; Roskos, H. G.; Scherf, U.; Lupton, J. M., Spin-conserving carrier recombination in conjugated polymers. *Nature Materials* **2005,** 4, (4), 340-346.

224. Rothe, C.; King, S. M.; Monkman, A. P., Direct measurement of the singlet generation yield in polymer light-emitting diodes. *Physical Review Letters* **2006,** 97, (7).

225. Wilson, J. S.; Dhoot, A. S.; Seeley, A.; Khan, M. S.; Kohler, A.; Friend, R. H., Spin-dependent exciton formation in pi-conjugated compounds. *Nature* **2001,** 413, (6858), 828-831.

226. Koch, N.; Duhm, S.; Rabe, J. P.; Vollmer, A.; Johnson, R. L., Optimized hole injection with strong electron acceptors at organic-metal interfaces. *Physical Review Letters* **2005,** 95, (23).

227. Koch, N.; Duhm, S.; Rabe, J. P.; Rentenberger, S.; Johnson, R. L.; Klankermayer, J.; Schreiber, F., Tuning the hole injection barrier height at organic/metal interfaces with (sub-) monolayers of electron acceptor molecules. *Applied Physics Letters* **2005,** 87, (10).

228. Bruner, E. L.; Koch, N.; Span, A. R.; Bernasek, S. L.; Kahn, A.; Schwartz, J., Controlling the work function of indium tin oxide: Differentiating bipolar from local surface effects. *Journal Of The American Chemical Society* **2002,** 124, (13), 3192-3193.

229. Wu, C. C.; Wu, C. I.; Sturm, J. C.; Kahn, A., Surface modification of indium tin oxide by plasma treatment: An effective method to improve the efficiency, brightness, and reliability of organic light emitting devices. *Applied Physics Letters* **1997,** 70, (11), 1348-1350.

230. Hanson, E. L.; Guo, J.; Koch, N.; Schwartz, J.; Bernasek, S. L., Advanced surface modification of indium tin oxide for improved charge injection in organic devices. *Journal Of The American Chemical Society* **2005,** 127, (28), 10058-10062.

231. Guo, J.; Koch, N.; Bernasek, S. L.; Schwartz, J., Enhanced hole injection in a polymer light emitting diode using a small molecule monolayer bound to the anode. *Chemical Physics Letters* **2006,** 426, (4-6), 370-373.

232. Blochwitz, J.; Pfeiffer, M.; Fritz, T.; Leo, K., Low voltage organic light emitting diodes featuring doped phthalocyanine as hole transport material. *Applied Physics Letters* **1998,** 73, (6), 729-731.

233. Gao, W. Y.; Kahn, A., Electrical doping: the impact on interfaces of pi-conjugated molecular films. *Journal Of Physics-Condensed Matter* **2003,** 15, (38), S2757-S2770.

234. Gao, W. Y.; Kahn, A., Effect of electrical doping on molecular level alignment at organic-organic heterojunctions. *Applied Physics Letters* **2003,** 82, (26), 4815-4817.

235. Chan, C. K.; Amy, F.; Zhang, Q.; Barlow, S.; Marder, S.; Kahn, A., N-type doping of an electron-transport material by controlled gas-phase incorporation of cobaltocene. *Chemical Physics Letters* **2006,** 431, (1-3), 67-71.

236. Chapin, D. M.; Fuller, C. S.; Pearson, G. L., A New Silicon P-N Junction Photocell For Converting Solar Radiation Into Electrical Power. *Journal Of Applied Physics* **1954,** 25, (5), 676-677.

237. Gratzel, M., Photoelectrochemical cells. *Nature* **2001,** 414, (6861), 338-344.

238. Carlson, D. E., Photovoltaic Technologies For Commercial Power-Generation. *Annual Review Of Energy* **1990,** 15, 85-98.

239. Zweibel, K., Thin-Films - Past, Present, Future. *Progress In Photovoltaics* **1995,** 3, (5), 279-293.

240. Shockley, W.; Queisser, H. J., Detailed Balance Limit Of Efficiency Of P-N Junction Solar Cells. *Journal Of Applied Physics* **1961,** 32, (3), 510-&.

241. Tang, C. W., 2-Layer Organic Photovoltaic Cell. *Applied Physics Letters* **1986,** 48, (2), 183-185.

242. Peumans, P.; Forrest, S. R., Very-high-efficiency double-heterostructure copper phthalocyanine/C-60 photovoltaic cells. *Applied Physics Letters* **2001,** 79, (1), 126-128.

243. Shaheen, S. E.; Ginley, D. S.; Jabbour, G. E., Organic-based photovoltaics. toward low-cost power generation. *Mrs Bulletin* **2005,** 30, (1), 10-19.

244. Gunes, S.; Neugebauer, H.; Sariciftci, N. S., Conjugated polymer-based organic solar cells. *Chemical Reviews* **2007,** 107, (4), 1324-1338.

245. Armstrong, N. R.; Wang, W. N.; Alloway, D. M.; Placencia, D.; Ratcliff, E.; Brumbach, M., Organic/Organic' Heterojunctions: Organic Light Emitting Diodes and Organic Photovoltaic Devices. *Macromolecular Rapid Communications* **2009,** 30, (9-10), 717-731.

246. Nelson, J., Organic photovoltaic films. *Current Opinion In Solid State & Materials Science* **2002,** 6, (1), 87-95.

247. Brown, T. M.; Kim, J. S.; Friend, R. H.; Cacialli, F.; Daik, R.; Feast, W. J., Built-in field electroabsorption spectroscopy of polymer light-emitting diodes incorporating a doped poly(3,4-ethylene dioxythiophene) hole injection layer. *Applied Physics Letters* **1999,** 75, (12), 1679-1681.

248. Gregg, B. A.; Hanna, M. C., Comparing organic to inorganic photovoltaic cells: Theory, experiment, and simulation. *Journal Of Applied Physics* **2003,** 93, (6), 3605-3614.

249. Rubinstein, I., *Physical Electrochemistry Principles, Methods, And Applications*. Marcel Dekkar, Inc.: NewYork, 1995.

250. Murray, R. W., *Molecular Design of Electrode Surfaces.* John Wiley and Sons Inc.: NewYork, 1992.

251. Elliott, C. M.; Murray, R. W., CHEMICALLY MODIFIED CARBON ELECTRODES. *Analytical Chemistry* **1976,** 48, (8), 1247-1254.

252. Fox, M. A.; Nobs, F. J.; Voynick, T. A., COVALENT ATTACHMENT OF ARENES TO SNO2-SEMICONDUCTOR ELECTRODES. *Journal Of The American Chemical Society* **1980,** 102, (12), 4029-4036.

253. Fox, M. A.; Nobs, F. J.; Voynick, T. A., CHEMICALLY MODIFIED ELECTRODES IN DYE-SENSITIZED PHOTOGALVANIC CELLS. *Journal Of The American Chemical Society* **1980,** 102, (12), 4036-4039.

254. Lane, R. F.; Hubbard, A. T., ELECTROCHEMISTRY OF CHEMISORBED MOLECULES .5. ROLE OF NON-AQUEOUS SOLVENTS IN LIGAND-BRIDGED ELECTROCHEMICAL INTERCONVERSION OF PLATINUM COMPLEXES. *Journal Of Physical Chemistry* **1977,** 81, (8), 734-739.

255. Moses, P. R.; Wier, L.; Murray, R. W., CHEMICALLY MODIFIED TIN OXIDE ELECTRODE. *Analytical Chemistry* **1975,** 47, (12), 1882-1886.

256. Watkins, B. F.; Behling, J. R.; Kariv, E.; Miller, L. L., CHIRAL ELECTRODE. *Journal Of The American Chemical Society* **1975,** 97, (12), 3549-3550.

257. Donley, C. L. Interfaces in Organic Electronic Devices: Surface Characterization and Modification and Their Effect on Microstructure in Molecular Assemblies. Dissertation, University of Arizona, Tucson, 2003.

258. Lindfors, T.; Ivaska, A., Potentiometric and UV-vis characterisation of N-substituted polyanilines. *Journal Of Electroanalytical Chemistry* **2002,** 535, (1-2), 65-74.

259. Tengstedt, C.; Crispin, A.; Hsu, C. H.; Zhang, C.; Parker, I. D.; Salaneck, W. R.; Fahman, M., Study and comparison of conducting polymer hole injection layers in light emitting devices. *Organic Electronics* **2005,** 6, (1), 21-33.

260. Marks, T. J.; Veinot, J. G. C.; Cui, J.; Yan, H.; Wang, A.; Edleman, N. L.; Ni, J.; Huang, Q.; Lee, P.; Armstrong, N. R., Progress in high work function TCO OLED anode alternatives and OLED nanopixelation. *Synthetic Metals* **2002,** 127, (1-3), 29-35.

261. Karg, S.; Scott, J. C.; Salem, J. R.; Angelopoulos, M., Increased brightness and lifetime of polymer light-emitting diodes with polyaniline anodes. *Synthetic Metals* **1996,** 80, (2), 111-117.

262. Malinsky, J. E.; Veinot, J. G. C.; Jabbour, G. E.; Shaheen, S. E.; Anderson, J. D.; Lee, P.; Richter, A. G.; Burin, A. L.; Ratner, M. A.; Marks, T. J.; Armstrong, N. R.; Kippelen, B.; Dutta, P.; Peyghambarian, N., Nanometer-scale dielectric self-assembly process for anode modification in organic light-emitting diodes. Consequences for charge injection and enhanced luminous efficiency. *Chemistry Of Materials* **2002,** 14, (7), 3054-3065.

263. Zhong, Z. Y.; Jiang, Y. D., Surface modification and characterization of indium-tin oxide for organic light-emitting devices. *Journal Of Colloid And Interface Science* **2006,** 302, (2), 613-619.

264. Chopra, K. L.; Major, S.; Pandya, D. K., TRANSPARENT CONDUCTORS - A STATUS REVIEW. *Thin Solid Films* **1983,** 102, (1), 1-46.

265. Luis, A.; de Carvalho, C. N.; Lavareda, G.; Amaral, A.; Brogueira, P.; Godinho, M. H., ITO coated flexible transparent substrates for liquid crystal based devices. *Vacuum* **2002,** 64, (3-4), 475-479.

266. Amaral, A.; de Carvalho, C. N.; Brogueira, P.; Lavareda, G.; Melo, L. V.; Godinho, M. H., ITO properties on anisotropic flexible transparent cellulosic substrates under different stress conditions. *Materials Science And Engineering B-Solid State Materials For Advanced Technology* **2005,** 118, (1-3), 183-186.

267. Lee, S. T.; Gao, Z. Q.; Hung, L. S., Metal diffusion from electrodes in organic light-emitting diodes. *Applied Physics Letters* **1999,** 75, (10), 1404-1406.

268. Schlatmann, A. R.; Floet, D. W.; Hilberer, A.; Garten, F.; Smulders, P. J. M.; Klapwijk, T. M.; Hadziioannou, G., Indium contamination from the indium-tin-oxide electrode in polymer light-emitting diodes. *Applied Physics Letters* **1996,** 69, (12), 1764-1766.

269. Carter, C. Modification of Indium Tin Oxide Surfaces: Enhancement of Solution Electron Transfer Rates and Efficiencies of Organic Thin Layer Devices. University of Arizona, Tucson, 2006.

270. Brumbach, M.; Veneman, P. A.; Marrikar, F. S.; Schulmeyer, T.; Simmonds, A.; Xia, W.; Lee, P.; Armstrong, N. R., Surface composition and electrical and electrochemical properties of freshly deposited and acid-etched indium tin oxide electrodes. *Langmuir* **2007,** 23, (22), 11089-11099.

271. Kim, J. S.; Granstrom, M.; Friend, R. H.; Johansson, N.; Salaneck, W. R.; Daik, R.; Feast, W. J.; Cacialli, F., Indium-tin oxide treatments for single- and double-layer polymeric light-emitting diodes: The relation between the anode physical, chemical, and morphological properties and the device performance. *Journal Of Applied Physics* **1998,** 84, (12), 6859-6870.

272. Milliron, D. J.; Hill, I. G.; Shen, C.; Kahn, A.; Schwartz, J., Surface oxidation activates indium tin oxide for hole injection. *Journal Of Applied Physics* **2000,** 87, (1), 572-576.

273. Sugiyama, K.; Ishii, H.; Ouchi, Y.; Seki, K., Dependence of indium-tin-oxide work function on surface cleaning method as studied by ultraviolet and x-ray photoemission spectroscopies. *Journal Of Applied Physics* **2000,** 87, (1), 295-298.

274. Chaney, J. A.; Pehrsson, P. E., Work function changes and surface chemistry of oxygen, hydrogen, and carbon on indium tin oxide. *Applied Surface Science* **2001,** 180, (3-4), 214-226.

275. Chan, I. M.; Hong, F. C. N., Plasma treatments of indium tin oxide anodes in carbon tetrafluorinde (CF4)/oxygen (O-2) to improve the performance of organic light-emitting diodes. *Thin Solid Films* **2003,** 444, (1-2), 254-259.

276. Chaney, J. A.; Koh, S. E.; Dulcey, C. S.; Pehrsson, P. E., Surface chemistry of carbon removal from indium tin oxide by base and plasma treatment, with implications on hydroxyl termination. *Applied Surface Science* **2003,** 218, (1-4), 258-266.

277. Choi, B.; Yoon, H.; Lee, H. H., Surface treatment of indium tin oxide by SF6 plasma for organic light-emitting diodes. *Applied Physics Letters* **2000,** 76, (4), 412-414.

278. Li, L.; Yu, J. S.; Lou, S. L.; Li, W. Z.; Jiang, Y. D.; Li, W., Surface modification and characterization of indium-tin oxide for organic light-emitting devices. *Journal Of Materials Science-Materials In Electronics* **2008,** 19, (12), 1214-1221.

279. Song, W.; So, S. K.; Cao, L., Angular-dependent photoemission studies of indium tin oxide surfaces. *Applied Physics a-Materials Science & Processing* **2001,** 72, (3), 361-365.

280. Steuber, F.; Staudigel, J.; Stossel, M.; Simmerer, J.; Winnacker, A., Reduced operating voltage of organic electroluminescent devices by plasma treatment of the indium tin oxide anode. *Applied Physics Letters* **1999,** 74, (23), 3558-3560.

281. Suess, C.; Wenzl, F. P.; Jakopic, G.; Wuchse, M.; Muellegger, S.; Koch, N.; Haase, A.; Lamprecht, K.; Schatzmayr, M.; Mitterbauer, C.; Hofer, F.; Leising, G., Combined XPS, AFM, TEM and ellipsometric studies on nanoscale layers in organic light emitting diodes. *Surface Science* **2002,** 507, 473-479.

282. You, Z. Z.; Dong, J. Y., Surface properties of treated ITO anodes for organic light-emitting devices. *Applied Surface Science* **2005,** 249, (1-4), 271-276.

283. Yu, H. Y.; Feng, X. D.; Grozea, D.; Lu, Z. H.; Sodhi, R. N. S.; Hor, A. M.; Aziz, H., Surface electronic structure of plasma-treated indium tin oxides. *Applied Physics Letters* **2001,** 78, (17), 2595-2597.

284. Carter, C.; Brumbach, M.; Donley, C.; Hreha, R. D.; Marder, S. R.; Domercq, B.; Yoo, S.; Kippelen, B.; Armstrong, N. R., Small molecule chemisorption on indium-tin oxide surfaces: enhancing probe molecule electron-transfer rates and the performance of organic light-emitting diodes. *Journal Of Physical Chemistry B* **2006,** 110, (50), 25191-25202.

285. Armstrong, N. R.; Shepard, V. R., VOLTAMMETRIC STUDIES OF SILANE-MODIFIED SNO2 SURFACES IN SELECTED AQUEOUS AND NON-AQUEOUS MEDIA. *Journal Of Electroanalytical Chemistry* **1980,** 115, (2), 253-265.

286. Nguyen, T. P.; Le Rendu, P.; Dinh, N. N.; Fourmigue, M.; Meziere, C., Thermal and chemical treatment of ITO substrates for improvement of OLED performance. *Synthetic Metals* **2003,** 138, (1-2), 229-232.

287. Jung, S.; Park, N. G.; Kwak, M. Y.; Kim, B. O.; Choi, K. H.; Cho, Y. J.; Kim, Y. K.; Kim, Y. S., Surface treatment effects of indium-tin oxide in organic light-emitting diodes. *Optical Materials* **2003,** 21, (1-3), 235-241.

288. Kim, J. S.; Cacialli, F.; Cola, A.; Gigli, G.; Cingolani, R., Increase of charge carriers density and reduction of Hall mobilities in oxygen-plasma treated indium-tin-oxide anodes. *Applied Physics Letters* **1999,** 75, (1), 19-21.

289. Sharma, A.; Haldi, A.; Hotchkiss, P. J.; Marder, S. R.; Kippelen, B., Effect of phosphonic acid surface modifiers on the work function of indium tin oxide and on the

charge injection barrier into organic single-layer diodes. *Journal Of Applied Physics* **2009,** 105, (7).

290. Paniagua, S. A.; Hotchkiss, P. J.; Jones, S. C.; Marder, S. R.; Mudalige, A.; Marrikar, F. S.; Pemberton, J. E.; Armstrong, N. R., Phosphonic acid modification of indium-tin oxide electrodes: Combined XPS/UPS/contact angle studies. *Journal Of Physical Chemistry C* **2008,** 112, (21), 7809-7817.

291. Hotchkiss, P. J.; Li, H.; Paramonov, P. B.; Paniagua, S. A.; Jones, S. C.; Armstrong, N. R.; Bredas, J. L.; Marder, S. R., Modification of the Surface Properties of Indium Tin Oxide with Benzylphosphonic Acids: A Joint Experimental and Theoretical Study. *Advanced Materials* **2009,** 21, (44), 4496-+.

292. Kim, J. S.; Cacialli, F.; Friend, R., Surface conditioning of indium-tin oxide anodes for organic light-emitting diodes. *Thin Solid Films* **2003,** 445, (2), 358-366.

293. Khodabakhsh, S.; Sanderson, B. M.; Nelson, J.; Jones, T. S., Using self-assembling dipole molecules to improve charge collection in molecular solar cells. *Advanced Functional Materials* **2006,** 16, (1), 95-100.

294. Koch, N.; Kahn, A.; Ghijsen, J.; Pireaux, J. J.; Schwartz, J.; Johnson, R. L.; Elschner, A., Conjugated organic molecules on metal versus polymer electrodes: Demonstration of a key energy level alignment mechanism. *Applied Physics Letters* **2003,** 82, (1), 70-72.

295. Kim, S. Y.; Hong, K.; Lee, J. L., Change of interface dipole energy with interfacial layer thickness and O-2 plasma treatment in metal/organic interface. *Applied Physics Letters* **2007,** 90, (18).

296. Khodabakhsh, S.; Poplavskyy, D.; Heutz, S.; Nelson, J.; Bradley, D. D. C.; Murata, F.; Jones, T. S., Using self-assembling dipole molecules to improve hole injection in conjugated polymers. *Advanced Functional Materials* **2004,** 14, (12), 1205-1210.

297. Ishii, H.; Sugiyama, K.; Yoshimura, D.; Ito, E.; Ouchi, Y.; Seki, K., Energy-level alignment at model interfaces of organic electroluminescent devices studied by UV photoemission: Trend in the deviation from the traditional way of estimating the interfacial electronic structures. *Ieee Journal of Selected Topics in Quantum Electronics* **1998,** 4, (1), 24-33.

298. Mutin, P. H.; Guerrero, G.; Vioux, A., Hybrid materials from organophosphorus coupling molecules. *Journal Of Materials Chemistry* **2005,** 15, (35-36), 3761-3768.

299. Breen, T. L.; Fryer, P. M.; Nunes, R. W.; Rothwell, M. E., Patterning indium tin oxide and indium zinc oxide using microcontact printing and wet etching. *Langmuir* **2002,** 18, (1), 194-197.

300. Gardner, T. J.; Frisbie, C. D.; Wrighton, M. S., SYSTEMS FOR ORTHOGONAL SELF-ASSEMBLY OF ELECTROACTIVE MONOLAYERS ON AU AND ITO - AN APPROACH TO MOLECULAR ELECTRONICS. *Journal Of The American Chemical Society* **1995,** 117, (26), 6927-6933.

301. Schulmeyer, T.; Paniagua, S. A.; Veneman, P. A.; Jones, S. C.; Hotchkiss, P. J.; Mudalige, A.; Pemberton, J. E.; Marder, S. R.; Armstrong, N. R., Modification of BaTiO3 thin films: adjustment of the effective surface work function. *Journal Of Materials Chemistry* **2007,** 17, (43), 4563-4570.

302. Sharma, A.; Haldi, A.; Potscavage, W. J.; Hotchkiss, P. J.; Marder, S. R.; Kippelen, B., Effects of surface modification of indium tin oxide electrodes on the performance of molecular multilayer organic photovoltaic devices. *Journal Of Materials Chemistry* **2009,** 19, (30), 5298-5302.

303. Appleyard, S. F. J.; Day, S. R.; Pickford, R. D.; Willis, M. R., Organic electroluminescent devices: enhanced carrier injection using SAM derivatized ITO electrodes. *Journal Of Materials Chemistry* **2000,** 10, (1), 169-173.

304. Appleyard, S. F. J.; Willis, M. R., Electroluminescence: enhanced injection using ITO electrodes coated with a self assembled monolayer. *Optical Materials* **1998,** 9, (1-4), 120-124.

305. Campbell, I. H.; Kress, J. D.; Martin, R. L.; Smith, D. L.; Barashkov, N. N.; Ferraris, J. P., Controlling charge injection in organic electronic devices using self-assembled monolayers. *Applied Physics Letters* **1997,** 71, (24), 3528-3530.

306. Guo, J.; Koch, N.; Schwartz, J.; Bernasek, S. L., Direct measurement of surface complex loading and surface dipole and their effect on simple device behavior. *Journal Of Physical Chemistry B* **2005,** 109, (9), 3966-3970.

307. Hatton, R. A.; Willis, M. R.; Chesters, M. A.; Rutten, F. J. M.; Briggs, D., Enhanced hole injection in organic light-emitting diodes using a SAM-derivatised ultra-thin gold anode supported on ITO glass. *Journal Of Materials Chemistry* **2003,** 13, (1), 38-43.

308. Ho, P. K. H.; Granstrom, M.; Friend, R. H.; Greenham, N. C., Ultrathin self-assembled layers at the ITO interface to control charge injection and electroluminescence efficiency in polymer light-emitting diodes. *Advanced Materials* **1998,** 10, (10), 769-774.

309. Yan, H.; Huang, Q. L.; Cui, J.; Veinot, J. G. C.; Kern, M. M.; Marks, T. J., High-brightness blue light-emitting polymer diodes via anode modification using a self-assembled monolayer. *Advanced Materials* **2003,** 15, (10), 835-+.

310. Ishii, H.; Sugiyama, K.; Ito, E.; Seki, K., Energy level alignment and interfacial electronic structures at organic metal and organic organic interfaces. *Advanced Materials* **1999,** 11, (8), 605-625.

311. Bruening, M.; Moons, E.; Yaronmarcovich, D.; Cahen, D.; Libman, J.; Shanzer, A., POLAR LIGAND ADSORPTION CONTROLS SEMICONDUCTOR SURFACE-POTENTIALS. *Journal Of The American Chemical Society* **1994,** 116, (7), 2972-2977.

312. Cui, J.; Huang, Q. L.; Wang, Q. W.; Marks, T. J., Nanoscale covalent self-assembly approach to enhancing anode/hole-transport layer interfacial stability and charge injection efficiency in organic light-emitting diodes. *Langmuir* **2001,** 17, (7), 2051-2054.

313. Zhou, X.; Pfeiffer, M.; Blochwitz, J.; Werner, A.; Nollau, A.; Fritz, T.; Leo, K., Very-low-operating-voltage organic light-emitting diodes using a p-doped amorphous hole injection layer. *Applied Physics Letters* **2001,** 78, (4), 410-412.

314. Gao, W. Y.; Kahn, A., Controlled p doping of the hole-transport molecular material N,N '-diphenyl-N,N '-bis(1-naphthyl)-1,1(')-biphenyl-4,4 '-diamine with tetrafluorotetracyanoquinodimethane. *Journal Of Applied Physics* **2003,** 94, (1), 359-366.

315. Murray, R. W., *Molecular design of electrode surfaces*. John Wiley and Sons, Inc.: NewYork, 1992.

316. Rubenstein, I., *Physical Electrochemistry*. Marcel Dekker, Inc.: NewYork, 1995.

317. *Handbook of Conducting Polymers*. 2nd ed.; Marcel Dekker: NewYork, 1998.

318. Groenendaal, L.; Zotti, G.; Aubert, P. H.; Waybright, S. M.; Reynolds, J. R., Electrochemistry of poly(3,4-alkylenedioxythiophene) derivatives. *Advanced Materials* **2003,** 15, (11), 855-879.

319. Feast, W. J.; Tsibouklis, J.; Pouwer, K. L.; Groenendaal, L.; Meijer, E. W., Synthesis, processing and material properties of conjugated polymers. *Polymer* **1996,** 37, (22), 5017-5047.

320. Shirakawa, H.; Louis, E. J.; Macdiarmid, A. G.; Chiang, C. K.; Heeger, A. J., Synthesis Of Electrically Conducting Organic Polymers - Halogen Derivatives Of Polyacetylene, (Ch)X. *Journal Of The Chemical Society-Chemical Communications* **1977**, (16), 578-580.

321. Chiang, C. K.; Fincher, C. R.; Park, Y. W.; Heeger, A. J.; Shirakawa, H.; Louis, E. J.; Gau, S. C.; Macdiarmid, A. G., Electrical-Conductivity In Doped Polyacetylene. *Physical Review Letters* **1977,** 39, (17), 1098-1101.

322. Nigrey, P. J.; Macdiarmid, A. G.; Heeger, A. J., Electrochemistry Of Polyacetylene, (Ch)X - Electrochemical Doping Of (Ch)X Films To The Metallic State. *Journal Of The Chemical Society-Chemical Communications* **1979**, (14), 594-595.

323. Heeger, A. J., Nobel Lecture: Semiconducting and metallic polymers: The fourth generation of polymeric materials. *Reviews Of Modern Physics* **2001,** 73, (3), 681-700.

324. Huang, W. S.; Humphrey, B. D.; Macdiarmid, A. G., Polyaniline, A Novel Conducting Polymer - Morphology And Chemistry Of Its Oxidation And Reduction In Aqueous-Electrolytes. *Journal Of The Chemical Society-Faraday Transactions I* **1986,** 82, 2385-&.

325. Yang, Y.; Heeger, A. J., Polyaniline As A Transparent Electrode For Polymer Light-Emitting-Diodes - Lower Operating Voltage And Higher Efficiency. *Applied Physics Letters* **1994,** 64, (10), 1245-1247.

326. Cao, Y.; Yu, G.; Zhang, C.; Menon, R.; Heeger, A. J., Polymer light-emitting diodes with polyethylene dioxythiophene-polystyrene sulfonate as the transparent anode. *Synthetic Metals* **1997,** 87, (2), 171-174.

327. Mortimer, R. J.; Dyer, A. L.; Reynolds, J. R., Electrochromic organic and polymeric materials for display applications. *Displays* **2006,** 27, (1), 2-18.

328. Focke, W. W.; Wnek, G. E.; Wei, Y., Influence Of Oxidation-State, Ph, And Counterion On The Conductivity Of Polyaniline. *Journal Of Physical Chemistry* **1987,** 91, (22), 5813-5818.

329. Kugler, T.; Salaneck, W. R.; Rost, H.; Holmes, A. B., Polymer band alignment at the interface with indium tin oxide: consequences for light emitting devices. *Chemical Physics Letters* **1999,** 310, (5-6), 391-396.

330. Nalwa, H. S., *Handbook of Organic Conducting Moleceules and Polymers*. John Wiley & Sons: NewYork, 1997.

331. Trivedi, D. C., *in Handbook of Organic Conductive Molecules and Polymers*. Wiley: Chichester, UK, 1997; Vol. 2.

332. Groenendaal, B. L.; Jonas, F.; Freitag, D.; Pielartzik, H.; Reynolds, J. R., Poly(3,4-ethylenedioxythiophene) and its derivatives: Past, present, and future. *Advanced Materials* **2000,** 12, (7), 481-494.

333. Leclerc, M.; Faid, K., Electrical and optical properties of processable polythiophene derivatives: Structure-property relationships. *Advanced Materials* **1997,** 9, (14), 1087-1094.

334. McCullough, R. D., The chemistry of conducting polythiophenes. *Advanced Materials* **1998,** 10, (2), 93-+.

335. Kraft, A.; Grimsdale, A. C.; Holmes, A. B., Electroluminescent conjugated polymers - Seeing polymers in a new light. *Angewandte Chemie-International Edition* **1998,** 37, (4), 402-428.

336. Roncali, J., Synthetic principles for bandgap control in linear pi-conjugated systems. *Chemical Reviews* **1997,** 97, (1), 173-205.

337. Yang, Y.; Pei, Q.; Heeger, A. J., Efficient blue polymer light-emitting diodes from a series of soluble poly(paraphenylene)s. *Journal Of Applied Physics* **1996,** 79, (2), 934-939.

338. Hou, L. T.; Hou, Q.; Mo, Y. Q.; Peng, J. B.; Cao, Y., All-organic flexible polymer microcavity light-emitting diodes using 3M reflective multilayer polymer mirrors. *Applied Physics Letters* **2005,** 87, (24).

339. Elschner, A.; Bruder, F.; Heuer, H. W.; Jonas, F.; Karbach, A.; Kirchmeyer, S.; Thurm, S., PEDT/PSS for efficient hole-injection in hybrid organic light-emitting diodes. *Synthetic Metals* **2000,** 111, 139-143.

340. Bayer, A. Eur. Patent 339 340. 1988.

341. Dietrich, M.; Heinze, J.; Heywang, G.; Jonas, F., Electrochemical And Spectroscopic Characterization Of Polyalkylenedioxythiophenes. *Journal Of Electroanalytical Chemistry* **1994,** 369, (1-2), 87-92.

342. Winter, I.; Reese, C.; Hormes, J.; Heywang, G.; Jonas, F., The Thermal Aging Of Poly(3,4-Ethylenedioxythiophene) - An Investigation By X-Ray-Absorption And X-Ray Photoelectron-Spectroscopy. *Chemical Physics* **1995,** 194, (1), 207-213.

343. Carlberg, J. C.; Inganas, O., Poly(3,4-ethylenedioxythiophene) as electrode material in electrochemical capacitors. *Journal Of The Electrochemical Society* **1997,** 144, (4), L61-L64.

344. Arias, A. C.; Granstrom, M.; Petritsch, K.; Friend, R. H., Organic photodiodes using polymeric anodes. *Synthetic Metals* **1999,** 102, (1-3), 953-954.

345. Kros, A.; van Hovell, W. F. M.; Sommerdijk, N.; Nolte, R. J. M., Poly(3,4-ethylenedioxythiophene)-based glucose biosensors. *Advanced Materials* **2001,** 13, (20), 1555-+.

346. Lin, R.; Stokbro, K.; Madsen, D. N.; Boubour, E.; Boggild, P., Optical detection of ion diffusion in electrochromic poly(3,4-ethylenedioxy)thiophene film using microcantilever electrodes. *Thin Solid Films* **2005,** 484, (1-2), 334-340.

347. Agfa, G. Eur. Patent 564 911. 1993.

348. Bayer, A. Eur. Patent 440 957. 1991.

349. Lang, U.; Naujoks, N.; Dual, J., Mechanical characterization of PEDOT:PSS thin films. *Synthetic Metals* **2009,** 159, (5-6), 473-479.

350. Arena, A.; Donato, N.; Saitta, G., Electrical characterization of solid-state heterojunctions between PEDOT : PSS and an anionic polyelectrolyte. *Microelectron. J.* **2007,** 38, (6-7), 678-681.

351. Lefebvre, M.; Qi, Z. G.; Rana, D.; Pickup, P. G., Chemical synthesis, characterization, and electrochemical studies of poly(3,4-ethylenedioxythiophene)/poly(styrene-4-sulfonate) composites. *Chemistry Of Materials* **1999,** 11, (2), 262-268.

352. Ballarin, B.; Fraleoni-Morgera, A.; Frascaro, D.; Marazzita, S.; Piana, C.; Setti, L., Thermal inkjet microdeposition of PEDOT : PSS on ITO-coated glass and characterization of the obtained film. *Synthetic Metals* **2004,** 146, (2), 201-205.

353. Louwet, F.; Groenendaal, L.; Dhaen, J.; Manca, J.; Van Luppen, J.; Verdonck, E.; Leenders, L., PEDOT/PSS: synthesis, characterization, properties and applications. *Synthetic Metals* **2003,** 135, (1-3), 115-117.

354. Hung, L. S.; Chen, C. H., Recent progress of molecular organic electroluminescent materials and devices. *Materials Science & Engineering R-Reports* **2002,** 39, (5-6), 143-222.

355. Jonsson, S. K. M.; Birgerson, J.; Crispin, X.; Greczynski, G.; Osikowicz, W.; van der Gon, A. W. D.; Salaneck, W. R.; Fahlman, M., The effects of solvents on the morphology and sheet resistance in poly (3,4-ethylenedioxythiophene)-polystyrenesulfonic acid (PEDOT-PSS) films. *Synthetic Metals* **2003,** 139, (1), 1-10.

356. Zotti, G.; Zecchin, S.; Schiavon, G.; Louwet, F.; Groenendaal, L.; Crispin, X.; Osikowicz, W.; Salaneck, W.; Fahlman, M., Electrochemical and XPS studies toward the role of monomeric and polymeric sulfonate counterions in the synthesis, composition,

and properties of poly(3,4-ethylenedioxythiophene). *Macromolecules* **2003,** 36, (9), 3337-3344.

357. Jukes, P. C.; Martin, S. J.; Higgins, A. M.; Geoghegan, M.; Jones, R. A. L.; Langridge, S.; Wehrum, A.; Kirchmeyer, S., Controlling the surface composition of poly(3,4-ethylene dioxythiophene)poly(styrene sulfonate) blends by heat treatment. *Advanced Materials* **2004,** 16, (9-10), 807-+.

358. Makinen, A. J.; Hill, I. G.; Shashidhar, R.; Nikolov, N.; Kafafi, Z. H., Hole injection barriers at polymer anode/small molecule interfaces. *Applied Physics Letters* **2001,** 79, (5), 557-559.

359. Nardes, A. M.; Janssen, R. A. J.; Kemerink, M., A morphological model for the solvent-enhanced conductivity of PEDOT : PSS thin films. *Advanced Functional Materials* **2008,** 18, (6), 865-871.

360. Scott, J. C.; Malliaras, G. G.; Chen, W. D.; Breach, J. C.; Salem, J. R.; Brock, P. J.; Sachs, S. B.; Chidsey, C. E. D., Hole limited recombination in polymer light-emitting diodes. *Applied Physics Letters* **1999,** 74, (11), 1510-1512.

361. Pei, Q. B.; Zuccarello, G.; Ahlskog, M.; Inganas, O., ELECTROCHROMIC AND HIGHLY STABLE POLY(3,4-ETHYLENEDIOXYTHIOPHENE) SWITCHES BETWEEN OPAQUE BLUE-BLACK AND TRANSPARENT SKY BLUE. *Polymer* **1994,** 35, (7), 1347-1351.

362. Chen, X. W.; Inganas, O., Three-step redox in polythiophenes: Evidence from electrochemistry at an ultramicroelectrode. *Journal Of Physical Chemistry* **1996,** 100, (37), 15202-15206.

363. Sakai, N.; Prasad, G. K.; Ebina, Y.; Takada, K.; Sasaki, T., Layer-by-layer assembled TiO2 nanoparticle/PEDOT-PSS composite films for switching of electric conductivity in response to ultraviolet and visible light. *Chemistry Of Materials* **2006,** 18, (16), 3596-3598.

364. Brewer, P. J.; Lane, P. A.; Huang, J. S.; DeMello, A. J.; Bradley, D. D. C.; DeMello, J. C., Role of electron injection in polyfluorene-based light emitting diodes containing PEDOT : PSS. *Physical Review B* **2005,** 71, (20).

365. Poplavskyy, D.; Nelson, J.; Bradley, D. D. C., Ohmic hole injection in poly(9,9-dioctylfluorene) polymer light-emitting diodes. *Applied Physics Letters* **2003,** 83, (4), 707-709.

366. Koch, N.; Elschner, A.; Johnson, R. L., Green polyfluorene-conducting polymer interfaces: Energy level alignment and device performance. *Journal Of Applied Physics* **2006,** 100, (2).

367. Huang, J. S.; Miller, P. F.; Wilson, J. S.; de Mello, A. J.; de Mello, J. C.; Bradley, D. D. C., Investigation of the effects of doping and post-deposition treatments on the conductivity, morphology, and work function of poly (3,4-ethylenedioxythiophene)/poly (styrene sulfonate) films. *Advanced Functional Materials* **2005,** 15, (2), 290-296.

368. Pingree, L. S. C.; MacLeod, B. A.; Ginger, D. S., The changing face of PEDOT : PSS films: Substrate, bias, and processing effects on vertical charge transport. *Journal Of Physical Chemistry C* **2008,** 112, (21), 7922-7927.

369. Huang, J.; Miller, P. F.; de Mello, J. C.; de Mello, A. J.; Bradley, D. D. C., Influence of thermal treatment on the conductivity and morphology of PEDOT/PSS films. *Synthetic Metals* **2003,** 139, (3), 569-572.

370. Kim, J. S.; Cacialli, F.; Granstrom, M.; Friend, R. H.; Johansson, N.; Salaneck, W. R.; Daik, R.; Feast, W. J., Characterisation of the properties of surface-treated indium-tin oxide thin films. *Synthetic Metals* **1999,** 101, (1-3), 111-112.

371. Aasmundtveit, K. E.; Samuelsen, E. J.; Pettersson, L. A. A.; Inganas, O.; Johansson, T.; Feidenhans, R., Structure of thin films of poly(3,4-ethylenedioxythiophene). *Synthetic Metals* **1999,** 101, (1-3), 561-564.

372. Kiebooms, R.; Aleshin, A.; Hutchison, K.; Wudl, F.; Heeger, A., Doped poly(3,4-ethylenedioxythiophene) films: Thermal, electromagnetical and morphological analysis. *Synthetic Metals* **1999,** 101, (1-3), 436-437.

373. Farrow, B.; Kamat, P. V., CdSe Quantum Dot Sensitized Solar Cells. Shuttling Electrons Through Stacked Carbon Nanocups. *Journal Of The American Chemical Society* **2009,** 131, (31), 11124-11131.

374. Harris, C.; Kamat, P. V., Photocatalysis with CdSe Nanoparticles in Confined Media: Mapping Charge Transfer Events in the Subpicosecond to Second Timescales. *Acs Nano* **2009,** 3, (3), 682-690.

375. Shallcross, R. C., D'Ambruoso, G. D., Korth, B. D., Hall, H. K., Zheng, Z. P., Pyun, J., Armstrong, N. R., Poly(3,4-ethylenedioxythiophene) - Semiconductor nanoparticle composite thin films tethered to indium tin oxide substrates via electropolymerization. *Journal of the American Chemical Society* **2007,** 129, 11310-+

376. Kamat, P. V., Meeting the clean energy demand: Nanostructure architectures for solar energy conversion. *Journal Of Physical Chemistry C* **2007,** 111, (7), 2834-2860.

377. Kongkanand, A.; Tvrdy, K.; Takechi, K.; Kuno, M.; Kamat, P. V., Quantum dot solar cells. Tuning photoresponse through size and shape control of CdSe-TiO2 architecture. *Journal Of The American Chemical Society* **2008,** 130, (12), 4007-4015.

378. Shallcross, R. C.; D'Ambruoso, G. D.; Korth, B. D.; Hall, H. K.; Zheng, Z. P.; Pyun, J.; Armstrong, N. R., Poly(3,4-ethylenedioxythiophene) - Semiconductor nanoparticle composite thin films tethered to indium tin oxide substrates via electropolymerization. *Journal Of The American Chemical Society* **2007,** 129, (37), 11310-+.

379. Agrios, A. G.; Cesar, I.; Comte, P.; Nazeeruddin, M. K.; Gratzel, M., Nanostructured composite films for dye-sensitized solar cells by electrostatic layer-by-layer deposition. *Chemistry Of Materials* **2006,** 18, (23), 5395-5397.

380. Carlson, B.; Leschkies, K.; Aydil, E. S.; Zhu, X. Y., Valence band alignment at cadmium selenide quantum dot and zinc oxide (10(1)over-bar0) interfaces. *Journal Of Physical Chemistry C* **2008,** 112, (22), 8419-8423.

381. Markus, T. Z.; Wu, M.; Wang, L.; Waldeck, D. H.; Oron, D.; Naaman, R., Electronic Structure of CdSe Nanoparticles Adsorbed on Au Electrodes by an Organic Linker: Fermi Level Pinning of the HOMO. *Journal Of Physical Chemistry C* **2009,** 113, (32), 14200-14206.

382. Campbell, I. H.; Crone, B. K., Efficient, visible organic light-emitting diodes utilizing a single polymer layer doped with quantum dots. *Applied Physics Letters* **2008,** 92, (4).

383. Niu, Y. H.; Munro, A. M.; Cheng, Y. J.; Tian, Y. Q.; Liu, M. S.; Zhao, J. L.; Bardecker, J. A.; Jen-La Plante, I.; Ginger, D. S.; Jen, A. K. Y., Improved performance light-emitting diodes quantum dot layer. *Advanced Materials* **2007,** 19, (20), 3371-+.

384. Huynh, W. U.; Dittmer, J. J.; Alivisatos, A. P., Hybrid nanorod-polymer solar cells. *Science* **2002,** 295, (5564), 2425-2427.

385. Huynh, W. U.; Dittmer, J. J.; Libby, W. C.; Whiting, G. L.; Alivisatos, A. P., Controlling the morphology of nanocrystal-polymer composites for solar cells. *Advanced Functional Materials* **2003,** 13, (1), 73-79.

386. Huynh, W. U.; Dittmer, J. J.; Teclemariam, N.; Milliron, D. J.; Alivisatos, A. P.; Barnham, K. W. J., Charge transport in hybrid nanorod-polymer composite photovoltaic cells. *Physical Review B* **2003,** 67, (11).

387. Colvin, V. L.; Alivisatos, A. P.; Tobin, J. G., VALENCE-BAND PHOTOEMISSION FROM A QUANTUM-DOT SYSTEM. *Physical Review Letters* **1991,** 66, (21), 2786-2789.

388. Ekimov, A. I.; Hache, F.; Schanneklein, M. C.; Ricard, D.; Flytzanis, C.; Kudryavtsev, I. A.; Yazeva, T. V.; Rodina, A. V.; Efros, A. L., Absorption And Intensity-Dependent Photoluminescence Measurements On Cdse Quantum Dots - Assignment Of The 1st Electronic-Transitions. *Journal Of The Optical Society Of America B-Optical Physics* **1993,** 10, (1), 100-107.

389. Wise, F. W., Lead salt quantum dots: The limit of strong quantum confinement. *Accounts Of Chemical Research* **2000,** 33, (11), 773-780.

390. Weiss, E. A.; Chiechi, R. C.; Geyer, S. M.; Porter, V. J.; Bell, D. C.; Bawendi, M. G.; Whitesides, G. M., Size-dependent charge collection in junctions containing single-size and multi-size arrays of colloidal CdSe quantum dots. *Journal Of The American Chemical Society* **2008,** 130, (1), 74-82.

391. Kagan, C. R.; Murray, C. B.; Bawendi, M. G., Long-range resonance transfer of electronic excitations in close-packed CdSe quantum-dot solids. *Physical Review B* **1996,** 54, (12), 8633-8643.

392. Murray, C. B.; Kagan, C. R.; Bawendi, M. G., Synthesis and characterization of monodisperse nanocrystals and close-packed nanocrystal assemblies. *Annual Review Of Materials Science* **2000,** 30, 545-610.

393. Klimov, V. I.; Mikhailovsky, A. A.; Xu, S.; Malko, A.; Hollingsworth, J. A.; Leatherdale, C. A.; Eisler, H. J.; Bawendi, M. G., Optical gain and stimulated emission in nanocrystal quantum dots. *Science* **2000,** 290, (5490), 314-317.

394. Tarucha, S.; Austing, D. G.; Honda, T.; vanderHage, R. J.; Kouwenhoven, L. P., Shell filling and spin effects in a few electron quantum dot. *Physical Review Letters* **1996,** 77, (17), 3613-3616.

395. Ding, Z. F.; Quinn, B. M.; Haram, S. K.; Pell, L. E.; Korgel, B. A.; Bard, A. J., Electrochemistry and electrogenerated chemiluminescence from silicon nanocrystal quantum dots. *Science* **2002,** 296, (5571), 1293-1297.

396. Chen, S. W.; Truax, L. A.; Sommers, J. M., Alkanethiolate-protected PbS nanoclusters: Synthesis, spectroscopic and electrochemical studies. *Chemistry Of Materials* **2000,** 12, (12), 3864-3870.

397. Haram, S. K.; Quinn, B. M.; Bard, A. J., Electrochemistry of CdS nanoparticles: A correlation between optical and electrochemical band gaps. *Journal Of The American Chemical Society* **2001,** 123, (36), 8860-8861.

398. Wehrenberg, B. L.; Guyot-Sionnest, P., Electron and hole injection in PbSe quantum dot films. *Journal Of The American Chemical Society* **2003,** 125, (26), 7806-7807.

399. Myung, N.; Ding, Z. F.; Bard, A. J., Electrogenerated chemiluminescence of CdSe nanocrystals. *Nano Letters* **2002,** 2, (11), 1315-1319.

400. Medintz, I. L.; Uyeda, H. T.; Goldman, E. R.; Mattoussi, H., Quantum dot bioconjugates for imaging, labelling and sensing. *Nature Materials* **2005,** 4, (6), 435-446.

401. Dahan, M.; Levi, S.; Luccardini, C.; Rostaing, P.; Riveau, B.; Triller, A., Diffusion dynamics of glycine receptors revealed by single-quantum dot tracking. *Science* **2003,** 302, (5644), 442-445.

402. Larson, D. R.; Zipfel, W. R.; Williams, R. M.; Clark, S. W.; Bruchez, M. P.; Wise, F. W.; Webb, W. W., Water-soluble quantum dots for multiphoton fluorescence imaging in vivo. *Science* **2003,** 300, (5624), 1434-1436.

403. Coe, S.; Woo, W. K.; Bawendi, M.; Bulovic, V., Electroluminescence from single monolayers of nanocrystals in molecular organic devices. *Nature* **2002,** 420, (6917), 800-803.

404. Stiff-Roberts, A. D.; Krishna, S.; Bhattacharya, P.; Kennerly, S., Low-bias, high-temperature performance of a normal-incidence InAs/GaAs vertical quantum-dot infrared photodetector with a current-blocking barrier. *Journal Of Vacuum Science & Technology B* **2002,** 20, (3), 1185-1187.

405. Oregan, B.; Gratzel, M., A Low-Cost, High-Efficiency Solar-Cell Based On Dye-Sensitized Colloidal Tio2 Films. *Nature* **1991,** 353, (6346), 737-740.

406. Nozik, A. J., Quantum dot solar cells. *Physica E-Low-Dimensional Systems & Nanostructures* **2002,** 14, (1-2), 115-120.

407. Milliron, D. J.; Gur, I.; Alivisatos, A. P., Hybrid organic - Nanocrystal solar cells. *Mrs Bulletin* **2005,** 30, (1), 41-44.

408. Forrest, S. R., The limits to organic photovoltaic cell efficiency. *Mrs Bulletin* **2005,** 30, (1), 28-32.

409. Shallcross, R. C.; D'Ambruoso, G. D.; Pyun, J.; Armstrong, N. R., Photoelectrochemical Processes in Polymer-Tethered CdSe Nanocrystals. *Journal Of The American Chemical Society* **2010,** 132, (8), 2622-2632.

410. Bae, Y.; Myung, N.; Bard, A. J., Electrochemistry and electrogenerated chemiluminescence of CdTe nanoparticles. *Nano Letters* **2004,** 4, (6), 1153-1161.

411. Guyot-Sionnest, P., Charging colloidal quantum dots by electrochemistry. *Microchimica Acta* **2008,** 160, (3), 309-314.

412. Guyot-Sionnest, P.; Wang, C., Fast voltammetric and electrochromic response of semiconductor nanocrystal thin films. *Journal Of Physical Chemistry B* **2003,** 107, (30), 7355-7359.

413. Inamdar, S. N.; Ingole, P. P.; Haram, S. K., Determination of Band Structure Parameters and the Quasi-Particle Gap of CdSe Quantum Dots by Cyclic Voltammetry. *Chemphyschem* **2008,** 9, (17), 2574-2579.

414. Wang, C. J.; Shim, M.; Guyot-Sionnest, P., Electrochromic nanocrystal quantum dots. *Science* **2001,** 291, (5512), 2390-2392.

415. Wang, C. J.; Shim, M.; Guyot-Sionnest, P., Electrochromic semiconductor nanocrystal films. *Applied Physics Letters* **2002,** 80, (1), 4-6.

416. Araci, Z. O.; Shallcross, R. C.; Armstrong, N. R.; Saavedra, S. S., Potential-Modulated Attenuated Total Reflectance Characterization of Charge Injection Processes in Monolayer-Tethered CdSe Nanocrystals. *The Journal of Physical Chemistry Letters* **2010,** 1, (12), 1900 - 1905.

417. Bradshaw, J. T.; Mendes, S. B.; Armstrong, N. R.; Saavedra, S. S., Broadband coupling into a single-mode, electroactive integrated optical waveguide for spectroelectrochemical analysis of surface-confined redox couples. *Analytical Chemistry* **2003,** 75, (5), 1080-1088.

418. Bradshaw, J. T.; Mendes, S. B.; Saavedra, S. S., Planar integrated optical waveguide spectroscopy. *Analytical Chemistry* **2005,** 77, (1), 28A-36A.

419. Saavedra, S. S.; Reichert, W. M., Integrated Optical Attenuated Total Reflection Spectrometry Of Aqueous Superstrates Using Prism-Coupled Polymer Wave-Guides. *Analytical Chemistry* **1990,** 62, (20), 2251-2256.

420. Hodes, G., Comparison of Dye- and Semiconductor-Sensitized Porous Nanocrystalline Liquid Junction Solar Cells. *Journal Of Physical Chemistry C* **2008,** 112, (46), 17778-17787.

421. Rabani, E.; Hetenyi, B.; Berne, B. J.; Brus, L. E., Electronic properties of CdSe nanocrystals in the absence and presence of a dielectric medium. *Journal Of Chemical Physics* **1999,** 110, (11), 5355-5369.

422. Qu, L. H.; Peng, X. G., Control of photoluminescence properties of CdSe nanocrystals in growth. *Journal Of The American Chemical Society* **2002,** 124, (9), 2049-2055.

423. Yu, W. W.; Qu, L. H.; Guo, W. Z.; Peng, X. G., Experimental determination of the extinction coefficient of CdTe, CdSe, and CdS nanocrystals. *Chemistry Of Materials* **2003,** 15, (14), 2854-2860.

424. Ratcliff, E. L.; Lee, P. A.; Armstrong, N. R., Work function control of hole-selective polymer/ITO anode contacts: an electrochemical doping study. *Journal Of Materials Chemistry* **2010,** 20, (13), 2672-2679.

425. Song, W. B.; Okamura, M.; Kondo, T.; Uosaki, K., Construction and electrochemical characteristics of multilayer assemblies of Au nanoclusters protected by mixed self-assembled monolayers on tin-doped indium oxide. *Physical Chemistry Chemical Physics* **2003,** 5, (23), 5279-5284.

426. Yan, C.; Zharnikov, M.; Golzhauser, A.; Grunze, M., Preparation and characterization of self-assembled monolayers on indium tin oxide. *Langmuir* **2000,** 16, (15), 6208-6215.

427. Munro, A. M.; Zacher, B.; Graham, A.; Armstrong, N. R., Photoemission Spectroscopy of Tethered CdSe Nanocrystals: Shifts in Ionization Potential and Local Vacuum Level As a Function of Nanocrystal Capping Ligand. *Acs Applied Materials & Interfaces* **2010,** 2, (3), 863-869.

428. Saavedra, S. S.; Reichert, W. M., Insitu Quantitation of Protein Adsorption Density by Integrated Optical Waveguide Attenuated Total Reflection Spectrometry. *Langmuir* **1991,** 7, (5), 995-999.

429. Skrdla, P. J.; Saavedra, S. S.; Armstrong, N. R.; Mendes, S. B.; Peyghambarian, N., Sol-gel-based, planar waveguide sensor for water vapor. *Analytical Chemistry* **1999,** 71, (7), 1332-1337.

430. Kelly, C. P.; Cramer, C. J.; Truhlar, D. G., Single-ion solvation free energies and the normal hydrogen electrode potential in methanol, acetonitrile, and dimethyl sulfoxide. *Journal Of Physical Chemistry B* **2007,** 111, (2), 408-422.

431. Brus, L. E., A SIMPLE-MODEL FOR THE IONIZATION-POTENTIAL, ELECTRON-AFFINITY, AND AQUEOUS REDOX POTENTIALS OF SMALL

SEMICONDUCTOR CRYSTALLITES. *Journal Of Chemical Physics* **1983,** 79, (11), 5566-5571.

432. Armstrong, N. R.; Veneman, P. A.; Ratcliff, E.; Placencia, D.; Brumbach, M., Oxide Contacts in Organic Photovoltaics: Characterization and Control of Near-Surface Composition in Indium-Tin Oxide (ITO) Electrodes. *Accounts Of Chemical Research* **2009,** 42, (11), 1748-1757.

433. Marikkar, F. S.; Carter, C.; Kieltyka, K.; Robertson, J. W. F.; Williamson, C.; Simmonds, A.; Zangmeister, R.; Fritz, T.; Armstrong, N. R., Conducting polymer diffraction gratings on gold surfaces created by microcontact printing and electropolymerization at submicron length scales. *Langmuir* **2007,** 23, (20), 10395-10402.

434. Clark, R. A.; Bowden, E. F., Voltammetric peak broadening for cytochrome c/alkanethiolate monolayer structures: Dispersion of formal potentials. *Langmuir* **1997,** 13, (3), 559-565.

435. Malliaras, G. G.; Scott, J. C., The roles of injection and mobility in organic light emitting diodes. *Journal Of Applied Physics* **1998,** 83, (10), 5399-5403.

436. Shen, Y. L.; Jacobs, D. B.; Malliaras, G. G.; Koley, G.; Spencer, M. G.; Ioannidis, A., Modification of indium tin oxide for improved hole injection in organic light emitting diodes. *Advanced Materials* **2001,** 13, (16), 1234-1238.

437. Ishii, H.; Seki, K., Energy level alignment at organic/metal interfaces studied by UV photoemission: Breakdown of traditional assumption of a common vacuum level at the interface. *Ieee Transactions on Electron Devices* **1997,** 44, (8), 1295-1301.

438. Kahn, A.; Koch, N.; Gao, W. Y., Electronic structure and electrical properties of interfaces between metals and pi-conjugated molecular films. *Journal of Polymer Science Part B-Polymer Physics* **2003,** 41, (21), 2529-2548.

439. Ginger, D. S.; Greenham, N. C., Charge injection and transport in films of CdSe nanocrystals. *Journal Of Applied Physics* **2000,** 87, (3), 1361-1368.

440. Jarosz, M. V.; Porter, V. J.; Fisher, B. R.; Kastner, M. A.; Bawendi, M. G., Photoconductivity studies of treated CdSe quantum dot films exhibiting increased exciton ionization efficiency. *Physical Review B* **2004,** 70, (19).

441. Talapin, D. V.; Murray, C. B., PbSe nanocrystal solids for n- and p-channel thin film field-effect transistors. *Science* **2005,** 310, (5745), 86-89.

442. Shalom, M.; Ruhle, S.; Hod, I.; Yahav, S.; Zaban, A., Energy Level Alignment in CdS Quantum Dot Sensitized Solar Cells Using Molecular Dipoles. *Journal Of The American Chemical Society* **2009,** 131, (29), 9876-+.

443. Soreni-Hararl, M.; Yaacobi-Gross, N.; Steiner, D.; Aharoni, A.; Banin, U.; Millo, O.; Tessler, N., Tuning energetic levels in nanocrystal quantum dots through surface manipulations. *Nano Letters* **2008,** 8, (2), 678-684.